

Advances in Geological and Geotechnical Engineering Research





Editor-in-Chief

Prof. Sayed Hemeed

Cairo University, Egypt

Prof. Wengang Zhang

Chongqing University, China

Associate Editor

Prof. Amin Beiranvand Pour

Universiti Malaysia Terengganu, Malaysia

Editorial Board Members

Alcides Nobrega Sial, Brazil	Sheng Hua Cui, China
Antonio Zanutta, Italy	Márton Veress, Hungary
Bojan Matoš, Croatia	Vincenzo Amato, Italy
Ezzedine Saïdi, Tunisia	Wang Dongdong, China
Irfan Baig, Norway	Wen-Chieh Cheng, China
Jian-Hong Wu, Taiwan, China	Zheng Han, China
Jinliang Zhang, China	Bing-Qi Zhu, China
Kamel Bechir Maalaoui, Tunisia	Mualla Cengiz, Turkey
Luqman Kolawole Abidoye, Nigeria	Hamdalla Abdel-Gawad Abdel-Aziz Wanas, Saudi Arabia
Mehmet İrfan Yesilnacar, Turkey	Ramesh Man Tuladhar, Nepal
Mirmahdi Seyedrahimi-Niaraq, Iran	Chaojun Jia, China
Mokhles Kamal Azer, Egypt	Olukayode Dewumi Akinyemi, Nigeria
Vladimir Aleksandrovich Naumov, Russia	Hu Li, China
Ntieche Benjamin, Cameroon	Raphael Di Carlo Santos, Brazil
Jianwen Pan, China	Zhaofei Chu, China
Salvatore Grasso, Italy	Zhenhua Zhou, China
Shaoshuai Shi, China	

Volume 5 Issue 4 • October 2023 • ISSN 2810-9384 (Online)

Advances in Geological and Geotechnical Engineering Research

Editor-in-Chief

Prof. Sayed Hemeed

Prof. Wengang Zhang

Advances in Geological and Geotechnical Engineering Research

Contents

Editorial


- 56** **Editorial for *Advances in Geological and Geotechnical Engineering Research*: Vol. 5 Issue 4 (2023)**
Amin Beiranvand Pour

Articles

- 1** **Groundwater Quality Assessment in Pul-e-Charkhi Region, Kabul, Afghanistan**
Hafizullah Rasouli, Ashok Vaseashta
- 22** **Integration of GIS with the Generalized Reciprocal Method (GRM) for Determining Foundation Bearing Capacity: A Case Study in Opolo, Yenagoa Bayelsa State, Nigeria**
Ebiegberi Oborie, Desmond Eteh
- 41** **Origin of the Dashuigou Independent Tellurium Deposit at the Southeastern Qinghai-Tibet Plateau: Based on the Abundances of Trace Elements in the Country Rocks**
Jianzhao Yin, Shoupu Xiang, Haoyu Yin, Hongyun Shi, Yuhong Chao
- 59** **Geophysical Approach for Groundwater Resource Assessment: A Case Study of Oda Community Akure, Southwestern Nigeria**
S. J. Abe, I. A. Adeyemo, O. J. Abosede-brown

ARTICLE

Groundwater Quality Assessment in Pul-e-Charkhi Region, Kabul, Afghanistan

Hafizullah Rasouli^{1*}, Ashok Vaseashta^{2*} 

¹ Department of Geology, Geoscience Faculty, Kabul University, Jamal Mina, Kabul, 1006, Afghanistan

² Applied Research, International Clean Water Institute Manassas, PO Box 258, VA, USA

ABSTRACT

We present the results of studies conducted on the assessment of groundwater quality observed on several water samples taken from water supply sources in the Pul-e-Charkhi region, which is located near the eastern part of Kabul and has seen steady growth in population after the U.S. completed its withdrawal from Afghanistan on 30 August 2021. The water in the basin serves as the main source of water supply and it consists of water discharge from nearby local industries, automobile repair and wash, Osman House, Gradation Place, International Standards Region, and many other regional sources that create a mix of contaminants in discharge to the basin. We collected several samples from each groundwater source for this investigation and transported them carefully to the research laboratory, maintaining the integrity of the samples. The main objective of this study is to assess groundwater quality for the determination of contaminants in groundwater to see what limitations it may pose for recycling and reuse. Such a study is necessary since the region requires persistent sources of water due to a steady increase in population and an associated shortage of water supply due to arid conditions. Furthermore, there is unavailability of similar data since the region served to support military operations since 2001. The samples were analyzed for temperature, electro-conductivity, dissolved oxygen, total dissolved solids, salinity, pH, color, turbidity, hardness, chemicals, and heavy metals. The results obtained suggest that the parameters can be used efficiently to design filtration strategies based on region-specific contamination for the specific catchments located in and around the Kabul Basin. An effort to add additional characterization techniques is described to detect micro/nano plastics and new and emerging contaminants. The efforts reported here are consistent with the 2030 agenda for Sustainable Development Goals.

Keywords: Groundwater; Water quality; Chemical parameter; Physical parameter; Geology

*CORRESPONDING AUTHOR:

Hafizullah Rasouli, Department of Geology, Geoscience Faculty, Kabul University, Jamal Mina, Kabul, 1006, Afghanistan; Email: hafizullah.rasouli133@gmail.com

Ashok Vaseashta, Applied Research, International Clean Water Institute Manassas, PO Box 258, VA, USA; Email: prof.vaseashta@ieee.org

ARTICLE INFO

Received: 27 August 2023 | Revised: 1 October 2023 | Accepted: 10 October 2023 | Published Online: 23 October 2023

DOI: <https://doi.org/10.30564/agger.v5i4.5949>

CITATION

Rasouli, H., Vaseashta, A., 2023. Groundwater Quality Assessment in Pul-e-Charkhi Region, Kabul, Afghanistan. *Advances in Geological and Geotechnical Engineering Research*. 5(4): 1-21. DOI: <https://doi.org/10.30564/agger.v5i4.5949>

COPYRIGHT

Copyright © 2023 by the author(s). Published by Bilingual Publishing Group. This is an open access article under the Creative Commons Attribution-NonCommercial 4.0 International (CC BY-NC 4.0) License. (<https://creativecommons.org/licenses/by-nc/4.0/>).

1. Introduction

This study concerns the assessment of the groundwater quality in the Pul-e-Charkhi region located near the eastern part of Kabul. The region has a lot of historical and political context. Historically, the region is on an Indian tectonic plate, formed by tectonic activities of the Gondwana since almost ~140 million years ago, and moving at a speed of ~20 cm/year toward the Asian plate. Generally, the east side of Kabul was separated along a fault line in the Tertiary (geological period) ~90 million years ago. The forming of the Himalayan Mountain occurred due to the movement of ~2000 miles over approximately 50 million years, following the collision of the Indian plate with the Asian plate in the Alpine orogeny^[1]. The Kabul Basin can be described as a valley filled with different sizes of sedimentary materials or regolith and surrounded by crystalline mountains (metamorphic) rocks^[2]. The ranges consist of different elevations of crystalline and sedimentary rocks^[3,4]. Quaternary sediments are > 100 m thick and are dispersed around Kabul^[5]. Underlying tertiary sediments in Kabul are estimated to be between 1500-2000 m thick, depending upon the area location of the valley^[6,7]. The adjoining mountains are predominantly comprised of Paleo-Proterozoic gneiss and Late Permian and Late Triassic sedimentary rocks^[7]. The gravel and sand in the river channels were deposited by the Lata-band formation as Quaternary terrace sediments of middle and younger Pleistocene age overlay these conglomerates. The Khengal and basement rocks are over-thrusted by schist *mélange*, which is termed the Cottagay Series in the northern Kohe-Safi range^[8], and are under-thrusted by *mélange* in the Kabul River valley^[9]. The eastern part of the Kabul Basin is exhibited by a few isolated yet linear faults and cliffs that exhibit normal dip-slip movement^[10]. The Granite in Paghman, Kabul spans from Precambrian^[11] and Khengal series. To further characterize the basin, it is important to note that Kabul is surrounded by different fault systems including Chamman-moqure^[12], Sarobi, and Mahi-par faults^[13]. The Kabul Basin is tectonically active in the transpressional deformation plate-bound-

ary region in the areas under investigation^[14,15]. The inter-basin ridges^[16,17] are accumulated from metamorphic core-complex rocks, consisting of Paleoproterozoic gneiss^[18]. The sediments of Khengal series were initiated since the Jurassic period^[19] and are situated in the Thythes Ocean in Afghanistan^[20].

The Pul-e-Charkhi Basin dates to the Quaternary (Pleistocene) and Neogen geological periods. The Pul-e-Charkhi sedimentary basin is situated on the east side of Kabul City and covers an area of ~580 km²^[21,22]. Most regolith and sediments are transported to this basin from different points of Loger and Asmayey mountains, formed by flashfloods and accumulation occurring in the Kabul River at different thicknesses and in different locations of this basin. Various sediments accumulate sequentially and form a morphology, which can be seen at different release points^[23]. Sediment types correspond to the nature of rocks located in the surrounding mountains, as we observe Garnete, Biotite, and Muscovite mineral particles. The surrounding mountains of this basin are formed from metamorphic rocks like Schist, Gneiss, and Slate. The Chelsaton Mountains are a series of Loger Mountain ranges, which are located from Southwest to Northeast, called Walayati and Khengal series^[24]. In these mountains, different kinds of rocks such as slate, Gneisses, Granite mica schist, and gravel for construction material^[25] are found. Further analysis reveals that there are additional sediments than Quartzite, Gneisses, and Schist. As per the morphology of Pul-e-Charkhi, there are three relief kinds, viz. high (upper course) in the mountain slopes, middle relief (middle course) in the hills, and plains (lower course) in the agricultural lands. Furthermore, Pul-e-Charkhi Basin is located between mountain ranges which are called intermountain backing basins, with the plain areas passing the Kabul River and its two laterals located on agricultural lands^[26]. Furthermore, Pul-e-Charkhi houses a military airfield nearby. Various strategic locations such as Pul-e-Charkhi prison, camp warehouse, and salt pit are all located nearby. However, since the 2021 withdrawal of U.S. forces from the region, there has been a lot of commercial interest and hence

subsequent pollution resulting from industrial activities. The discharge water also ends up in the basin. Hence, the main objective of this investigation is to assess the groundwater quality which is extracted for selection for different types of usage, such as drinking water, agriculture, and industries. As proposed by the authors, an efficient water filtration strategy is to filter out region-specific contaminants^[27]. The thickness, and sizes of soil and sediment vary year-to-year in hydro-meteorological conditions of the basin thus impacting groundwater percolation, surface, and groundwater pollution^[28].

The Pul-e-Charkhi region has experienced significant industrial growth ranging from pharmaceuticals, metals, auto-repair, construction, and even bakeries—all producing CO and CO₂ emissions as well as a mixture of waste discharge in the water basin including micro/nano plastics, metals, volatile organic compounds, and new and emerging contaminants. Several of these contaminants are emitted into the environment and remain suspended locally due to the high mountains in the region. The suspended particles get mixed with precipitation by absorption and leaching and contaminate the surface waters and the earth's surface and soil. Some of these factories use metals such as Arsenic (As), Cadmium (Cd), and Lead (Pb), which have severe consequences, should they be discharged into the water basin. Several health centers in the region also pose concerns about the likelihood of medical waste being released into the water basin. Lastly, the ubiquitous presence of plastics from single-use plastic bottles and grocery bags is a major concern as most of the plastic waste ends up in landfills and subsequently in surface waters through estuaries and rivers. Therefore, geological and pedogenic research for the future of this region is critically important for the efficient management and planning of groundwater. This research is essential to studying groundwater quality, with almost no previous research available pertaining to this basin^[29].

1.1 Geology of Kabul

First, we present a brief overview of the geology

of the Kabul Basin which dates to the Quaternary (Pleistocene) period^[30,16]. Sediments to this basin come from Aliabad, Asmayie, Paghman, Qorugh, and Logger mountains. These mountains are in the surrounding areas of Kabul Basin and these sediments are carried by water at varied periods of time and form different thicknesses. The upper and middle parts of Kabul Basin terraces accumulate some heavy and light minerals, which originate from the mother rocks located in the surrounding mountain areas of Kabul Basin. For example, Epidote, Cyanite, and Granite can be found in some terraces of the Kabul River Basin as they arise from Metamorphic (Crystalline) rocks. Also, there are some other minerals, such as Rutile and Zircon which come from igneous rocks of the Paghman Mountains range^[17,31]. In addition, there are some other minerals such as Muscovite and Biotite, as metamorphic rocks from the surrounding mountains of Kabul Basin. Biotite and Rutile minerals in the middle and lower terraces of the Paghman River also come from igneous rocks of the Paghman Mountain range, and all sediments are carried by water and accumulate in terraces^[32,18]. All rivers of Kabul Basin conjoin at different locations, and all run about from west to east, and sediments of Kabul Basin belong to Tertiary (Eocene and Oligocene), and the age of sediments between the upper and middle parts of Kabul is ~ (20-45) million years, called Tertiary formations^[19]. The upper part of these sediments is covered by younger sediments of lower Quaternary (Pleistocene) sediments, and it consists of the terraces above. It has different complexes, altitudes, and locations. For example, the upper part of the Kabul River Basin originated from the Quaternary, as we observe combined and dispersed gravel sediments, as compared with the middle part of the Kabul River Basin, which comes from the Tertiary. All mountains surrounding Kabul Province are made of metamorphic rocks, while the Paghman Mountains change of metamorphic rocks arises from some pyrogenous rocks. The radiometry method found that the lifetime of these metamorphic rocks of approximately (928 ± 8) million years^[21,34]. The older of the two is located in the Khair Khana

Mountains while the younger one is in the Shawaky and Qorugh Mountains range ^[12,36,37] (**Figure 1**).



Figure 1. The geological map of Pul-e-Charkhi, Kabul, Afghanistan.

1.2 Geographical location

The Pul-e-Charkhi (lat: 34.54132°, long: 69.36764°) is one of the bigger areas of Kabul province and is located in the east part of Kabul province (**Figure 2**). It has a total area of ~48,800,000 km², agricultural land of ~4800 ha, an urban area is ~15,800,000 km², and an unplanned area is approximately 3,300,000 km². The surrounding areas consist of the Loger River located at the west side ^[38,22], with

south and east sides Botkhak and Bagرامي, and the Kabul River flows at the north side ^[22,39,40]. The total population living in these areas is ~325000 ^[22,41].

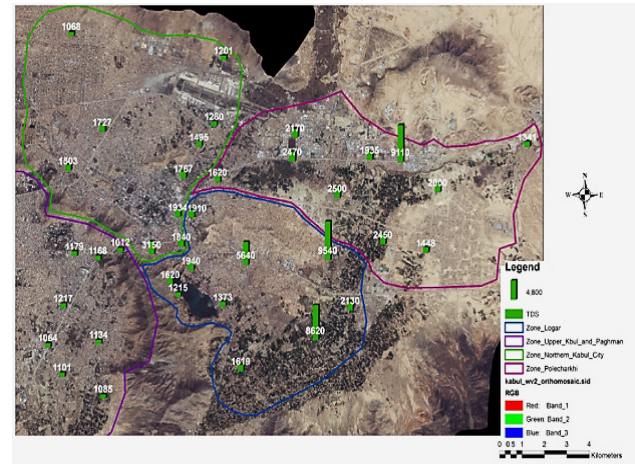


Figure 2. The location map of Pul-e-Charkhi.

2. Methods and materials

The area under investigation consists of the Pul-e-Charkhi region, a province of Kabul, where we identified water sources from 10 ring wells. The samples were collected, transported to the laboratory, and then subsequently analyzed at the laboratory of the Department of Geology, Kabul University. The results of various characterizations are provided below. **Tables 1 and 2** list various parameters that were characterized and instrumentation used for the measurements.

Table 1. Physical parameters of groundwater in Pul-e-Charkhi regions.

No	Name	Formula	Unite	The device of measurement	Location of analysis
1	Color	Col	DOS	Color test kit, Model#: CO-1, HACH	Laboratory
2	Temperature	T	°C	Potable groundwater temperature Multi 341 Instrument	Laboratory
3	Electroconductivity	EC	µs/cm	Potable groundwater Conductivity meter, Model#: Multi 340i	Laboratory
4	Solutions	TDS	mg/L	Potable groundwater temperature Conductivity meter, Model#: Multi 340i	Laboratory
5	Saline	Sal	mg/L	Potable groundwater temperature Conductivity meter, Model#: Multi 340i	Laboratory
6	Solution of Oxygen	DO	mg/L	Dissolved Oxygen Sensor, Model#: Multi 340i	Laboratory

Table 2. Chemical parameters of groundwater in Pul-e-Charkhi regions.

No	Name	Symbol	Unite	Measurement Instrument	Location of analyzed
1	Calcium	Na	mg/L	Spectra photometer # DR3900	Laboratory
2	Magnesium	Mg	mg/L	Spectra photometer # DR3900	Laboratory
3	Sodium	Na	mg/L	Spectra photometer # DR3900	Laboratory
4	Hydroxide	OH	mg/L	Spectra photometer # DR3900	Laboratory
5	Carbonates	CO ₃	mg/L	Spectra photometer # DR3900	Laboratory
6	Bicarbonates	HCO ₃	mg/L	Spectra photometer # DR3900	Laboratory
7	Chloride	Cl ₂	mg/L	Spectra photometer # DR3900	Laboratory
8	Fluorides	F	mg/L	Spectra photometer # DR3900	Laboratory
9	Sulfite	SO ₄	mg/L	Spectra photometer # DR3900	Laboratory
10	Phosphate	PO ₄	mg/L	Spectra photometer # DR3900	Laboratory
11	Potassium	K	mg/L	Spectra photometer # DR3900	Laboratory
12	Nitride	NO ₃	mg/L	Spectra photometer # DR3900	Laboratory
13	Nitrite	NO ₄	mg/L	Spectra photometer # DR3900	Laboratory
14	Ammonia	NH ₃	mg/L	Spectra photometer # DR3900	Laboratory
15	Iron	Fe	mg/L	Spectra photometer # DR3900	Laboratory
16	Manganese	Mn	mg/L	Spectra photometer # DR3900	Laboratory
17	Copper	Cu	mg/L	Spectra photometer # DR3900	Laboratory
18	Aluminum	Al	mg/L	Spectra photometer # DR3900	Laboratory
19	Arsenic	Ar	mg/L	Spectra photometer # DR3900	Laboratory
20	Cyanides	CN	mg/L	Spectra photometer # DR3900	Laboratory

3. Results and discussions

In this study, we used physical and chemical limitations at the groundwater of Pul-e-Charkhi regions, of Kabul Province, Afghanistan. Here, we collected different groundwater samples from the general water supply, Bricks center, Washing of Cars, Osman House, Gradation place, International Standards, etc. regions of Kabul. These measurement parameters include temperature, electro-conductivity, dissolved oxygen, total dissolved solids, salinity, pH, color, turbidity, T hardness from CaCO₃, calcium, magnesium, sodium, alkalinity, passphrase, OH, CO₃, HCO₃, chlorides, florid, sulfate, phosphate, potassium, nitrite, nitrate, ammonia, iron, manganese, copper, aluminium, arsenic, and cyanide, as described in **Table 3**.

It should be noted that water passing through the tables of gravel continues to be filtered through a variety of mechanisms. On the other hand, there are old practices of burying waste in the ground, which over a period of time leaches into water tables with high acidic contents due to decomposition. Hence,

regular monitoring of these contaminants is essential in providing guidance to the local municipalities on water purification strategies. From this investigation, our objective is to establish in-field testing as well as laboratory-based testing of water samples to consistently monitor different types of pollutants in water, such as organic materials, micro/nano plastics, metals from industrial discharge, raw sewage, and other new and emerging contaminants. We have also studied temperature dependence which tends to dissolve more chemicals causing changes in electroconductivity. In addition, we studied the redox process for self-purification of water due to catalysis. Likewise, characterization of TDS (total dissolved solids) provides turbidity due to soluble and salty rocks and salinity, while pH provides data on salinity. In the following section, we describe several methods that are used to characterize these contaminants. In parallel, we continue to develop additional capabilities to characterize new and emerging contaminants using Atomic Absorption Spectroscopy, Raman, and Fourier Transform Infrared (FTIR) spectrophotometer.

Table 3. Groundwater physical and chemical parameters in Pul-e-Charkhi regions.

Parameters	Units	Well locations					
		Water supply	Bricks center	Washing of cars	Osman house	Gradation place	International standards
Temperature	°C	25	24	15	30	20	25-30
EC	μs/cm	1619	2150	2470	1942	9140	1500 (WHO2006)
pH		7.18	7.35	7.89	8.208	8.186	6.5-8.5
DO	mg/L	25	39	37	35	26	
TDS	mg/L	1445.22	1645.02	1288.12	6067.26	3075.20	1000
Salinity	mg/L	0.8	1.1	1.2	0.9	5.1	
Color	APHA	0	0	0	0	0	No acceptable
Turbidity	NTU	0	0	0	0	0	5 NTU
T hardness as CaCO ₃	mg/L	800	1000	1140	750	2050	500
Calcium	mg/L	24	76	18.4	72.1	120.2	75
Magnesium	mg/L	478.9	599.9	721.3	357.8	153.8	30
Sodium	mg/L	6	0	32	27	140	200
T Alkalinity	mg/L	475	650	575	350	150	NGVS
Phosphorus	mg/L	0	0	0	0	0	NGVS
OH	mg/L	0	0	0	0	0	NGVS
CO ₃	mg/L	0	0	0	0	0	NGVS
HCO ₃	mg/L	475	650	575	350	150	NGVS
Chlorides	mg/L	0	0	0	0	0.02	250
Fluoride	mg/L	0	0	0	0	1.21	1.5
Sulfate	mg/L	95	92	116	127	1000	250
Phosphate	mg/L	0.19	0.59	0.44	0.33	2.12	NGVS
Potassium	mg/L	11.1	8.5	7.1	6	33.9	NGVS
Nitrite	mg/L	0.001	0.001	0.021	0.022	0.121	3
Nitrate	mg/L	1.2	0.4	2.2	0.15	1.2	50
Ammonia	mg/L	0.19	0.17	0.15	0.08	0.16	NGVS
Iron	mg/L	0.16	0.61	0	0	0.07	0.3
Manganese	mg/L	0.8	0.9	1	0.8	1	0.3
Copper	mg/L	0.05	0.06	0.05	0.05	0.22	0.2
Aluminum	mg/L	0.03	0.011	0.027	0	0.036	0.2
Arsenic	mg/L	0	0	0	0	0	0.05
Cyanide	mg/L	0	0.001	0.002	0.002	0.002	0.05

3.1 Temperature

The temperature of groundwater is generally between 5-15 °C, which is normally colder than surface water. At the location of the brick center, the water temperature is generally lower than the Kabul River. The temperature of the water near the well of the washing area is higher than the regional standard, which results in lower water quality for the villagers,

due to a decrease in the amount of oxygen. Furthermore, it results in decomposition due to an increase in bacterial formation bacteria (**Figure 3**). The temperature of groundwater varies with the depth of groundwater, volcanic eruptions, and geographical locations. From the viewpoint of temperature, the ground is divided into six categories as it consists of very cold (5 °C), less cold (10 °C), warm water (18 °C), almost warm (25 °C), warm (37 °C), and very

warm (more than 40 °C). In this investigation, all groundwater temperature is around 22 °C, which is suitable for drinking and most all other usages^[42].

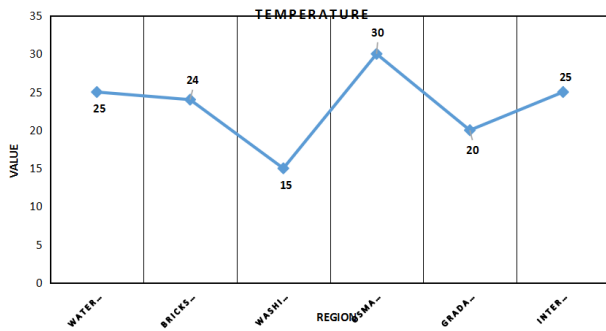


Figure 3. Groundwater temperature in Pul-e-Charkhi regions.

3.2 Electro-conductivity (EC)

Conductivity is the measurement of the primary current in any solution, and it shows the quantity of salt dissolved in water. The electro-conductivity is also dependent on the temperature of the water temperature during the measurement. Using a WTW GmbH, Weilheim Multi 340i pH/Dissolved Oxygen/Conductivity Measuring Instrument, the investigation could easily be conducted at the site, although samples were transported to the laboratory for assessment. To obtain an accurate value, it was necessary to measure the electro-conductivity at least three times for each sampling. The EC was higher at the Gradation place (9140 $\mu\text{S}/\text{cm}$) as compared to the international standard (1500 $\mu\text{S}/\text{cm}$) (Figure 4). Conforming to the norms of Afghanistan the EC, the World Health Organization (WHO), and Asian countries the electro-conductivity is 1500 $\mu\text{S}/\text{cm}$ ^[43].

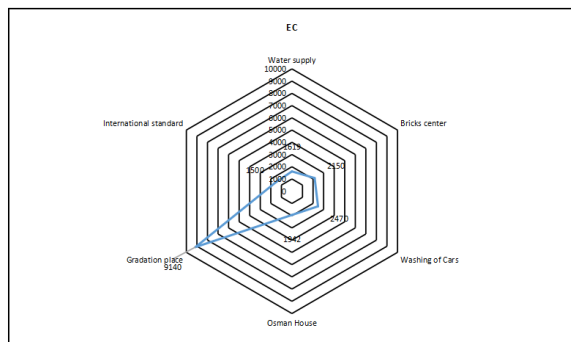


Figure 4. Groundwater electro-conductivity in Pul-e-Charkhi region.

3.3 pH

pH stands for the “power of hydrogen”. The numerical value of pH is determined by the molar concentration of hydrogen ions (H^+). The pH determination is because of hydrogen ions (H^+) and hydroxyl ions (OH^-) on pH. The higher the H^+ concentration, the lower the pH, and the higher the OH^- concentration, the higher the pH. At a neutral pH of 7 (pure water), the concentration of both H^+ ions and OH^- ions is 10^{-7} M. Thus, the ions H^+ and OH^- are always paired—as the concentration of one increases, the other will decrease; regardless of pH. For this investigation, the pH of groundwater was measured and was observed to be between (6.5 to 8.5). As per WHO, the water can be used for drinking and irrigation water (Figure 5). Generally, a WTW GmbH, Weilheim Multi 340i pH/Dissolved Oxygen/Conductivity Measuring Instrument was used for the determination of pH for measuring the acidic and basic nature of water samples. We determined that the pH of water is within the range agreement with WHO guidelines of 6.5-8.5, and also for the Asian countries^[44]. The hydroxyl group (OH) is due to the alkalinity of water. When the pH is higher than 7, the water displays a higher OH group.

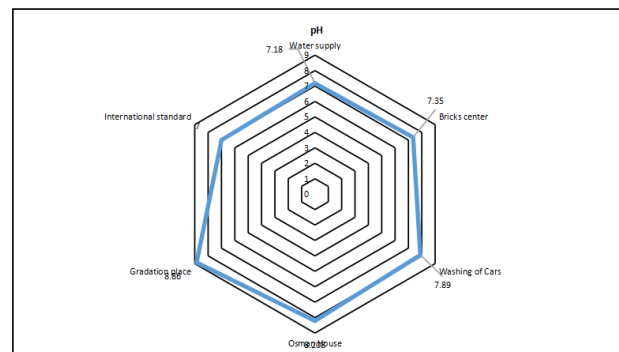


Figure 5. Groundwater pH in Pul-e-Charkhi regions.

3.4. Dissolved oxygen (DO)

The DO (dissolved oxygen), in Asiab regions is attributed to the location. For the measured samples, it was found to be more than recommended by WHO. Usually, from the observed values, we can find the main reason, which generally is due to the

location and the height of the well with respect to the mean sea level (**Figure 6**).

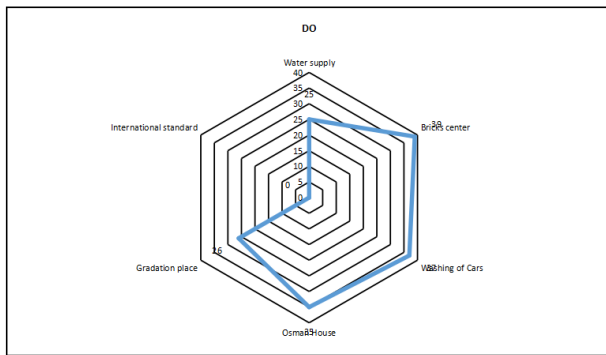


Figure 6. Groundwater DO in Pul-e-Charkhi regions.

3.5 TDS

For this part of the investigation, the TDS (total dissolved solid) shows the concentration of the solution (dissolved) material in water, such as salts, carbonates, and gypsum. The measured value of TDS is higher than the WHO standard (~1000 mg/L) ^[45]. From this measurement, we can estimate that the main reason for higher TDS will be due to the limestone coming from the surrounding mountains. Furthermore, since the surrounding mountains have more carbonates and limestones, the solids leach from different layers of aquifers producing higher TDS (**Figure 7**).

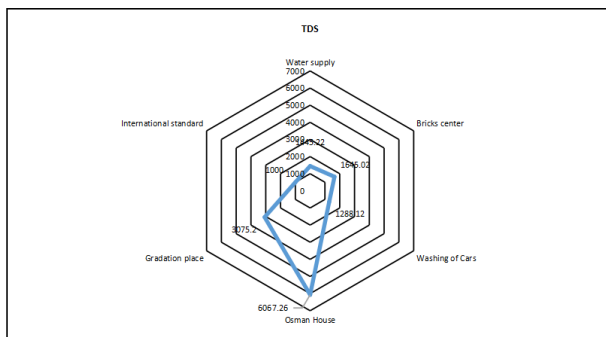


Figure 7. Groundwater TDS in Pul-e-Charkhi regions.

3.6 Salinity

Generally, in groundwater, we can find some amount of salinity, and the type and concentration of salt pertain to the source and the layers that infiltrate

the groundwater. Generally, the amount of salt in the groundwater is more than the surface water. The main sources of salinity are due to the compositions of saline lithology in groundwater layers, that come in contact and are attributed to the duration of salt percolation to surface water as well. The concentration of salt is also due to the composition of minerals and rocks that come in contact with the groundwater. Also, the amount of salinity is due to the evaporation, because Afghanistan is one the countries where we have more evapotranspiration than precipitation. Arising due to arid- the semi-arid climate of Afghanistan, there is more evaporation than precipitation, hence the amount of salinity in some places is due to the amount of salts from the igneous rocks, as such rocks contain Na, and Ca elements as compositional elements. Additionally, in this region, we also find some granite (**Figure 8**).

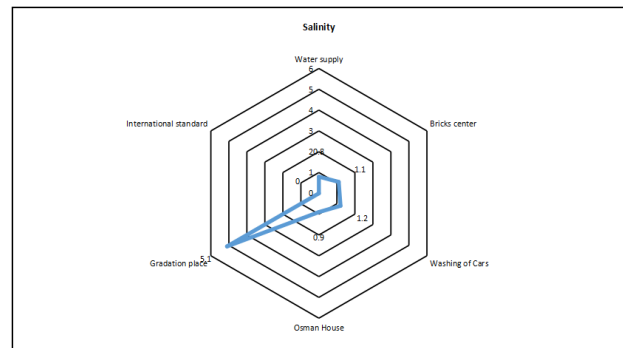


Figure 8. Groundwater total dissolved solids (TDS) in Pul-e-Charkhi regions.

3.7 Color

The groundwater color for this investigation is measured as per the WHO standard. In general, color is a great indication of the quality and contents of water, which generally has a slight green color, while every other color arises due to the existence of organic and inorganic materials in soluble forms. The existence of organic materials is typically displayed as brown, while the organic acidic dissolved solids have a yellow color. The existence of iron and hydrogen sulfides is shown by the red color, and the manganese shows a black color ^[46]. Generally, the color of groundwater is divided into five separate

categories, viz: blue, green, yellow, red, and colored. While the blue color of the water is desirable, care must be taken for use for drinking water and all other uses. In general, green color is also good but it may have some negative effects, due to bacteria, algae, and uncertainty being unstable. To mitigate the negative effects of coloration, it is necessary to measure color and we used Color Test Kit, Model CO-1, Product #: 223400 (HACH, Colorado, USA). The sample measurements and their comparison to local and international standards are shown in **Figure 9**.

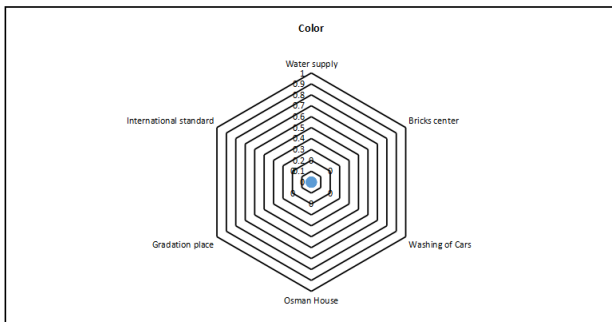


Figure 9. Groundwater color in Pul-e-Charkhi regions.

3.8 Turbidity

The turbidity in this study was measured by a turbidity meter since it measures the soluble solid materials in the water, but the turbidity cannot sum up in the watercolor. Generally, the turbidity is created by non-soluble materials in which the amount is lower in terms of high quantity that caused turbidity of water. The standard units for turbidity are ppm of non-soluble materials. According to WHO standards, the turbidity of water must be lower than 5. In this study, all the points are between 4 to 3^[47], as shown in **Figure 10**.

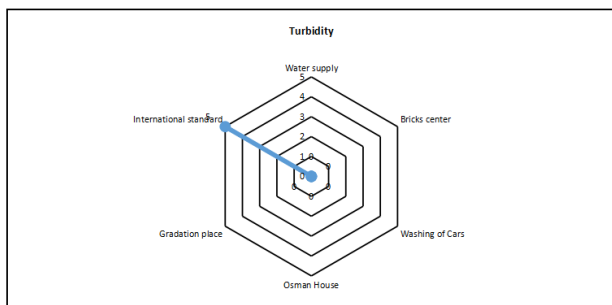


Figure 10. Groundwater turbidity in Pul-e-Charkhi regions.

3.9 Hardness as CaCO₃

The amount of carbonates results in varying pH (acid and basic) conditions, and it plays a very important role in the solution of soluble materials. Generally, in surface water, the amount of CO₂ should be fewer than 10 mg/L, but in groundwater, the amount is far more than 100 mg/L. In this study, the amount of carbonates is more than the recommended WHO standard (500 mg/L). The main reason is due to the existence of carbonate rocks in the surrounding mountains (**Figure 11**).

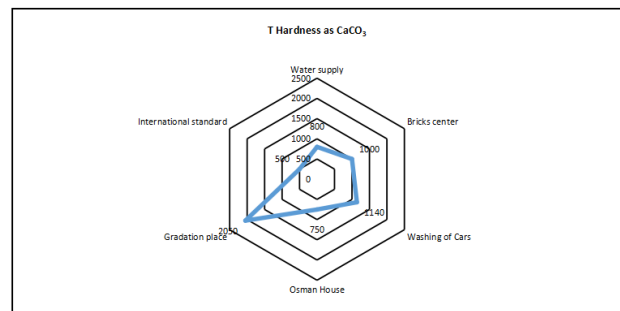


Figure 11. Groundwater T hardness as CaCO₃ in Pul-e-Charkhi regions.

3.10 Calcium

Calcium is one of the basic metals of the earth, and during reaction with water, it makes calcium hydroxides. Calcium is one of the important elements for the vertebral column bone, and the existence of calcium in water is good for the protection of human bone. We can find calcium in water, as it comes from certain rock formations in nature, and generally, it is found in the forms of calcium carbonates, carbonates, and sulfides. Although beneficial, a higher amount of calcium causes the hardness of the water. According to the WHO standard, the amount of calcium is 75 mg/L. The samples show that the amount of calcium in groundwater is near the WHO limit, as shown in **Figure 12**. However, after normal filtration, the water can be used for general purposes. Only in the Alishang region the amount of calcium was observed to be very high (~120 mg/L), which is due to the igneous rocks in that specific location^[48].

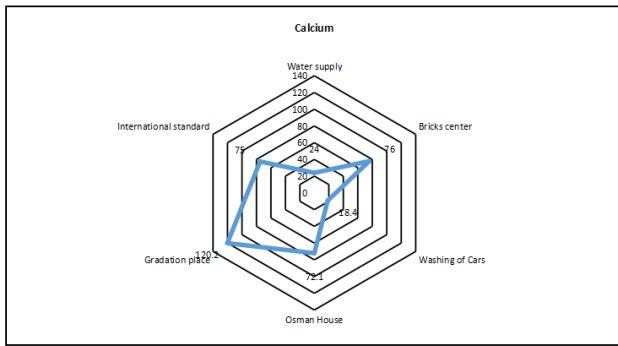


Figure 12. Groundwater calcium in Pul-e-Charkhi regions.

3.11 Magnesium

Magnesium is also one the basic metals of the earth, and with the fire having bright light and made magnesium oxides. Magnesium is used for normal activities of muscles and as an anti-acid for digestive tracks. The usage in water is ~250 mg/24 h. Magnesium is one the very important cations of water, which makes different soluble salts in water. In this study, the amount of Mg is observed to be more than recommended by WHO standard (30 mg/L), the main reason will be the mother rocks having Mg in the composition (Figure 13). A higher amount of Mg in water can induce a diarrheal response in humans.

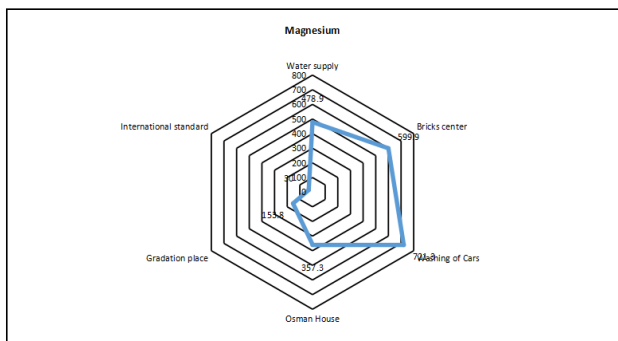


Figure 13. Groundwater magnesium in Pul-e-Charkhi regions.

3.12 Sodium

Sodium is one the important constituents of NaCl, which serves as an important part of our diet, as it is used for pH balance for the human body. The concentration of Na is due to the location and composition of rocks. The concentration of Na in freshwater

is ~500 mg/L. For those places where there is no precipitation, the concentration exceeds 500 mg/L. In ocean waters, the concentration of Na is up to 1100 mg/L, since Na is one of the soluble elements [49], and in saline water, the amount is approx. 1-100 mg/L. In this study, the amount of Na is lower than the WHO standard (200 mg/L), hence the water can be used for drinking and other usages (Figure 14), following standard municipality water cleaning procedures.

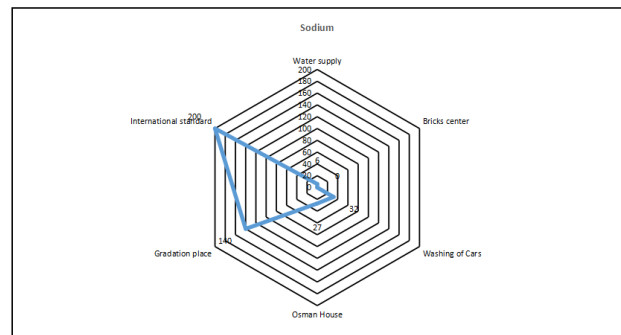


Figure 14. Groundwater sodium in Pul-e-Charkhi regions.

3.13 Alkalinity

Alkalinity is the buffering capacity of a water body; a measure of the ability of the water body to neutralize acids to maintain a fairly stable pH level. The ions that contribute to alkalinity are carbonate, bicarbonate, and hydroxide. Alkalinity may also include contributions from borates, phosphates, silicates, or other bases. When the pH is higher than 7, the solution is more alkaline in nature. Some of the pollutants, such as soap solution in urban areas and water from canals, etc. can also raise the pH. For the area under investigation, the alkalinity is found to be more than the WHO standard and the main reason is due to the composition of surrounding rocks from mountains (Figure 15). In general, pH electrodes are used for alkalinity titration using the preset endpoint technique. It is very important to calibrate the pH electrode before the analysis when using the preset end-point titration method. Interferences for the titration method are soaps, oily matter, suspended solids, or precipitates, which may coat the glass electrode and cause a sluggish response.

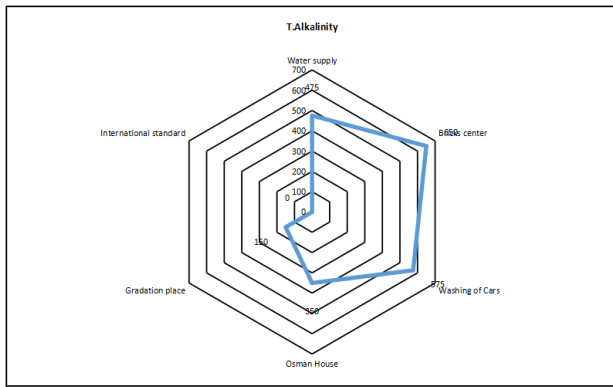


Figure 15. Groundwater alkalinity in Pul-e-Charkhi regions.

3.14 Phosphorus

Phosphorus results from several industrial activities, agricultural feed, and fertilizers since a vast majority of phosphorus compounds mined are consumed as fertilizers. Additionally, phosphate mines contain fossils because phosphate is present in the fossilized deposits of animal remains and excreta. Low phosphate levels are an important limit to growth in several plant ecosystems. Phosphate is needed to replace the phosphorus that plants remove from the soil and with increasing population its annual demand is rising. As per this study, the amount of phosphorus observed is consistent with limits established by the WHO standards and hence can be used for drinking water and other usages after standard water cleaning at the local municipality.

3.15 CaCO_3

Carbonates are one of the very important components of rock formations, found as minerals calcite and aragonite, most remarkably in chalk and limestone, eggshells, shellfish skeletons, gastropod shells, and pearls. Materials containing a lot of calcium carbonate are termed calcareous. Calcium carbonate is the active component in agricultural lime and is generated when calcium ions in hard water react with carbonate ions to create limescale. It has medical use as a calcium supplement or as an antacid, but excessive consumption can be hazardous and cause hypercalcemia and digestive issues. However, for

the region under investigation, the observed value of CaCO_3 is within the WHO range. Chemically, it is represented as follows^[50].



In the titration of the carbonate ions, we can find in the two steps, as it changes to the acids in the first stage as HCO_3^- , an intermediate form in the deprotonation of carbonic acid. It is a polyatomic anion with the chemical formula HCO_3^- . Bicarbonate serves a crucial biochemical role in the physiological pH buffering system. When acids are added to water, the amount of CO_3 decreases, and it changes to HCO_3^- . In this study, the amount of HCO_3^- is higher than the WHO standard and the main reason for this is the composition of lithology and surrounding mountain rocks (Figure 16).

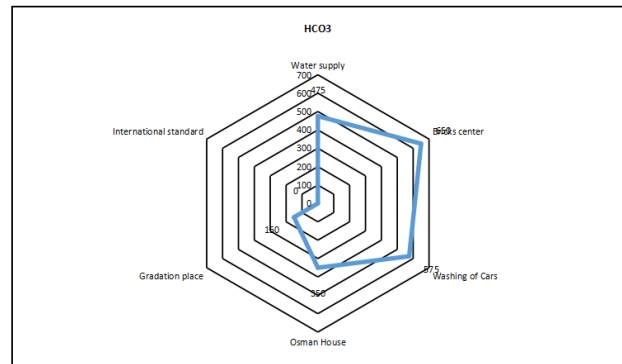


Figure 16. Groundwater calcium carbonates in Pul-e-Charkhi regions.

3.16 Chloride

Chloride refers either to a negatively charged (Cl^-) chlorine atom, or a non-charged chlorine atom covalently bonded to the rest of the molecule by a single bond (Cl). It is an essential electrolyte in body fluids responsible for maintaining acid/base balance, transmitting nerve impulses, and regulating liquid flow in and out of cells. Due to high reactivity, it also has corrosive characteristics and increased concentrations of chloride can cause a variety of ecological effects in both aquatic and terrestrial environments. The concentration of chlorides in groundwater under observation is 10 mg/L. The concentration of

chlorides in such places is due to salts, and seawater infiltration. For this investigation, the quantity of chlorides is much lower than WHO standard (250 mg/L), and hence the water can be used for daily consumption following standard municipality filtration methods (**Figure 17**).

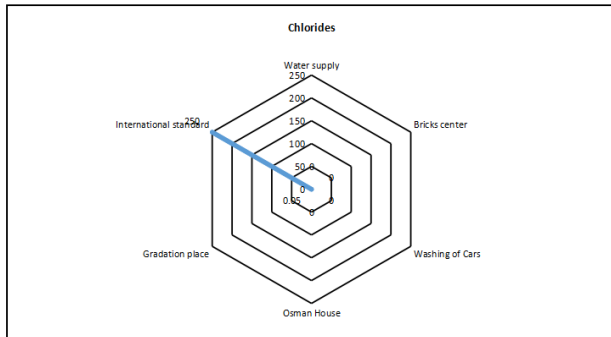


Figure 17. Groundwater chlorides in Pul-e-Charkhi regions.

3.17 Fluoride

Fluoride, a mineral, is naturally present in many foods and available as a dietary supplement. Generally, soil, water, plants, and foods contain trace amounts of fluoride. Most of the fluoride that people consume comes from fluoridated water, foods, and beverages prepared with such water, and use of toothpaste and other dental products. Fluoride in its ionic form of the element fluorine inhibits the initiation and progression of dental decay and stimulates new bone formation. The concentration of fluoride in surface water that is not polluted is about ~0.1-0.3 mg/L [51], but generally in groundwater the concentration is observed to be ~0.1-0.3 mg/L, and in some of the locations is observed to be about 12 mg/L. In most of the areas under investigation, the amount of fluoride is observed to be lower than the WHO standard (1.5 mg/L), hence the water can be used for drinking and all usages following standard municipality cleaning procedures (**Figure 18**).

Sulfates occur as microscopic aerosols resulting from fossil fuel and biomass combustion. They increase the acidity of the atmosphere and form acid rain. In groundwater, it is found in the form of magnesium sulfate (commonly known as Epsom salts), which is used in therapeutic baths. The concentration of sulfate in freshwater is less than 10 mg/L. However, for water directly discharged from mining industries to the groundwater, the amount of sulfate is observed to be ~500 mg/L. The concentration of sulfate in natural water fluctuates from 1-1000 mg/L. For this investigation, the quantity of sulfate is observed to be lower than the WHO standard (250 mg/L), and we can use it for drinking and other usages (**Figure 19**) following standard municipality cleaning procedures.

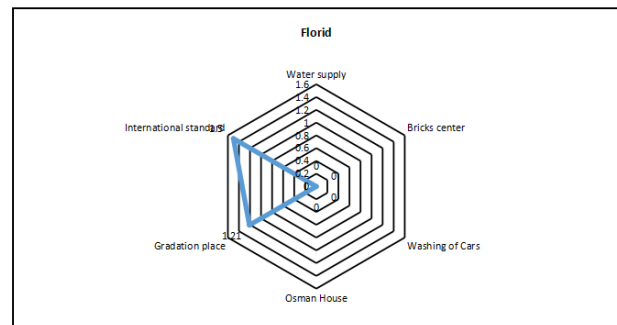


Figure 18. Groundwater fluoride in Pul-e-Charkhi regions.

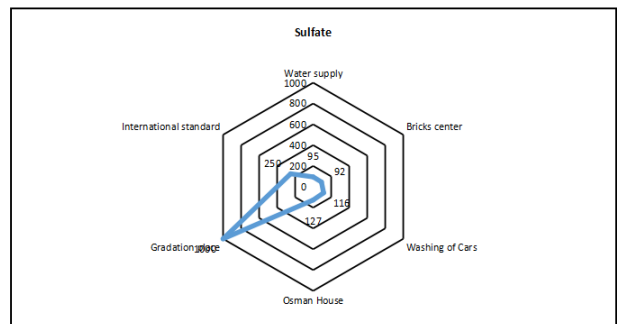


Figure 19. Groundwater sulfate in Pul-e-Charkhi regions.

3.18 Sulfate

Sulfate is an important polyatomic anion with the empirical formula SO_4^{2-} . Salts, acid derivatives, and peroxides of sulfate are widely used in various

3.19 Phosphate

Phosphate is another very important element that occurs in groundwater. Phosphate arises from any of numerous chemical compounds related to phosphoric acid (H_3PO_4). Derivatives are composed of salts containing the phosphate ion (PO_4^{3-}), the hy-

drogen phosphate ion (HPO_4^{2-}), or the dihydrogen phosphate ion (H_2PO_4^-), and positively charged ions such as those of sodium or calcium. A second group is composed of esters, in which the hydrogen atoms of phosphoric acid have been replaced by organic combining groups such as ethyl (C_2H_5) or phenyl (C_6H_5). Phosphates are a common constituent of agricultural fertilizers, manure, and organic wastes in sewage and industrial effluent. Furthermore, phosphates are chemicals containing the element phosphorous, and they affect water quality by causing excessive growth of algae. Phosphates in water feed algae, which grow out of control in water ecosystems and create imbalances, which destroy other life forms and produce harmful toxins. For this study, the amount of phosphate is close to the limit of WHO standards. Depending upon location, for the most part, the water can be used for drinking and other usages pending standard cleaning procedures (Figure 20).

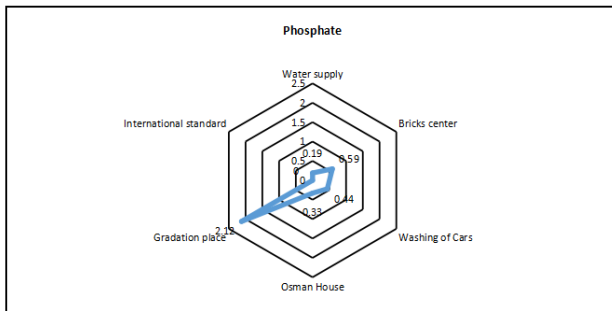


Figure 20. Groundwater phosphate in Pul-e-Charkhi regions.

3.20 Potassium

Potassium (K) is yet another important element in the groundwater. There is a growing movement to use potassium in conjunction with sodium to treat and soften drinking water. This would cause the level of potassium in drinking water to rise. The level of potassium in drinking water depends on the type of treatment used. Water that goes through potassium permanganate has lower levels of potassium than water that uses a potassium-based water softener. The concentration of potassium in clean water is about 2-5 mg/L. Generally, the concentration of K in

natural water is 30 mg/L. In this study, the amount of K is observed to be higher than the WHO guidelines and it may cause some issues if consumed untreated beyond standard clean procedures (Figure 21).

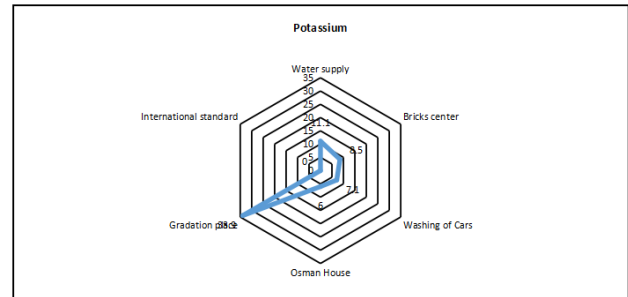


Figure 21. Groundwater potassium in Pul-e-Charkhi regions.

3.21 Nitrite

The nitrite ion has the chemical formula NO_2^- and is widely used throughout chemical and pharmaceutical industries. Nitrite can be reduced to nitric oxide or ammonia by many species of bacteria. Under hypoxic conditions, nitrite may release nitric oxide, which causes potent vasodilation. Sodium nitrite is used to speed up the curing of meat and also impart an attractive color and hence is used by the food industry. However, excess amounts of nitrites are known to be carcinogens. The returned nitrites in water are lower than 2 mg/L. Additionally, the reason for the presence of nitrites is due to the decomposition of sewage and industrial activities, such as dyes. In this study, the presence of NO_2^- is within the limit set by the WHO standard, and hence the water can be used for drinking and other usages following standard municipality cleaning (Figure 22).

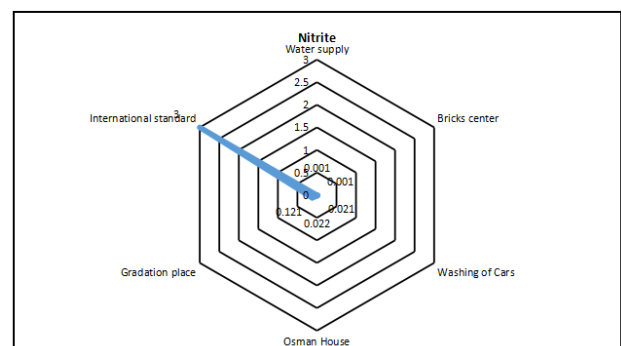


Figure 22. Groundwater nitrate in Pul-e-Charkhi regions.

3.22 Nitrate

Nitrate is a polyatomic ion with the chemical formula NO_3^- and salts containing this ion are called nitrates, which is a common component of fertilizers and explosives. Almost all inorganic nitrates are soluble in water and hence are used in agriculture, firearms, medicine, and even in the food industry. Nitrate salts are found naturally on earth in arid environments as large deposits, particularly of nitratine, a major source of sodium nitrate. Lightning strikes in Earth's nitrogen- and oxygen-rich atmosphere produce a mixture of oxides of nitrogen, which form nitrous ions and nitrate ions, which are washed from the atmosphere by rain or in occult deposition. Nitrates are also produced industrially from nitric acid. In freshwater or estuarine systems close to land, nitrate can reach concentrations that are lethal to fish. While nitrate is much less toxic than ammonia, levels over 30 ppm of nitrate can inhibit growth, impair the immune system, cause stress in aquatic species, and are known to produce methemoglobinemia. In clean water, the amount of NO_3^- is lower than 2 mg/L. In this study, the amount of NO_3^- is within the WHO guidelines of 50 mg/L, and hence water can be used for drinking and other usages following normal filtering and cleaning (Figure 23).

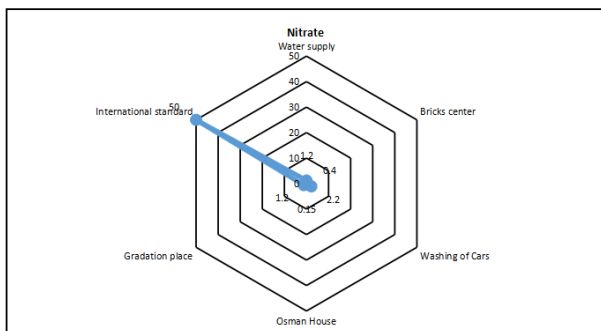


Figure 23. Groundwater nitrate in Pul-e-Charkhi regions.

3.23 Ammonia

Ammonia is an inorganic compound of nitrogen and hydrogen, NH_3 , a stable binary hydride, which is a colorless gas with a distinct pungent smell. Biologically, it is a common nitrogenous waste, particularly

among aquatic organisms, and it contributes significantly to the nutritional needs of terrestrial organisms by serving as a precursor to food and fertilizers. Ammonia readily dissolves in water. In an aqueous solution, it can be expelled by boiling. The aqueous solution of ammonia is basic. The maximum concentration of ammonia in water (a saturated solution) has a density of 0.880 g/cm^3 . In wells, the quality of water can be improved by decomposing nitrates by suitable catalysts into constituent elements. In this study, the amount of ammonia is within the WHO guidelines and hence water can be used for drinking water purposes pending standard cleaning and filtering (Figure 24).

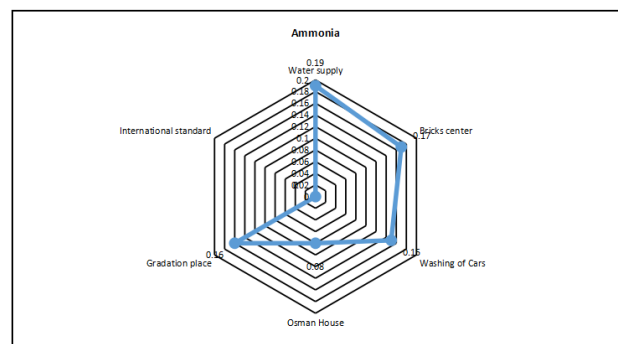


Figure 24. Groundwater ammonia in Pul-e-Charkhi regions.

3.24 Iron

Well waters are generally rich in iron since it exists in different forms, such as in suspended colloidal forms, and in complex forms of organic or inorganic materials. This iron element is not harmful to the human body, but it changes the physical properties of water (including smell) and has a bitter taste. After sedimentation, one can separate iron oxides. In this study, the amount of iron is according to the WHO standard (0.3 mg/L), and we can use it for drinking water (Figure 25).

3.25 Manganese

Manganese is an essential human dietary element, important in macronutrient metabolism, bone formation, and free radical defence systems. It is a critical component in dozens of proteins and enzymes. It is

found mostly in the bones, but also in the liver, kidneys, and brain. In the human brain, manganese is bound to manganese metalloproteins, most notably glutamine synthetase in astrocytes. Yet, manganese is a common impurity in private well water supplies. Also, manganese is naturally occurring in rocks and soil, so it gets into groundwater that seeps through the earth, collecting minerals. Manganese is used as an additive in gasoline and is released into the environment in exhaust gases. For the water samples in this study, the amount of manganese is within the limits set by the WHO and hence water can be consumed for drinking water and other usages following standard cleaning and filtration procedures (Figure 26).

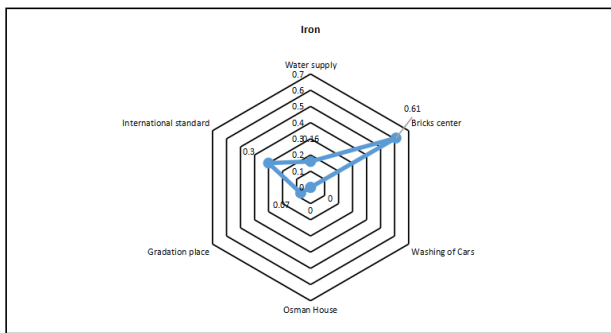


Figure 25. Groundwater iron in Pul-e-Charkhi regions.

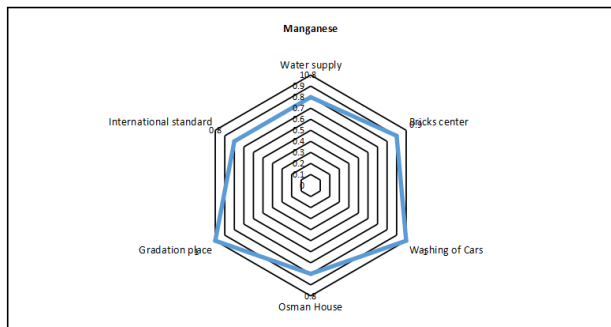


Figure 26. Groundwater manganese in Pul-e-Charkhi regions.

3.26 Copper

Cu is also one of the very important elements in nature. It is located in the rocks and lithology of the earth at varying compositions. In households, copper is used for cooking utensils and also in the plumbing. Copper is a mineral and metallic element that's essential to human health. However, too much copper will have side effects. Copper leaching is es-

pecially likely in acidic water with a low pH. In this study, the amount of Cu is at a slightly elevated level than recommended by the WHO standard (0.2 mg/L). However, with some precautions and using standard cleaning and filtration procedures, the water can be used for drinking and other usages (Figure 27).

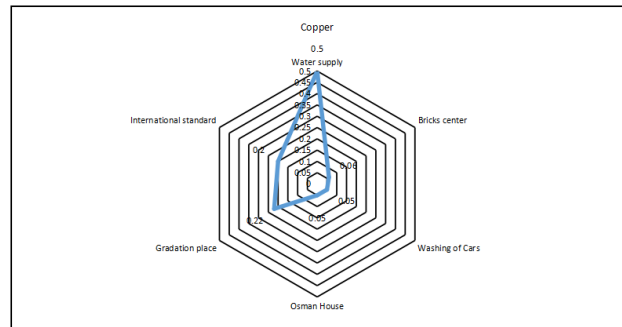


Figure 27. Groundwater copper in Pul-e-Charkhi regions.

3.27 Aluminum

Aluminum is one of the most common heavy metals found in drinking water and is also found abundantly in the earth's crust. This lightweight, silvery-white metal is used in a variety of products, including airplane parts, cans, kitchen utensils, foils, and satellite dishes. Unlike other metals, like iron and zinc, aluminum is non-essential to humans and is considered toxic. There is no recommended daily aluminum intake required by the human body. The most common way that aluminum gets into drinking water is through surface runoff and soil seepage. Water flows over rocks or through soil with high concentrations of aluminum, and traces of the metal dissolve into the water. Acid rain resulting from industrial activity is another common cause of high aluminum concentrations in surface water. In this study, the amount of aluminum was found to be within the WHO standard (0.2 mg/L) and the water can be used for drinking and other usage activities following standard cleaning procedures at the municipality (Figure 28).

3.28 Arsenic

Arsenic is one of the most toxic elements in wa-

ter. It is found in those places near metal mining, and industrial-scale insecticide production with discharge into the groundwater. Another common source of arsenic is water from freeways entering into the groundwater. There has been a substantial amount of research done to address arsenic in groundwater and drinking water supplies around the world. In drinking water supplies, arsenic poses a problem because it is toxic at low levels and is a known carcinogen. Long-term exposure to inorganic arsenic, mainly through drinking water and food, can lead to chronic arsenic poisoning. Skin lesions and skin cancer are the most characteristic effects. In 2001, the USEPA lowered the MCL for arsenic in public water supplies to 10 micrograms per liter ($\mu\text{g/L}$) from 50 $\mu\text{g/L}$. In this study, the amount of Arsenic is according to the WHO standard (0.05 mg/L), and we can use the water for drinking water and other usages following standard cleaning procedures (**Figure 29**).

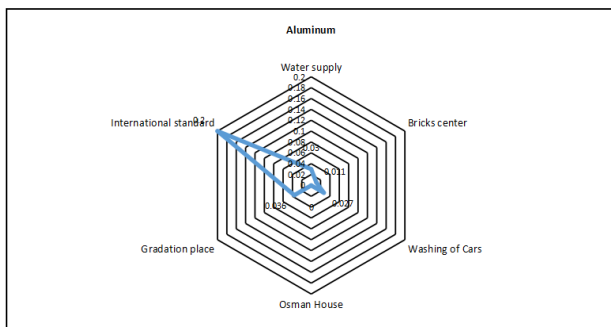


Figure 28. Groundwater ammonium in Pul-e-Charkhi regions.

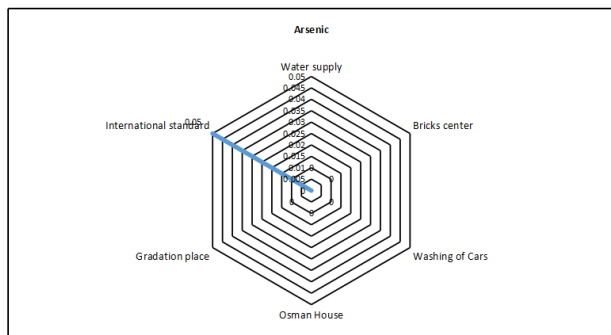


Figure 29. Groundwater arsenic in Pul-e-Charkhi regions.

3.29 Cyanides

HCN and its components are found in industrial and mining waters that contain a chemical com-

pound with the formula HCN and structural formula $\text{H}-\text{C}\equiv\text{N}$. It is a colorless, extremely poisonous, and flammable liquid that boils slightly above room temperature. Hydrogen cyanide is a linear molecule, with a triple bond between carbon and nitrogen. The tautomer of HCN is HNC, hydrogen isocyanide. Hydrogen cyanide is weakly acidic, and it partially ionizes in a water solution to give the cyanide anion, CN^- . A solution of hydrogen cyanide in water, represented as HCN, is called hydrocyanic acid. The salts of the cyanide anion are known as cyanides. HCN has a faint bitter almond-like odour, which is difficult to detect, and a volatile compound has been used as inhalation rodenticide and human poison, as well as for killing whales. Furthermore, cyanide ions interfere with iron-containing respiratory enzymes. The lethal dose concentration (LC_{50}) is 501 ppm (for rats, 200 ppm for mammals, and 357 ppm for humans). Using this investigation, we determined the amount of HCN at 0.05 mg/L , which is below the WHO standard and can be used for drinking and other usages (**Figure 30**), after normal municipality cleaning processes.

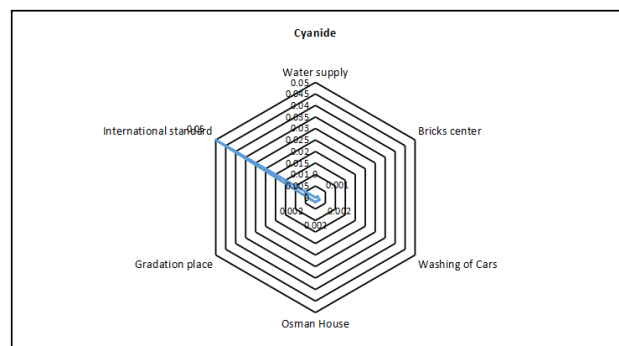


Figure 30. Groundwater cyanides in Pul-e-Charkhi regions.

4. Conclusions and discussion

During this investigation, we assessed the physical and chemical characteristics of the groundwater in the Pul-e-Charkhi region of Kabul Province, Afghanistan. We collected different samples of groundwater from various locations of water supply consisting of discharge from Bricks center, Washing of Cars, Osman House, Gradation Place, International Standards, and other similar regions of Kabul.

Several parameters were measured, such as temperature, EC, DO, TDS, salinity, pH, color, turbidity, T hardness as CaCO_3 , calcium, magnesium, sodium, alkalinity, phosphorus, OH, CO_3 , HCO_3 , chlorides, florid, sulfate, phosphate, potassium, nitrite, nitrate, ammonia, iron, manganese, copper, aluminum, arsenic, and cyanide respectively. The groundwater samples and parameters still show good results with national and international standards, indicating that water can be recycled using standard coagulation, flocculation, and bleaching methods. These results also suggest that the groundwater quality can still be used efficiently in the other districts of Kabul and other provinces in Afghanistan. As discharge now consists of new and emergent materials, including nanomaterials, it is necessary to improve the cleaning procedures and study life cycle analysis^[52] to assess and remediate new and emergent contaminants, including microplastics^[53-55]. One of the primary goals of the World Health Organization (WHO) and its member states is that “all people, whatever their stage of development and their social and economic conditions, have the right to have access to an adequate supply of safe drinking water.” The novelty of this investigation is to initiate a study of this kind that aims to provide comprehensive data on pollutants in this region. The level of contaminants is increasing and soon, the region will need to implement an improved and comprehensive approach to mitigate these contaminants. Also, in view of micro/nano plastics and new and emerging contaminants such as returned pharmaceuticals, volatile organic compounds, degreasers containing acetone, trichloroethylene, and other large chain hydrocarbons such as per-and polyfluoroalkyl substances (PFAS), also known as forever chemicals, we need better characterization facilities. Using our international network and with support from our local funding agencies, we would like to keep local municipalities and the general population aware of the contaminants and adverse health impacts that can result from using contaminated water. This is also consistent with the Sustainable Development Goals (SDG). The study conducted here is consistent with SDG-6 to support access to clean

water for all.

Author Contributions

Hafizullah Rasouli (H.R.), Ashok Vaseashta (A.V.), Conceptualization: H.R., A.V.; Methodology: H.R.; Software: H.R., A.V.; Validation, H.R., A.V.; Formal analysis, H.R., A.V.; Investigation, H.R.; Resources, H.R., A.V.; Data curation, H.R., A.V.; Writing-original and draft preparation, H.R., A.V.; Visualization, H.R., A.V.

Conflicts of Interest

The authors declare no conflicts of interest—financial or otherwise.

Funding

This research received no external funding.

References

- [1] Arian, H., Kayastha, R.B., Bhattarai, B.C., et al., 2015. Application of the snowmelt runoff model in the Salang river basin, Afghanistan using MODIS satellite data. *Journal of Hydrology and Meteorology*. 9(1), 109-118.
DOI: <https://doi.org/10.3126/jhm.v9i1.15586>
- [2] Rasouli, H., Safi, A.G., 2021. Geological, soil and sediment studies in Chelsaton sedimentary basin, Kabul, Afghanistan. *International Journal of Geosciences*. 12(2), 170-193.
DOI: <https://doi.org/10.4236/ijg.2021.12201120>
- [3] Rasouli, H., Sarwari, M.H., Rasikh, K., et al., 2020. Geological study of Tangi Mahi-Par Mountain Range along Kabul Jalalabad Road, Afghanistan. *Open Journal of Geology*. 10(10), 971.
DOI: <https://doi.org/10.4236/ojg.2020.1010044>
- [4] Rasouli, H., 2020. Application of soil physical and chemical parameters and its Comparing in Kabul Sedimentary basins, Kabul, Afghanistan. *International Journal of Recent Scientific Research*. 11(2), 37368-37380.
DOI: <https://doi.org/10.24327/ijrsr.2020.1102.5095>

- [5] Hamdard, M.H., Soliev, I., Rasouli, H., et al., 2022. Groundwater quality assessment in Chak Karstic Sedimentary Basin, Wardak Province, Afghanistan. *Central Asian Journal of Water Research*. 8(2), 102-109.
DOI: <https://doi.org/10.29258/CAJWR/2022-R1.v8-2/110-127.eng>
- [6] Rasouli, H., 2021. Analysis of groundwater quality in Jabal Sarage and Charikar Districts, Parwan, Afghanistan. *Journal of Geological Research*. 3(4), 45-55.
DOI: <https://doi.org/10.30564/jgr.v3i4.3717>
- [7] Rasouli, H., 2019. A study on some river sediments, hydrology and geological characteristics in Chak Sedimentary Basin, Wardak, Afghanistan. *International Journal of Geology, Earth & Environmental Sciences*. 9(2), 46-61.
- [8] Shamal, S., Rasouli, H., 2018. Comparison between pH, EC, CaCO₃ and mechanical analysis of Qala Wahid and Company Areas soil, Kabul, Afghanistan. *International Journal of Science and Research*. 8(5), 429-433.
DOI: <https://doi.org/10.21275/ART20197318>
- [9] Rasouli, H., 2020. Well design and stratigraphy of Sheerkhana Deep Well in Chak District, Wardak, Afghanistan. *International Journal of Geology, Earth & Environmental Sciences*. 10(2), 54-68.
- [10] Rasouli, H., Kayastha, R.B., Bhattarai, B.C., et al., 2015. Estimation of discharge from Upper Kabul River Basin, Afghanistan using the snow-melt runoff model. *Journal of Hydrology and Meteorology*. 9(1), 85-94.
DOI: <https://doi.org/10.3126/jhm.v9i1.15584>
- [11] Rasouli, H., Quraishi, R., Belhassan, K., 2021. Investigations on river sediments in Chak Sedimentary Basin, Wardak Province, Afghanistan. *Journal of Geological Research*. 3(4), 21-29.
DOI: <https://doi.org/10.30564/jgr.v3i4.3574>
- [12] Rasouli, H., 2022. Climate change impacts on water resource and air pollution in Kabul Sub-basins, Afghanistan. *Advances in Geological and Geotechnical Engineering Research*. 4(1), 11-27.
- [13] Rasouli, H., 2022. Methods of well construction complication, design and developing for sixteen observation and test wells at the eight locations of Zarange District, Nimroz, Afghanistan. *International Journal of Earth Sciences Knowledge and Applications*. 4(3), 426-448.
- [14] Rasouli, H., Vaseashta, A., Hamdard, M.H., 2023. Sedimentological study of Chack Hydro-power Reservoir, Wardak, Afghanistan. *International Journal of Earth Sciences Knowledge and Applications*. 5(1), 21-32.
- [15] Rasouli, H., Vaseashta, A., Belhassan, K., 2023. Mechanical analysis of Khair Abad Village, Surskhrud District, Nangarhar Province, Afghanistan. *International Journal of Earth Sciences Knowledge and Applications*. 5(1), 103-120.
- [16] Rasouli, H., Vaseashta, A., Hamdard, M.H., 2023. Study of physicochemical properties of soil at Qargha Dam Areas in Paghman District, Kabul, Afghanistan. *International Journal of Earth Sciences Knowledge and Applications*. 5(2), 244-251.
- [17] Tünnemeier, T., Houben, G., 2005. Hydrogeology of Kabul Basin Part 1: Geology, Aquifer Characteristics, Climate, and Hydrography [Internet]. Available from: https://www.bgr.bund.de/EN/Themen/Wasser/Projekte/abgeschlossen/TZ/Afghanistan/hydrogeology_kabul_basin_1.pdf?__blob=publicationFile&v=3
- [18] Arsenic in Drinking Water: Background Document for Development of WHO Guidelines for Drinking-water Quality [Internet]. WHO; 2019. Available from: <https://www.who.int/publications/i/item/arsenic-in-drinking-water-background-document-for-development-of-who-guidelines-for-drinking-water-quality>
- [19] Preventing Disease through Healthy Environments. Exposure to Arsenic: A Major Public Health Concern [Internet]. WHO; 2019. Available from: <https://www.who.int/publications/i/item/WHO-CED-PHE-EPE-19.4.1>
- [20] WHO Handbook on Indoor Radon: A Public Health Perspective [Internet]. WHO; 2009.

- Available from: <https://www.who.int/publications/i/item/9789241547673>
- [21] Uranium in Drinking Water. Background Document, for Development of WHO Guidelines for Drinking Water Quality [Internet]. WHO; 2005. Available from: <https://www.who.int/docs/default-source/wash-documents/wash-chemicals/uranium-background-document.pdf>
- [22] Anthony, E.J., Héquette, A., 2007. The grain-size characterisation of coastal sand from the Somme estuary to Belgium: Sediment sorting processes and mixing in a tide-and storm-dominated setting. *Sedimentary Geology*. 202(3), 369-382.
DOI: <https://doi.org/10.1016/j.sedgeo.2007.03.022>
- [23] Coe, A.L., 2003. The sedimentary record of sea-level change. Cambridge University Press: Cambridge.
- [24] Ball, M.M., 1967. Carbonate sand bodies of Florida and the Bahamas. *Journal of Sedimentary Research*. 37(2), 556-591.
- [25] Belhassan, K., 2020. Hydrogeology of the Ribaa-Bittit springs in the Mikkes Basin (Morocco). *International Journal of Water Resources and Environmental Science*. 9(1), 07-15.
DOI: <http://doi.org/10.5829/idosi.ijwres.2020.9.1.14537>
- [26] Belhassan, K., 2020. Relationship between river and groundwater: Water table piezometry of the Mikkes Basin (Morocco). *International Journal of Water Resources and Environmental Sciences*. 9(1), 1-6.
DOI: <http://doi.org/10.5829/idosi.ijwres.2020.9.1.14536>
- [27] Vaseashta, A., Gevorgyan, G., Kavaz, D., et al., 2021. Exposome, biomonitoring, assessment and data analytics to quantify universal water quality. Water safety, security and sustainability: Threat detection and mitigation. Springer International Publishing: Cham. pp. 67-114.
DOI: https://doi.org/10.1007/978-3-030-76008-3_4
- [28] Broshears, R.E., Akbari, M.A., Chornack, M.P., et al., 2005. Inventory of Ground-water Resources in the Kabul Basin, Afghanistan [Internet]. U. S. Geological Survey. Available from: <https://pubs.usgs.gov/sir/2005/5090/>
- [29] Maps of Quadrangle 3468, Chak Wardak-Syahgerd (509) and Kabul (510) Quadrangles, Afghanistan [Internet]. U.S. Geological Survey; 2007. Available from: <https://www.usgs.gov/publications/maps-quadrangle-3468-chak-wardak-syahgerd-509-and-kabul-510-quadrangles-afghanistan>
- [30] Maps of Quadrangle 3468, Chak Wardak-Syahgerd (509) and Kabul (510) Quadrangles, Afghanistan [Internet]. U.S. Geological Survey; 2005. Available from: <https://pubs.usgs.gov/publication/ofr20051107>
- [31] Colella, A., Di Geronimo, I., 1998. Surface sediments and macrofaunas of the Grati submarine fan (Ionian sea, Italy). *Sedimentary Geology*. 51(3), 257-277.
- [32] Elliott, T., 1986. Deltas, sedimentary environments and facies, 2nd ed. Black Wall Scientific Pub.: Oxford. pp. 154.
- [33] Folk, R.L., 1962. Spectral subdivision of limestone types. *Classification of Carbonate Rocks: AAPG Memoir*. 1, 62-84.
- [34] Goff, J., McFadgen, B.G., Chagué-Goff, C., 2004. Sedimentary differences between the 2002 Easter storm and the 15th-century Okoropunga tsunami, southeastern North Island, New Zealand. *Marine Geology*. 204(1-2), 235-250.
DOI: [https://doi.org/10.1016/S0025-3227\(03\)00352-9](https://doi.org/10.1016/S0025-3227(03)00352-9)
- [35] Horikawa, K., Ito, M., 2009. Non-uniform across-shelf variations in thickness, grain size, and frequency of turbidites in a transgressive outer-shelf, the Middle Pleistocene Kakinokidai Formation, Boso Peninsula, Japan. *Sedimentary Geology*. 220(1-2), 105-115.
DOI: <https://doi.org/10.1016/j.sedgeo.2009.07.002>
- [36] Kortekaas, S., Dawson, A., 2007. Distinguishing tsunami and storm deposits: An example from Martinhal, SW Portugal. *Sedimentary Geology*. 200, 208-210.
DOI: <https://doi.org/10.1016/j.sedgeo.2007.01.004>
- [37] Sree Devi, P., Srinivasulu, S., Kesava Raju, K., 2001. Hydrogeomorphological and groundwa-

- ter prospects of the Pageru river basin by using remote sensing data. *Environmental Geology*. 40(9), 1088-1094.
- [38] Grillot, J.C., Chaffaut, I., Mountaz, R., 1988. Effect of the environment on the hydrochemical characteristic of an alluvial aquifer following an exceptional multiyear drought (Mediterranean seashore, Herault, France): Part I—Recharge of the aquifer. *Environmental Geology and Water Sciences*. 11(2), 163-173.
- [39] Grillot, J.C., Chaffaut, I., Mountaz, R., 1988. Effect of the environment on the hydrochemical characteristic of an alluvial aquifer following an exceptional multiyear drought (Mediterranean seashore, Herault, France): Part II—Climatology and Agronomy. *Environmental Geology and Water Sciences*. 11(2), 175-181.
- [40] Fakir, Y., 1991. Hydrogéologique et hydrochimique des aquifères côtières du Sahel de Safi à Oualidia (Meseta côtière, Maroc) (French) [Hydrogeological and hydrochemical characterization of the coastal aquifers of the Sahel Safi to Oualidia (coastal Meseta, Morocco)] [Ph.D. thesis]. Marrakech, Morocco: Faculty of Sciences Semlalia, Cadi Ayyad University.
- [41] Alibou, J., 2002. Impacts des changements climatiques sur les ressources en eau et les zones humides du Maroc (French) [Impacts of climate change on water resources and wetlands of Morocco]. École Hassania des Travaux Publics (EHTP).
- [42] Technical Report on Groundwater Management in the Mediterranean and the Water Framework Directive [Internet]. Mediterranean Groundwater Working Group; 2007. Available from: <http://hdl.handle.net/20.500.11822/2303>
- [43] Rafik, A., Bahir, M., Beljadid, A., et al., 2021. Surface and groundwater characteristics within a semi-arid environment using hydrochemical and remote sensing techniques. *Water*. 13, 277. DOI: <https://doi.org/10.3390/w13030277>
- [44] Murthy, K.S.R., 2000. Ground water potential in a semi-arid region of Andhra Pradesh-a geographical information system approach. *International Journal of Remote Sensing*. 21(9), 1867-1884.
- [45] Sree Devi, P., Srinivasulu, S., Kesava Raju, K., 2001. Hydrogeomorphological and groundwater prospects of the Pageru river basin by using remote sensing data. *Environmental Geology*. 40(9), 1088-1094.
- [46] Ligtenberg, J.H., 2005. Detection of fluid migration pathways in seismic data: implications for fault seal analysis. *Basin Research*. 17(1), 141-153.
- [47] Chenini, I., Mammou, A.B., Turki, M.M., et al., 2010. Piezometric levels as possible indicator of aquifer structure: Analysis of the data from Maknassy basin aquifer system (Central Tunisia). *Arabian Journal of Geosciences*. 3(1), 41-47. DOI: <https://doi.org/10.1007/s12517-009-0050-4>
- [48] Castany, G., 1967. Unité des eaux de surface et des eaux souterraines, principe fondamental de la mise en valeur des ressources hydrologiques (French) [Unit of surface water and groundwater, a fundamental principle of the development of water resources]. *Bull. A.I.H.S.* 3, 22-30.
- [49] Horikawa, K., Ito, M., 2009. Non-uniform across-shelf variations in thickness, grain size, and frequency of turbidites in a transgressive outer-shelf, the Middle Pleistocene Kakinokidai Formation, Boso Peninsula, Japan. *Sedimentary Geology*. 220(1-2), 105-115. DOI: <https://doi.org/10.1016/j.sedgeo.2009.07.002>
- [50] Bogdevich, O., Duca, G., Sidoroff, M.E., et al., 2022. Groundwater resource investigation using isotope technology on river-sea systems. *Handbook of research on water sciences and society*. IGI Global: Hershey. pp. 87-100. DOI: <https://doi.org/10.4018/978-1-7998-7356-3.ch004>
- [51] Vaseashta, A., Duca, G., Culighin, E., et al., 2020. Smart and connected sensors network for water contamination monitoring and situational awareness. *Functional nanostructures and sensors for CBRN defence and environmental safety and security*. Springer: Netherlands. pp. 283-

296.
DOI: https://doi.org/10.1007/978-94-024-1909-2_20
- [52] Vaseashta, A., 2015. Life cycle analysis of nanoparticles: Risk, Assessment, and Sustainability. Destech Publications: Lancaster, PA, USA.
- [53] Stabnikova, O., Stabnikov, V., Marinin, A., et al., 2021. Microbial life on the surface of microplastics in natural waters. *Applied Sciences*. 11(24), 11692.
DOI: <https://doi.org/10.3390/app112411692>
- [54] Stabnikova, O., Stabnikov, V., Marinin, A., et al., 2022. The role of microplastics biofilm in accumulation of trace metals in aquatic environments. *World Journal of Microbiology and Biotechnology*. 38(7), 117.
DOI: <https://doi.org/10.1007/s11274-022-03293-6>
- [55] Vaseashta, A., Ivanov, V., Stabnikov, V., et al., 2021. Environmental safety and security investigations of neustonic microplastic aggregates near water-air interphase. *Polish Journal of Environmental Studies*. 30(4), 3457-3469.
DOI: <https://doi.org/10.15244/pjoes/131947>

ARTICLE

Integration of GIS with the Generalized Reciprocal Method (GRM) for Determining Foundation Bearing Capacity: A Case Study in Opolo, Yenagoa Bayelsa State, Nigeria

Ebiegberi Oborie^{*} , Desmond Eteh[®] 

Department of Geology, Niger Delta University, Wilberforce Island, Bayelsa State, 560103, Nigeria

ABSTRACT

This study addresses the pressing need to assess foundation bearing capacity in Opolo, Yenagoa, Bayelsa State, Nigeria. The significance lies in the dearth of comprehensive geotechnical data for construction planning in the region. Past research is limited and this study contributes valuable insights by integrating Geographic Information System (GIS) with the Generalized Reciprocal Method (GRM). To collect data, near-surface seismic refraction surveys were conducted along three designated lines, utilizing ABEM Terraloc Mark 6 equipment, Easy Refract, and ArcGIS 10.4.1 software. This methodology allowed for the determination of key geotechnical parameters essential for soil characterization at potential foundation sites. The results revealed three distinct geoseismic layers. The uppermost layer, within a depth of 0.89 to 1.50 meters, exhibited inadequate compressional and shear wave velocities and low values for oedometric modulus, shear modulus, N-value, ultimate bearing capacity, and allowable bearing capacity. This indicates the presence of unsuitable, soft, and weak alluvial deposits for substantial structural loads. In contrast, the second layer (1.52 to 3.84 m depth) displayed favorable geotechnical parameters, making it suitable for various construction loads. The third layer (15.00 to 26.05 m depth) exhibited varying characteristics. The GIS analysis highlighted the unsuitability of the uppermost layer for construction, while the second and third layers were found to be fairly competent and suitable for shallow footing and foundation design. In summary, this study highlights the importance of geotechnical surveys in Opolo's construction planning. It offers vital information for informed choices, addresses issues in the initial layer, and suggests secure, sustainable construction options.

Keywords: Generalized reciprocal method (GRM); Geographic information system (GIS); Foundation bearing capacity; Seismic refraction

*CORRESPONDING AUTHOR:

Ebiegberi Oborie, Department of Geology, Niger Delta University, Wilberforce Island, Bayelsa State, 560103, Nigeria; Email: ebixl14@gmail.com

ARTICLE INFO

Received: 16 September 2023 | Revised: 23 October 2023 | Accepted: 25 October 2023 | Published Online: 15 November 2023

DOI: <https://doi.org/10.30564/agger.v5i4.5969>

CITATION

Oborie, E., Eteh, D., 2023. Integration of GIS with the Generalized Reciprocal Method (GRM) for Determining Foundation Bearing Capacity: A Case Study in Opolo, Yenagoa Bayelsa State, Nigeria. *Advances in Geological and Geotechnical Engineering Research*. 5(4): 22-40. DOI: <https://doi.org/10.30564/agger.v5i4.5969>

COPYRIGHT

Copyright © 2023 by the author(s). Published by Bilingual Publishing Group. This is an open access article under the Creative Commons Attribution-NonCommercial 4.0 International (CC BY-NC 4.0) License. (<https://creativecommons.org/licenses/by-nc/4.0/>).

1. Introduction

The assessment of foundation bearing capacity holds a pivotal role in the planning and execution of diverse civil engineering projects, encompassing the construction of buildings, bridges, and various infrastructural undertakings^[1,2]. The stability of any structure firmly hinges on the soil's appropriateness for a foundation. The utilization of compressible soil in foundation construction often leads to subsidence issues, thereby underscoring the critical need for an accurate evaluation of soil characteristics to ensure the stability and long-term functionality of these structures^[3,4]. Traditionally, geotechnical investigations have heavily relied on invasive techniques like boreholes and laboratory tests to amass data indispensable for foundation design^[5]. Nevertheless, these approaches can be labor-intensive and cost-prohibitive, and may not furnish a comprehensive comprehension of subsurface conditions^[6,7]. In recent years, the integration of Geographic Information System (GIS) methods with geotechnical engineering has emerged as a potent instrument for site characterization and foundation design^[8]. GIS offers an efficient means of organizing, visualizing, and analyzing geospatial data, thereby empowering engineers to make well-informed decisions grounded in precise and current information^[9]. One notable application of GIS in geotechnical engineering involves the utilization of the Generalized Reciprocal Method (GRM) for the determination of foundation bearing capacity. The Generalized Reciprocal Method (GRM) constitutes a non-invasive geophysical approach widely employed in seismic refraction surveys^[10]. It serves the purpose of establishing the seismic velocity structure of subsurface materials, which is invaluable information in a myriad of geophysical and engineering contexts, including site characterization, geological mapping, and the assessment of bedrock depth or other geological strata. Through the estimation of shear wave velocity, engineers can gauge the soil's stiffness, and by extension, its bearing capacity^[11]. Yenagoa, the capital city of Bayelsa State in Nigeria, has undergone a rapid process of urbanization and

witnessed a substantial upsurge in its population in recent years. Consequently, there exists an escalating demand for the development of infrastructure, encompassing the construction of residential, commercial, and public edifices^[12]. Nevertheless, the region grapples with intricate geological and geotechnical conditions that pose substantial challenges for foundation design. This case study is specifically geared towards the application of GIS techniques and the Generalized Reciprocal Method (GRM) for the assessment of foundation bearing capacity in Yenagoa, Bayelsa State, Nigeria. The study area is marked by a heterogeneous geological composition, encompassing soft clay, silt, and sand deposits, each of which can exert a significant influence on the mechanical properties of the soil and, consequently, its bearing capacity.

Study area

The focus of our investigation is Opolo, situated in Yenagoa, the capital city of the south-south geopolitical region of Nigeria. Opolo is a swiftly developing urban area within this region^[2]. Our study encompasses an area of approximately 170 square kilometers and benefits from a well-developed road network that links various parts of Yenagoa city and its environs. This particular zone can be pinpointed between longitudes 006°14'30" and 006°21'30" east of the prime meridian and latitudes 04°55'0" and 05°0'30" north of the equator, positioned in the coastal region of the Niger Delta (see **Figure 1**).

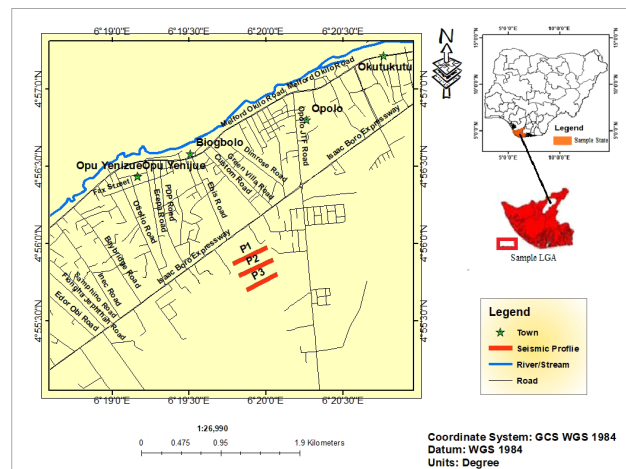


Figure 1. Map of the study area.

2. Materials and methods

2.1 Materials

ABEM Terraloc Mark 6 A sledgehammer and metal plate; a group of 12 vertical geophones at 14 Hz; seismic cable reels; Wire reel, 12-volt DC battery, log book, Global Positioning System device (GPS), measuring tape.

2.2 Methods

Seismic refraction

Seismic refraction is a geophysical method that entails the measurement of the time it takes for seismic waves to propagate through different underground layers of the Earth's crust^[13]. This technique is of utmost importance in aiding engineers and geologists in acquiring a deeper understanding of the geological features and characteristics beneath the Earth's surface. The data gathered from seismic refraction surveys holds significant value for a diverse set of purposes, including but not limited to foundation design, site assessment, and geotechnical engineering^[2,14].

Generalized reciprocal method (GRM)

The Generalized Reciprocal Method (GRM) is a mathematical approach employed in seismic refraction surveys for the determination of subsurface velocity profiles and the depths of different geological layers^[15]. Seismic refraction surveys are commonly employed to investigate subsurface geology, aiming to ascertain the characteristics and depths of various geological strata, like bedrock and sedimentary deposits^[10]. The GRM serves as an extension of the conventional seismic refraction method, proving particularly valuable when dealing with intricate subsurface structures characterized by irregular layer boundaries or variations in lateral velocity^[16]. It enables geophysicists to enhance the precision of their interpretations of subsurface conditions by accounting for these complexities. Nevertheless, it necessitates meticulous data collection and analysis, and the outcomes are typically presented in the form of velocity-depth models, offering valuable insights

into the geological attributes at a specific location.

Seismic data acquisition

Seismic refraction was conducted in an undeveloped area, involving three profiles surveyed using the 12-channel ABEM Terraloc Mark 6. The equipment included the seismograph, geophones, a 15 kg sledgehammer, measuring tapes, and more. Profiles spanned 75 m, with geophones placed 5 m apart to capture accurate data and depth details. The study area's isolation from noise sources like traffic and human activity enhanced data quality. Seismic waves were generated using a sledgehammer and detected by geophones, with both P-waves and S-waves recorded using 14-Hz geophones. Five stacks were produced per shot location, capturing critically refracted waves. The refracted energy was converted into digital signals and stored in memory. The research encompassed three profile lines, each 75 m long, marked by GPS for accurate geophone and shot position data using the generalized reciprocal method (GRM). The method allowed for imaging subsurface boundaries based on seismic wave behavior.

Data processing

The utilization of Easy Refract and ArcGIS software version 10.5 for handling the data. The result of this data manipulation unveiled valuable subsurface characteristics, which served as vital inputs for geotechnical and engineering evaluations in various projects (as shown in **Figures 2a to 2i**). Additionally, a spatial distribution map was generated to visually represent the geographical spread of the data. This comprehensive analysis greatly assists decision-making in the fields of geotechnical and engineering endeavors.

The GRM process can be outlined as follows:

- 1) Manual identification of initial arrivals, either through direct entry or copy-paste commands. **Figures 2a-2e** display the selected first arrival times from collected wave records.

- 2) Custom definition of time travel curves, achieved by drawing lines through the selected first arrival times or by utilizing software to fit a curve to the data. The outcome of this step is demonstrated in

Figure 2f.

3) Automated detection of slope change points on the time travel curves, performed with the assistance of software to identify the points where the slope changes.

Figure 2g illustrates the results of this stage.

4) Selection of the optimal XY value on the velocity function diagram. The velocity function is a plot of refractor velocity against XY distance. The optimal XY value is where the velocity function is most stable and exhibits the fewest changes, as shown in **Figure 2h**.

5) Selection of the optimal XY value on the time-depth function diagram. The time-depth function displays the depth of the refractor against XY distance. The optimal XY value is the one where the time-depth function is smoothest and provides the most detail, as depicted in **Figure 2i**.

After determining the optimal XY value, you can calculate the depth to the refractor at any point along the survey line using the following equation:

$$\text{Depth} = (XY/2) * (1/\text{Velocity}) \quad (1)$$

where:

- Depth represents the depth to the refractor in meters.
- XY is the preferred XY distance in meters.
- Velocity is the refractor velocity in meters per second.

The GRM is a robust and versatile seismic refraction technique used to obtain precise and detailed information about subsurface conditions. It finds application in various fields, including engineering and geotechnical investigations, groundwater exploration, mineral exploration, and environmental assessments.

Table 1 holds a pivotal position in understanding the properties of P-waves, S-waves, and a variety of geotechnical parameters. It not only furnishes precise definitions but also encompasses the mathematical expressions associated with primary, shear wave, and geotechnical properties.

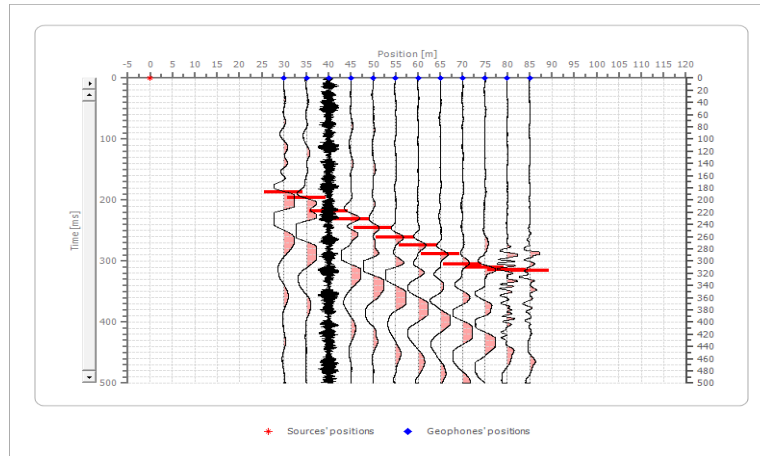


Figure 2a. A sample of a picked first wave arrival time from the collected wave records at 0 m.

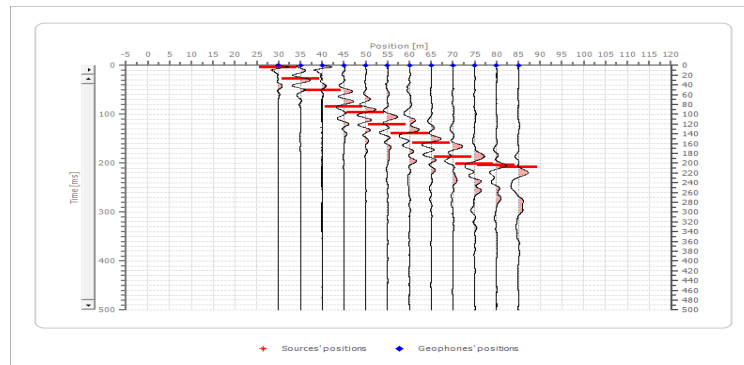


Figure 2b. A sample of a picked first wave arrival time from the collected wave records at 30 m.

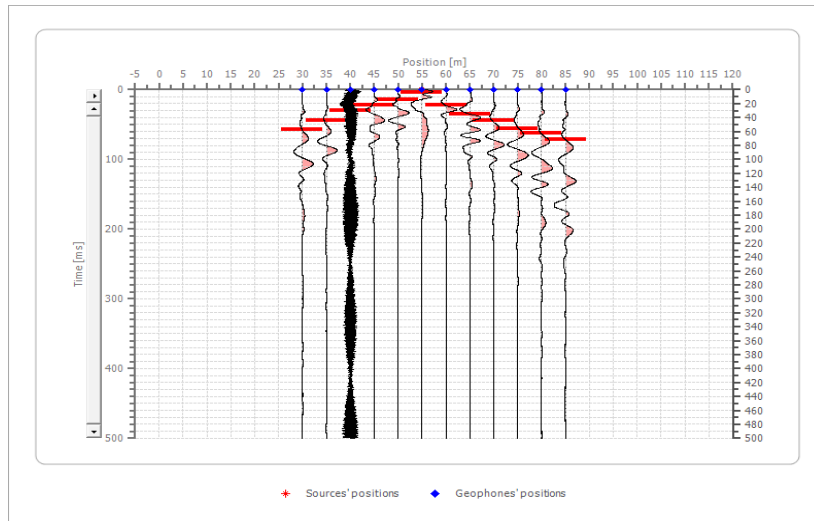


Figure 2c. A sample of a picked first wave arrival time from the collected wave records 55 m.

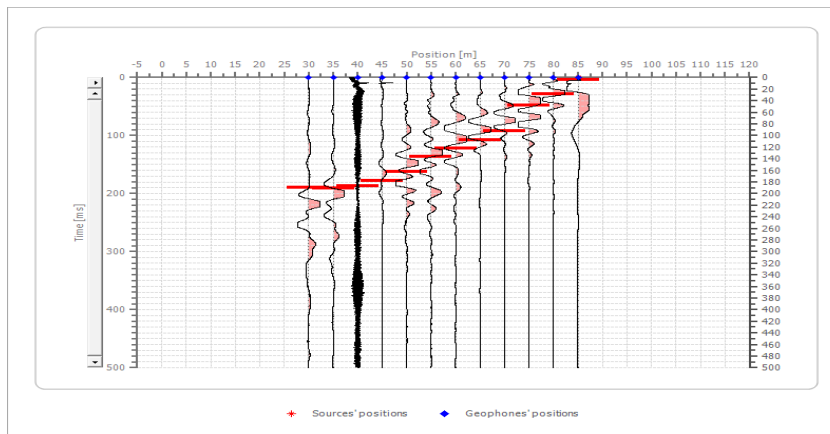


Figure 2d. A sample of a picked first wave arrival time from the collected wave records at 85 m.

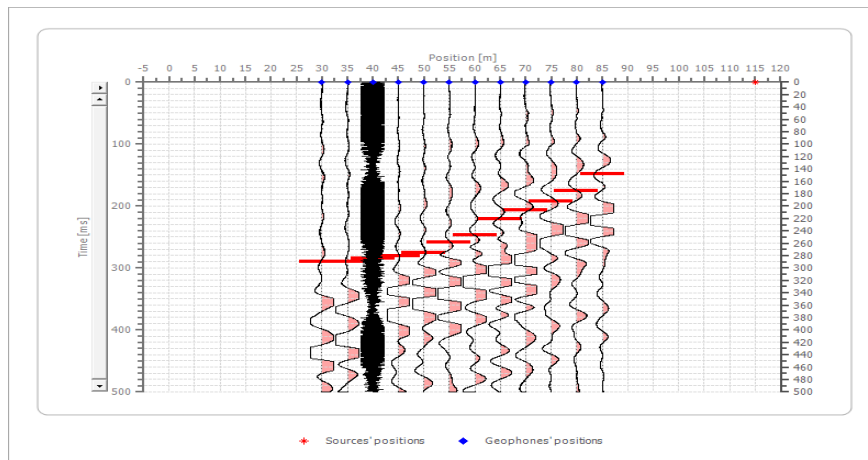


Figure 2e. A sample of a picked first wave arrival time from the collected wave records at 115 m.

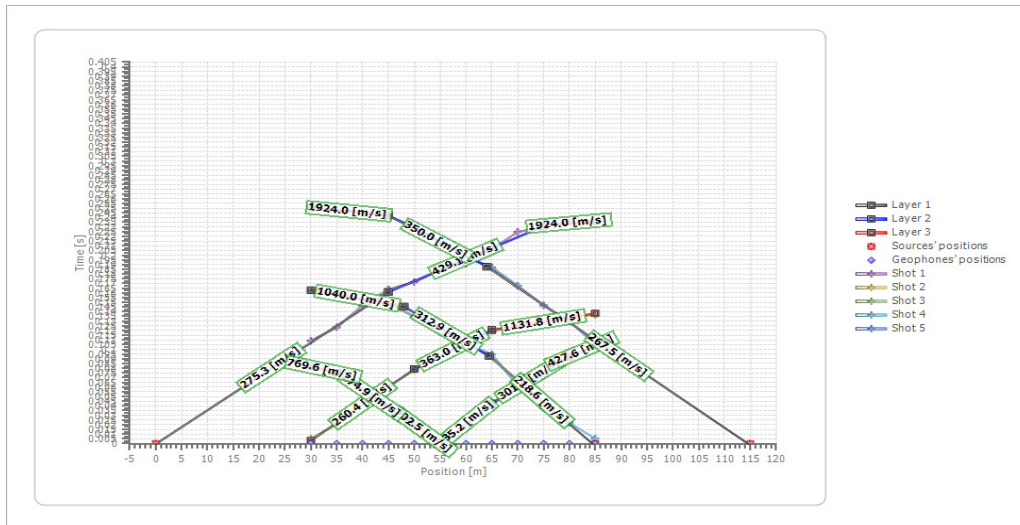


Figure 2f. Time travel curves.

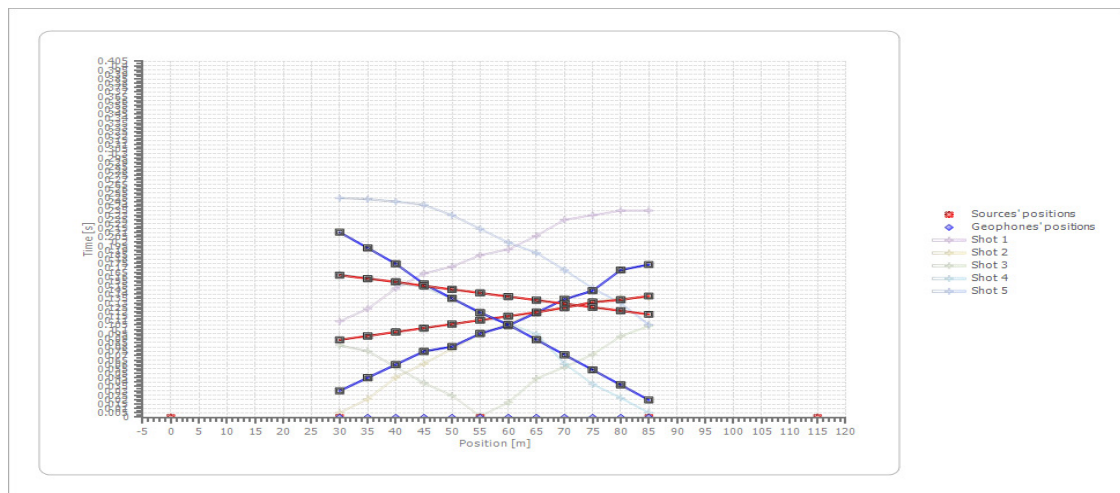


Figure 2g. Slope change points.

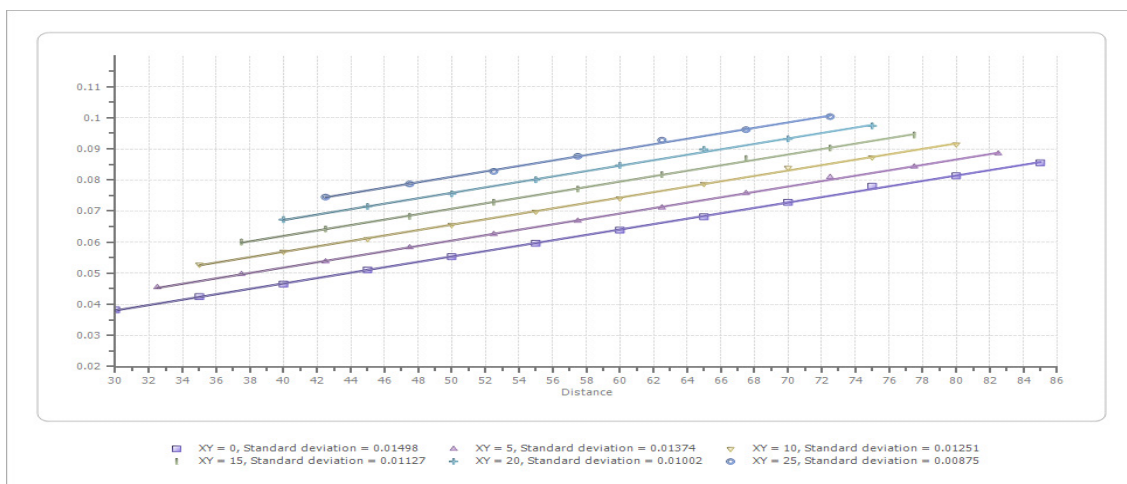


Figure 2h. Velocity function.

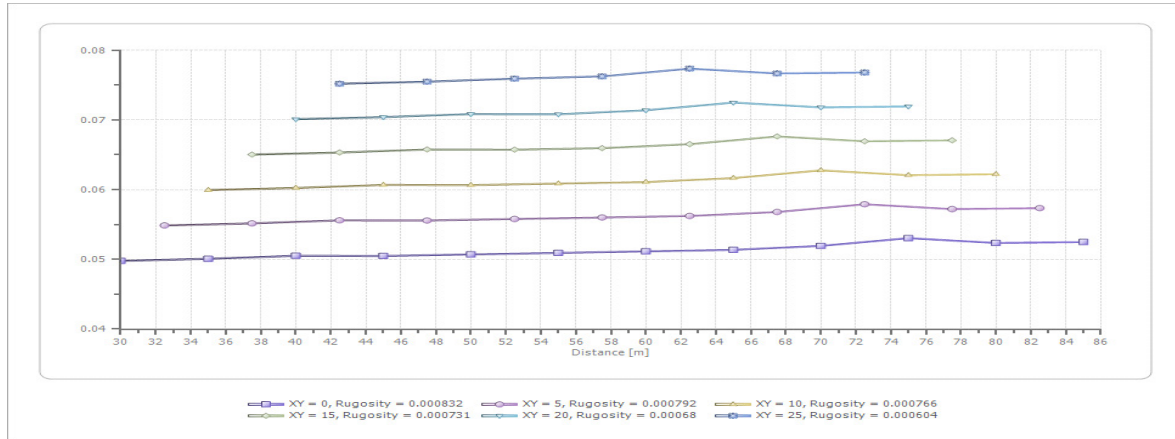


Figure 2i. Time-depth function.

Spatial analysis using kriging interpolation

GIS provides spatial analysis, visualization, and data management, helping engineers and geologists assess site suitability, predict geological risks, and optimize infrastructure design. This synergy improves project efficiency, reduces costs, and minimizes environmental impacts, ensuring safer and more sustainable outcomes. Therefore, kriging claims that the distance or direction between the sampling points can be used to explain the surface variation. This involves exploratory statistical data analysis, simulation of variograms, surface creation and discovery of layers of variance (possibly). If you know that the data involves a spatially-based distance or directional bias, Kriging is more suitable. Kriging interpolation is mostly used in geology, geophysics and soil science. The GIS application was used to analyze all data layers through the process called “Overlay”. The spatial strategy consists of using a thematic scheme to apply Index Overlay to overlay one layer to another, thereby creating a new layer. In this analysis, different value scores were assigned to the map classes produced on each added map, and different weights were given to the maps^[17]. In the selection site suitability for foundation in the study area, this approach has identified and resolved multi-criteria problems. Kriging believes that a spatial comparison can be used to describe the surface variability by the distance or direction between the

sampling points. Kriging is the weights of the relevant calculated values to achieve a forecast for an unknown position.

The formula of the kriging interpolators is the weighted sum of the data:

$$\hat{Z}(s_0) = \sum_{i=1}^N \lambda_i Z(s_i) \quad (2)$$

where:

$Z(s_i)$ = measured value at the i th location

λ_i = an unknown weight for the measured value at the i th location

s_0 = Prediction location

N = Number of measured values

Geotechnical parameters

The provided **Table 2** presents a range of geotechnical parameters and their corresponding soil descriptions. These parameters have been sourced from various authors and studies^[31-36].

Table 3 shows the conventional p-wave velocities associated with various soil classifications as described by Nwankwoala and Amadi in their^[37]. This table includes statistics on typical p-wave velocities for various soil types, acting as a resource for researchers and experts in the field. As stated by Nwankwoala and Amadi^[37], it incorporates crucial information regarding the p-wave velocities of diverse soil kinds, providing a thorough knowledge of soil properties and assisting in geotechnical and seismic studies.

Table 1. Definition of primary, shear wave and geotechnical parameters.

Parameter	Definition	Formula	Citations
Primary wave velocity (P-wave) (m/s)	Propagate through the medium faster than other forms of waves and P waves often called compression waves or longitudinal waves	$V_p = \sqrt{\frac{k + 4/3 \mu}{\rho}}$ (K) Bulk modulus, (μ) Shear modulus, and (ρ) density.	[18,19,20]
Secondary wave velocity (S-wave) (m/s)	The shear or transverse wave which propagates more slowly through a medium than the primary wave.	$V_s = \sqrt{\mu/\rho}$ $V_p \approx 1.7V_s$	[21,18,19,20]
Bulk density (ρ) (kg/m ³)	The mass of soil per unit volume	$P = \gamma/g$ g is the acceleration due to gravity = 9.8 m/s ² .	[22,23]
Poisson's ratio (σ)	The ratio of lateral strain to axial strain in a material	Poisson's (σ) = $\frac{1}{2} \left[1 - \frac{1}{(V_p/V_s)^2 - 1} \right]$	[21,19]
Young's modulus (E) (Mpa)	The measure of stiffness of a material	$E = 2\mu(1 + \sigma)$	[24]
Oedometeric modulus (Ec) (Mpa)	The measure of stiffness of soil under one-dimensional compression	$E_c = \frac{(1 - \sigma)E}{(1 + \sigma)(1 - 2\sigma)}$	[25]
Bulk modulus (K) (Mpa)	The measure of a material's resistance to uniform compression	$K = \frac{E}{3(1 - 2\sigma)}$	[26]
Shear modulus (μ) (Mpa)	The measure of a material's resistance to shear deformation	$\mu = \frac{\sigma E}{(1 + \sigma)(1 - 2\sigma)}$	[27]
N-value (N)	A standardized measure of soil consistency and density	$N = \left(\frac{V_s}{76.55} \right)^{2.24719}$	[28,29]
Ultimate bearing capacity (Qult) (Kpa)	The maximum load a soil can withstand before failure	$Q_{ult} = \log(30N)$	[30]
Allowable bearing capacity (Qa) (Kpa)	The maximum load a soil can bear without exceeding the allowable settlement or deformation limits	$Q_a = Q_{ult}/F$ The factor of safety equals 2 and 3 for the cohesionless and cohesive soils, respectively. Also, (Qa) can be estimated by using shear wave velocity $\log Q_a = 2.932 \log V_s - 4.553$ for soft soil	[31]

Table 2. Serves as a reference for classifying soils based on specific engineering and geotechnical characteristics.

Soil/Rock description parameters	Weak		Fair		Good
	Incompetent		Fairly competent		Competent
	Very soft	Soft	Fairly compacted	Moderately compacted	Compacted
Concentration index (Ci)	3.5-4.0	4.0-4.5	4.5-5.0	5.0-5.5	5.5-6.0
Material index (Mi)	< -0.6	-0.6-0.2	-0.2-0.2	0.2-0.6	0.6-1.0
Stress ratio (Si)	0.7-0.61	0.61-0.52	0.52-0.43	0.43-0.34	0.34-0.25
Bearing capacity (Qult) (Kpa)	0-50	50-100	100-550	550-5000	5000-8000
Reaction modulus (Rm) (Mpa)	0-10	10-30	30-1000	1000-4800	4800-6000
Poisson's ratio	0.4-0.49		0.35-0.27	0.25-0.16	0.12-0.03

Table 3. Standard p-wave velocities for different soil types.

Rock/soil types	P-wave velocity (m/s)
Top soil	100-250
Sandy clay	300-500
Sand with gravel(dry)	500-700
Sand with gravel (wet)	700-1150
Coarse sand (wet)	1150-2000
Clay	1500-4200
Sandstone	1400-4300
Loose sand	1500-2000

Source: [37].

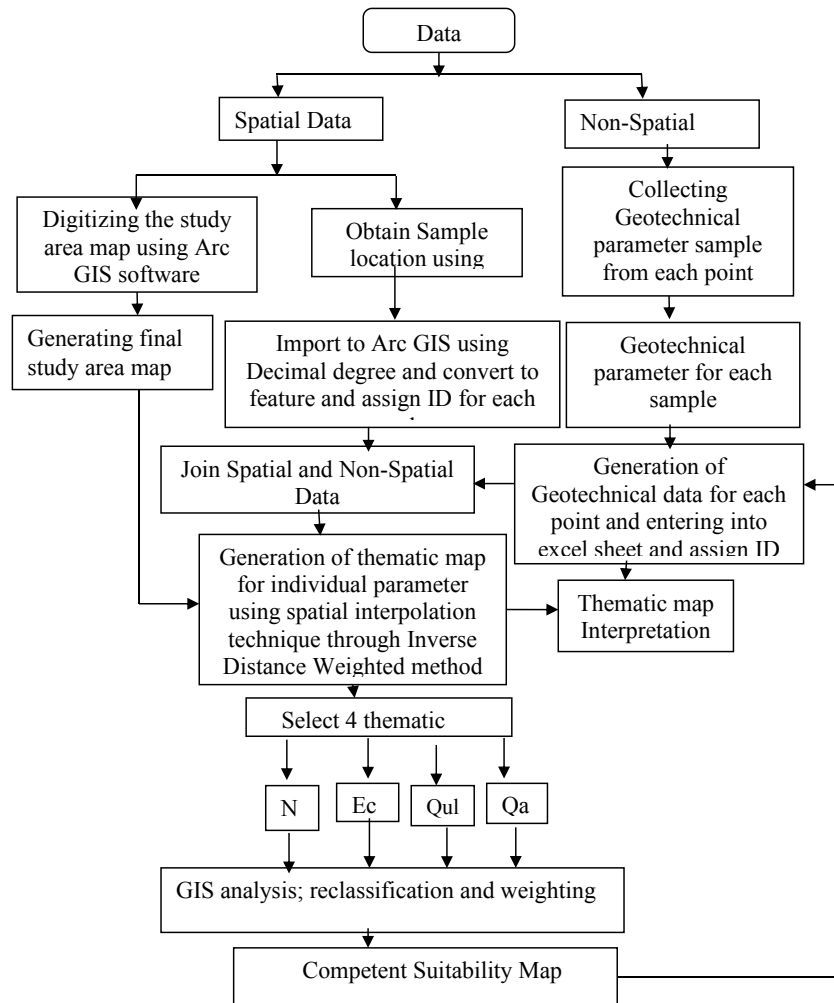


Figure 2j. Flow diagram.

3. Results and discussion

3.1 Results

Table 4 provides essential data related to seismic velocities in three different layers. This data is critical for assessing the foundation bearing capacity, which is crucial for construction and infrastructure development.

Seismic velocities

Seismic velocities are fundamental in understanding the subsurface geology and, in turn, the bearing capacity of the soil. The table provides seismic velocity data for the following parameters in three different layers (Layer I, Layer II, and Layer III):

- **Thickness (m):** This parameter represents the thickness of each layer. Layer I has a minimum thickness of 0.89 m, a maximum of 1.48 m, and a mean thickness of 1.162 m. Layer II and Layer III have similar statistics.

- **Primary Velocity (Vp) (m/s):** Primary velocity values vary across the layers. Layer I has a minimum of 236.2 m/s, a maximum of 264.4 m/s, and a mean value of 248.9 m/s. Layer II and Layer III exhibit similar trends.

- **Shear Velocity (Vs) (m/s):** Similar to primary velocity, shear velocity shows variation across the layers. Layer I has a minimum of 138.9 m/s, a maximum of 155.5 m/s, and a mean value of 146.38 m/s. Layer II and Layer III follow a similar pattern.

Foundation bearing capacity

Table 4 also provides data on the foundation bearing capacity of each layer, as determined by the following parameters:

- **Unit Weight of the Soil (Y) (kgN/m³):** Unit weight, which represents the density of the soil, shows variation among the layers. Layer I has a minimum of 16.47 kgN/m³, a maximum of 16.53 kgN/m³, and a mean value of 16.498 kgN/m³. Layer II and Layer III display similar trends.

- **Bulk Density (ρ) (kg/m³):** Bulk density, which is another measure of soil density, exhibits variation. Layer I has a minimum of 1.681 kg/m³, a maximum of 1.687 kg/m³, and a mean value of 1.6836 kg/m³. Layer II and Layer III follow similar patterns.

- **Poisson's Ratio (σ):** Poisson's ratio remains

constant across all layers, indicating that this parameter does not vary with depth.

- **Young's Modulus (E) (Mpa):** Young's modulus shows variation among the layers, with Layer I having a minimum of 0.08 Mpa, a maximum of 0.101 Mpa, and a mean value of 0.0894 Mpa. Layer II and Layer III exhibit similar trends.

- **Oedometric Modulus (Ec) (Mpa):** Similar to Young's modulus, Oedometric modulus varies across the layers. Layer I has a minimum of 0.094 Mpa, a maximum of 0.118 Mpa, and a mean value of 0.1048 Mpa. Layer II and Layer III follow a similar pattern.

- **Bulk Modulus (K) (Mpa):** Bulk modulus exhibits variation among the layers, with Layer I having a minimum of 0.051 Mpa, a maximum of 0.064 Mpa, and a mean value of 0.0568 Mpa. Layer II and Layer III display similar trends.

- **Shear Modulus (μ) (Mpa):** Shear modulus varies among the layers, with Layer I having a minimum of 0.033 Mpa, a maximum of 0.041 Mpa, and a mean value of 0.0364 Mpa. Layer II and Layer III exhibit similar trends.

- **Concentration Index (Ci):** Concentration index remains constant across all layers, indicating a consistent level of soil concentration.

- **Stress Ratio (Si):** Stress ratio is also constant across all layers, suggesting a uniform stress level within the site.

- **Material Index (Mi):** Material index remains constant, indicating uniform material properties across the layers.

- **Reaction Modulus (Rm) (Mpa):** Reaction modulus shows variation across the layers, with Layer I having a minimum of 4.6112 Mpa, a maximum of 6.3286 Mpa, and a mean value of 5.37782 Mpa. Layer II and Layer III exhibit similar trends.

- **Ultimate Bearing Capacity (Qult) (Kpa):** Ultimate bearing capacity varies across the layers, with Layer I having a minimum of 114.5 Kpa, a maximum of 147.6 Kpa, and a mean value of 129.31 Kpa.

- **Allowable Bearing Capacity (Qa) (Kpa):** Allowable bearing capacity also varies among the layers. Layer I has a minimum of 57.249 Kpa, a maximum of 73.802 Kpa, and a mean value of 64.6552 Kpa.

Table 4. Seismic velocities of the investigated site as obtained from the refraction profiles and the corresponding calculated from **Table 1** for Minimum, maximum, mean values in Opolo.

Parameters	Layer I Opolo			Layer II Opolo			Layer III Opolo		
	Min	max	Mean	Min	max	Mean	min	max	mean
Thickness (m)	0.89	1.48	1.162	0.63	2.42	1.558	12.62	21	16.032
Primary velocity (Vp) (m/s)	236.2	264.4	248.9	421	471.6	449.68	1117	1153	1138.2
Shear velocity (Vp) (m)	138.9	155.5	146.38	247.6	277.4	264.5	657.1	678	669.46
Unit weight of the Soil (Y) (kgN/m ³)	16.47	16.53	16.498	16.84	16.94	16.898	19.23	19.31	19.276
Bulk density (p) (kg/m ³)	1.681	1.687	1.6836	1.719	1.729	1.7246	1.963	1.97	1.9672
Possion's ratio (σ)	0.235	0.235	0.235	0.235	0.235	0.235	0.235	0.235	0.235
Young's modulus (E) (Mpa)	0.08	0.101	0.0894	0.261	0.329	0.2994	2.094	2.238	2.179
Oedometeric modulus (Ec) (Mpa)	0.094	0.118	0.1048	0.305	0.385	0.3502	2.449	2.617	2.5482
Bulk modulus (K) (Mpa)	0.051	0.064	0.0568	0.164	0.207	0.1884	1.319	1.409	1.3722
Shear modulus (μ) (Mpa)	0.033	0.041	0.0364	0.105	0.133	0.1208	0.848	0.906	0.8822
Concentration index (Ci)	5.248	5.248	5.248	5.248	5.248	5.248	5.248	5.248	5.248
Stress ratio (Si)	0.308	0.308	0.308	0.308	0.308	0.308	0.308	0.308	0.308
Material index (Mi)	0.058	0.058	0.058	0.058	0.058	0.058	0.058	0.058	0.058
Reaction modulus (Rm) (Mpa)	4.6112	6.3286	5.37782	23.284	31.998	28.1982	385.22	391.06	388.424
N-value (N)	3.8163	4.9198	4.31016	13.99	18.054	16.2856	125.36	134.5	130.762
Ultimate bearing capacity (Qult) (Kpa)	114.5	147.6	129.31	460.15	541.63	504.76	3761	4034.6	3922.74
Allowable bearing capacity (Qa) (Kpa)	57.249	73.802	64.6552	230.08	270.81	252.38	1880.5	2017.3	1961.38

3.2 Discussion

Primary wave velocity

Tables 4 and 5 at the specified location present profiles consisting of three distinct geoseismic layers. Within the first layer, P-wave velocities in Opolo are relatively low, ranging from 236.2 m/s to 264.4 m/s. This initial layer extends in depth from 0.89 m to 1.48 m in Opolo. These reduced velocities likely arise from the loose and soft nature of the soil, indicating lower elastic moduli and densities when compared to the values provided in **Table 3**^[37]. At the Opolo site, the second layer exhibits velocities ranging from 421.00 m/s to 471.6 m/s, accompanied by layer thickness variations spanning from 0.63 m to 2.42 m. This suggests the presence of sandy clay in this layer, deviating from the standard P-wave velocities listed in **Table 3**. Moving on to the third geoseismic layer, observed exclusively at the Opolo sites, it displays higher velocities compared to the layers preceding it. In Opolo, velocities within this layer range from 1117 m/s to 1153 m/s, with depths ranging from 12 m to 21 m. This pattern suggests the presence of wet to coarse sand in this third layer. Spatial

distribution maps visually depict a transition in P-wave velocities, as indicated by blue areas in the first layer, shifting to increasing velocities represented by green, yellow, and red in the subsequent layers. **Figure 3** provides a graphical representation of this observed trend.

Shear wave velocity

The shear seismic wave velocity measurements obtained from the Opolo region exhibit distinct ranges for the first, second, and third geoseismic layers. For the initial layer, the velocities span 138.9 m/s to 155.5 m/s Opolo in **Tables 4 and 5**, indicating loose, unconsolidated sediments comprising surface soil and alluvial deposits. Conversely, the second layer displays higher shear wave velocities of 247.60 m/s to 277.40 m/s, suggesting more solid earth materials. The third layer, which marks the study's probing depth limit, showcases shear wave velocities ranging from 657.10 m/s to 678.00 m/s for Opolo. Spatially, Opolo's upper layer exhibits gradually increasing shear wave velocities from deep blue to white, while the second layer demonstrates a progressive velocity rise illustrated by colors transitioning from purple to red, as depicted in **Figure 4** below.

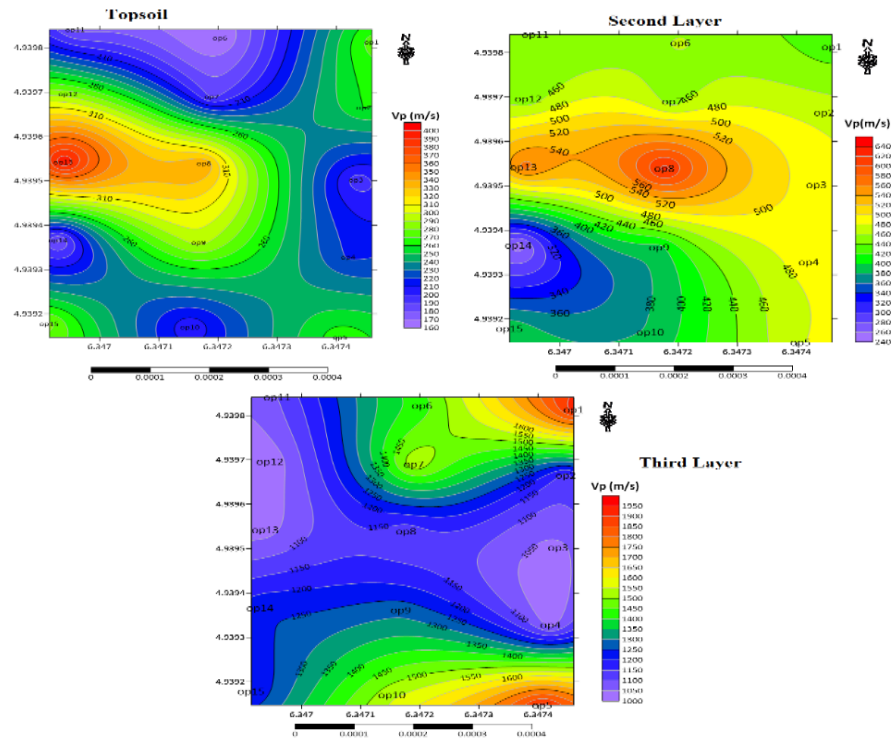


Figure 3. Distribution map of primary wave velocity in Opolo.

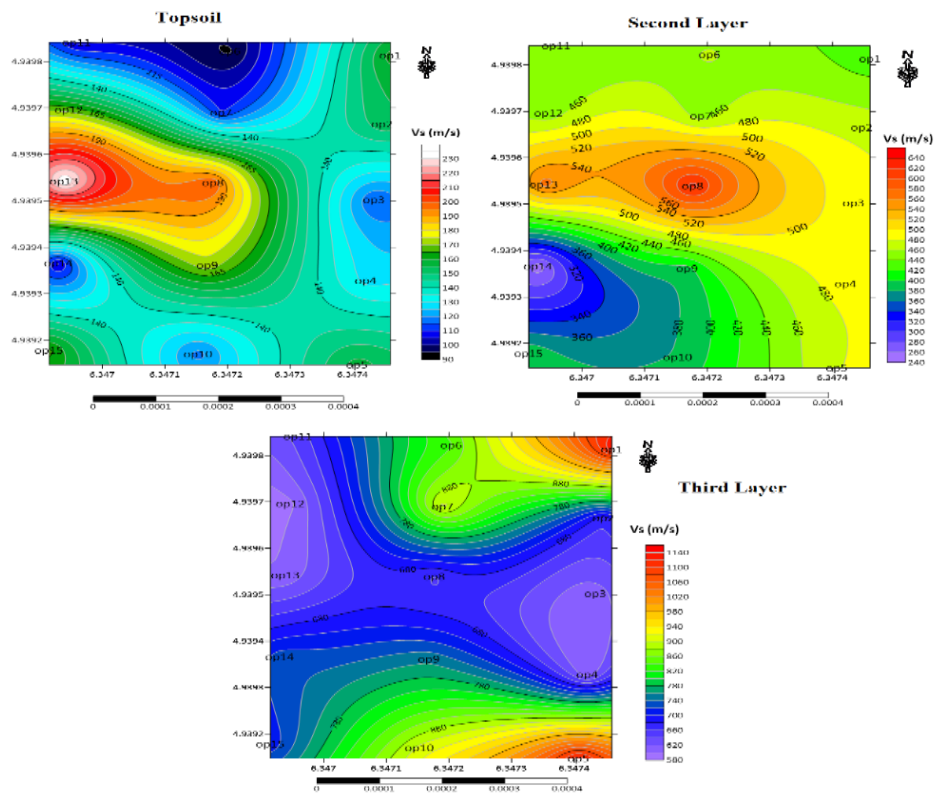


Figure 4. Distribution map of shear wave velocity in Opolo.

Table 5. Seismic velocities of the investigated site as obtained from five receiver geophones each in refraction survey and the corresponding calculated elastic moduli in Opolo.

Layer I Opolo								Layer II Opolo						Layer III Opolo					
Long	lat	Vp	Vs	Ec	N	Qult	Qa	Vp	Vs	Ec	N	Qult	Qa	Vp	Vs	Ec	N	Qult	Qa
6.34746	4.93981	275.3	161.941	0.1275	5.386	161.585	80.7923	429.1	252.4118	0.1275	5.386	161.585	80.7923	1924	1131.7647	7.2923	425.39	12761.4	6380.72
6.34745	4.93967	260.4	153.177	0.114	4.7529	142.594	71.2968	471.8	277.5294	0.114	4.7529	142.594	71.2968	1131.8	665.7647	2.523	129.109	3873.47	1936.73
6.34743	4.9395	194.5	114.647	0.0639	2.4786	74.3533	37.1766	489.4	287.8824	0.0639	2.4786	74.3533	37.1766	1040	611.7647	2.1306	125.916	4142.86	2071.43
6.34742	4.93933	218.6	128.588	0.0804	3.2077	96.2277	48.1138	488.7	287.4706	0.0804	3.2077	96.2277	48.1138	1029.3	605.4706	2.0794	106.758	5130.98	2565.49
6.34741	4.93915	267.5	157.353	0.1202	5.0491	151.461	75.7304	479	281.7647	0.1202	5.0491	151.461	75.7304	1924	1131.7647	7.291	425.39	12761.4	6380.72
6.3472	4.93982	160.3	94.2941	0.0433	1.5976	47.9292	23.9646	462.1	271.8235	0.0433	1.5976	47.9292	23.9646	1425.2	838.3529	4.001	214.988	6449.11	3224.56
6.34719	4.93969	186.99	109.994	0.0588	2.2582	67.733	33.8665	449.9	264.6471	0.0588	2.2582	67.733	33.8665	1539.2	905.4118	4.6663	257.639	7728.59	3864.29
6.34718	4.93954	339.06	199.447	0.1939	8.6014	258.048	129.024	628.28	369.5765	0.1939	8.6014	258.048	129.024	1119.26	658.3882	2.4588	125.916	3777.46	1888.73
6.34717	4.93936	293.9	172.882	0.1454	6.2383	187.37	93.685	392.8	231.0588	0.1454	6.2383	187.37	93.685	1282.7	754.5294	3.2411	171.042	5130.98	2565.49
6.34715	4.93917	200.6	118	0.0676	5.6444	79.3232	39.6616	382.92	225.2471	0.0676	5.6444	79.3232	39.6616	1539.2	905.4118	4.6663	257.639	7728.59	3864.29
6.34696	4.93984	176.4	103.765	0.0524	1.98	59.4292	29.7146	444.2	261.2941	0.0524	1.98	59.4292	29.7146	1099.5	646.7647	2.3814	120.976	3629.11	1814.55
6.34695	4.9397	285.5	167.941	0.137	5.8448	175.348	87.6738	447.3	263.1176	0.137	5.8448	175.348	87.6738	1012.7	595.7059	2.02	100.564	3017.17	1508.59
6.34694	4.93954	400.55	235.618	0.2706	12.5089	375.319	187.659	568.2	334.2353	0.2706	12.5089	375.319	187.659	1029.3	605.4706	2.0794	104.306	3128.96	1564.48
6.34693	4.93937	176.8	104	0.0526	1.991	59.731	29.8655	249.3	146.6471	0.0526	1.991	59.731	29.8655	1241.3	730.1765	3.0353	171.042	4766.5	2383.25
6.34692	4.93918	282.9	166.412	0.1345	5.7259	171.791	85.8954	396	232.9412	0.1345	5.7259	171.791	85.8954	1202.5	707.3529	2.848	257.639	4438.13	2219.06

Competent site suitability map for foundation

The spatial distribution maps depicted in **Figures 5, 6, and 7** illustrate the variations in geotechnical parameters, namely oedometric modulus (E_c), N-value, ultimate bearing capacity (Q_{ult}), and allowable bearing capacity (Q_a) in **Tables 3, 4 and 5**, within the distinct Opolo geological layers 1, 2, and 3. These alterations are visually represented using the Kriging method, a geostatistical technique employed for comprehensive analysis. **Figure 8**, on the other hand, specifically presents the competent site suitability map for foundation sites, encompassing topsoil (layer 1), as well as layers 2 and 3, and employs the index overlay method. This method involves assigning score values based on multiple criteria as per established geotechnical standards (as detailed in **Tables 1 and 2**). These criteria consider factors such as oedometric modulus (E_c), N-value, ultimate bearing capacity (Q_{ult}), and allowable bearing capacity (Q_a), which are also illustrated in **Figures 5, 6, and 7**. The resultant maps serve the purpose of identifying areas competent for foundation construction. Within **Figure 8**, the regions shaded in red signify zones unsuitable for foundation construction due to their geological incompetence. Yellow areas represent reasonably competent regions, while light blue areas indicate a higher level of competence, and blue areas are deemed highly competent for foundation purposes. This assessment is applicable within a depth range of 0.89 meters to 1.48 meters. Consequently, the red areas are deemed unsuitable for foundation construction, primarily due to their geological characteristics. Moving on to the second geological layer, the red regions now exhibit a level of competence, while yellow areas indicate competence, and blue areas signify a high level of competence for shallow foundation applications, typically at depths ranging from 1.52 meters to 3.84 meters. This analysis allows for informed decision-making regarding the suitability of the geological layers for different types of foundation construction. Furthermore, the third geological layer, as displayed in **Figure 8**, highlights areas of competence (yellow) and high competence

(blue) suitable for deep foundation applications, generally exceeding a depth of 3 meters. This geotechnical evaluation serves as a valuable resource for engineers and geologists to identify areas within the Opolo geological layers that are well-suited for the specific requirements of shallow and deep foundation construction projects.

Implications

The implications of this research are significant for construction and geotechnical engineering in Opolo, Yenagoa, Bayelsa State, Nigeria. The utilization of near-surface seismic refraction surveys, combined with the Generalized Reciprocal Method (GRM), has provided valuable insights into the geotechnical characteristics of the study area. Firstly, the identification of three distinct geoseismic layers underscores the importance of a detailed geotechnical investigation before construction projects. It allows for a comprehensive understanding of the subsurface conditions, which is crucial for designing foundations that can safely support the intended structural loads. The findings regarding the first layer's unsuitability for supporting substantial structural loads have immediate practical implications. Builders and developers in Opolo need to be aware of this soft and weak alluvial deposit layer, which could pose challenges to construction projects. This knowledge can help avoid costly construction failures and ensure the safety and stability of structures. Conversely, the positive geotechnical parameters of the second layer make it a promising option for construction. The higher ultimate and allowable bearing capacities suggest that this layer can support a wide range of construction loads. This information is valuable for architects and engineers when planning and designing buildings and infrastructure in Opolo. Furthermore, the geographic information system (GIS) analysis provides a spatial perspective on the suitability of different areas within Opolo. It highlights variations in soil competence, which can guide site selection for specific projects and inform decisions about foundation types and construction techniques.

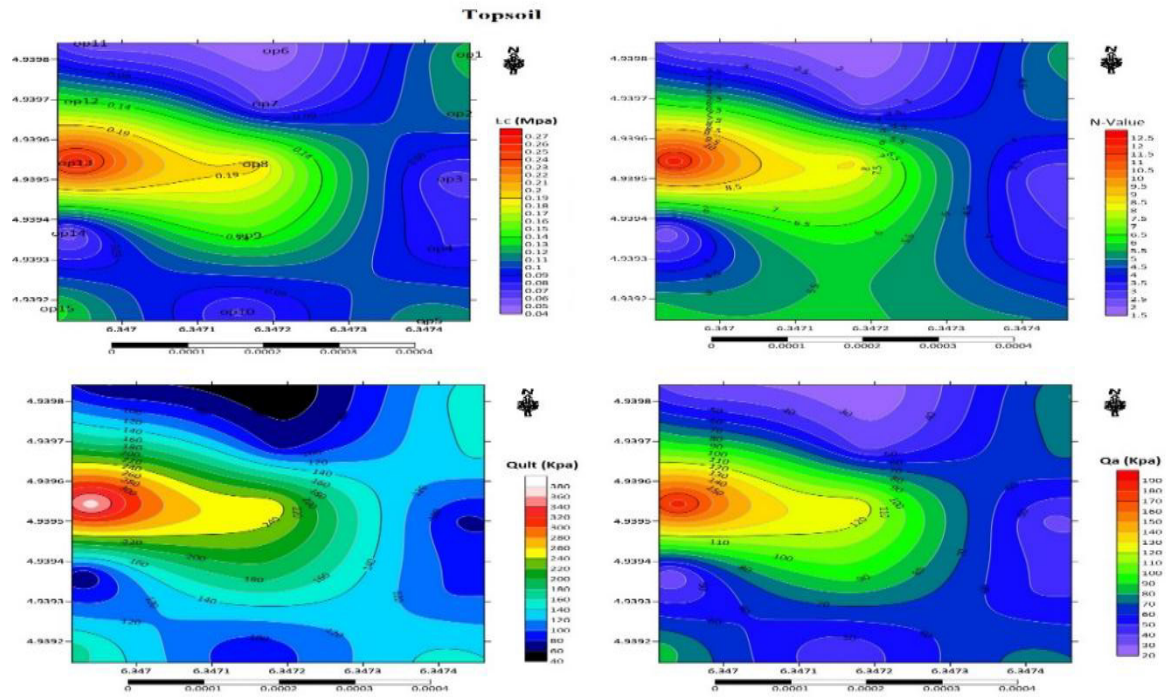


Figure 5. Distribution map of oedometric modulus (E_c), N-value, ultimate bearing capacity (Q_{ult}) and allowable bearing capacity (Q_a) for topsoil Opolo.

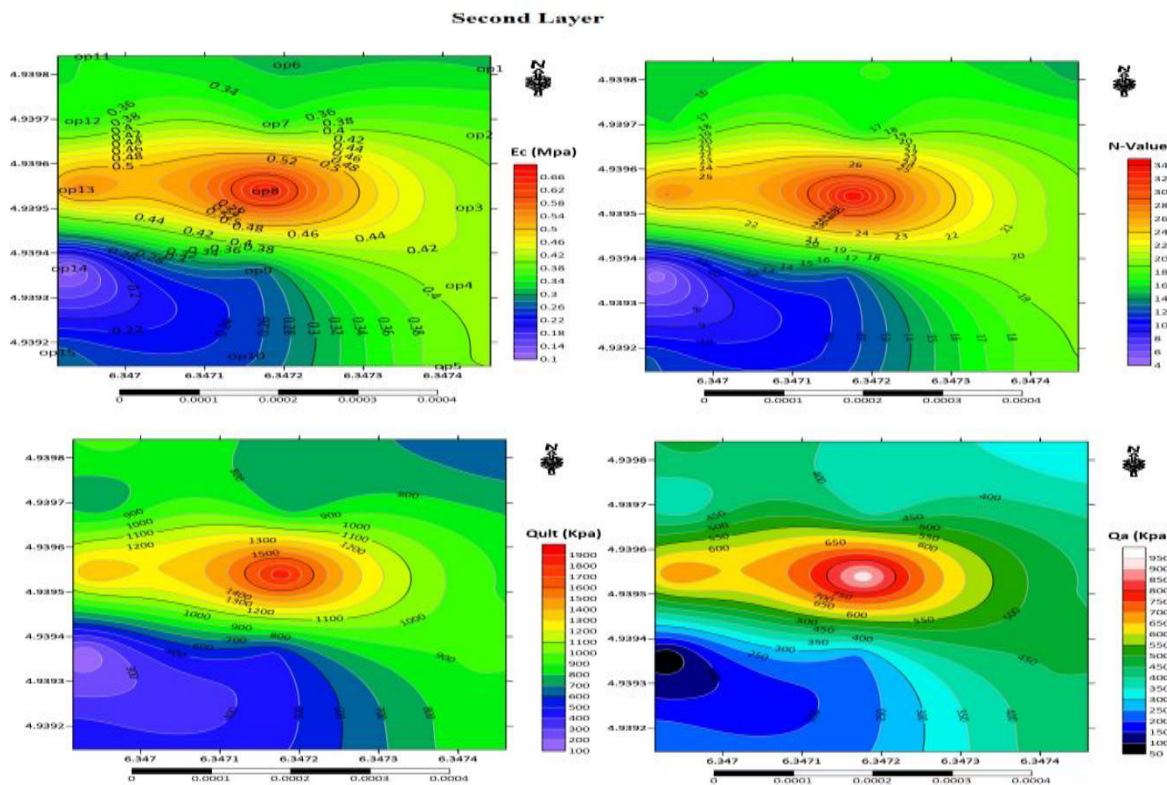


Figure 6. Distribution map of oedometric modulus (E_c), N-value, ultimate bearing capacity (Q_{ult}) and allowable bearing capacity (Q_a) for second layer Opolo.

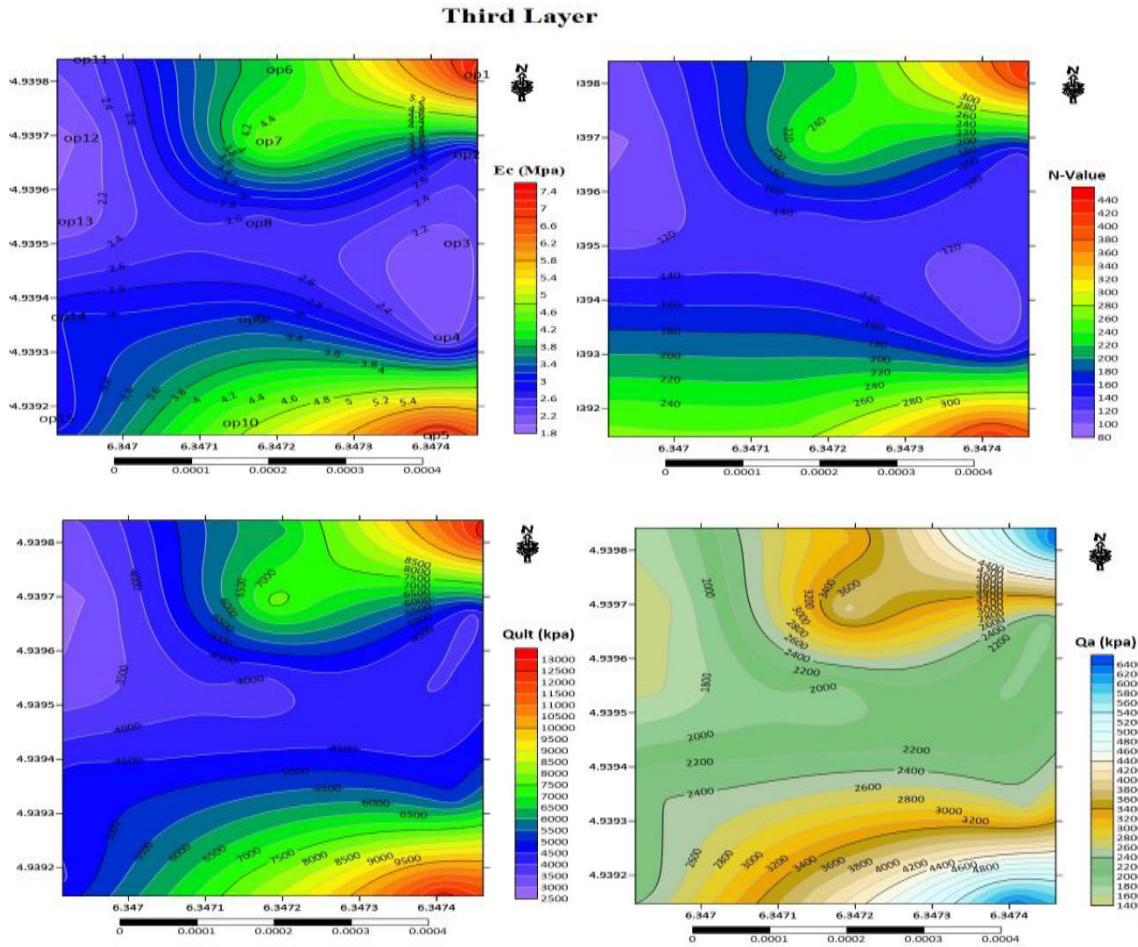


Figure 7. Distribution map of oedometric modulus (E_c), N-value, ultimate bearing capacity (Q_{ult}) and allowable bearing capacity (Q_a) for third layer Opolo.

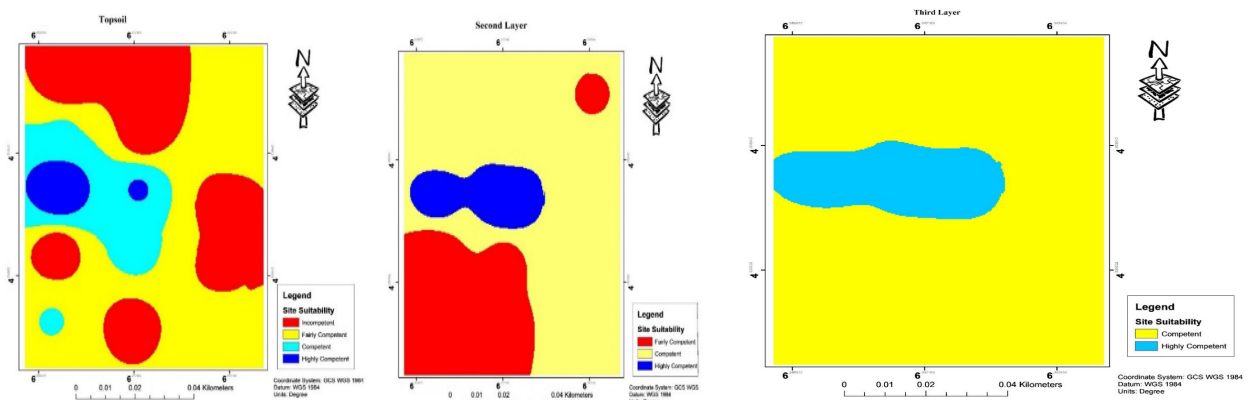


Figure 8. Competent site suitability maps from topsoil to third layer in Opolo study area.

4. Conclusions and recommendations

4.1 Conclusions

This research illustrates the utilization of near-surface seismic refraction surveys to establish crucial geotechnical parameters for soil characterization in potential construction locations. The study was carried out in Opolo, Yenagoa, Bayelsa State, Nigeria, involving the implementation of seismic profiling along three designated lines. Through meticulous analysis, three distinct geoseismic layers were identified, and their geotechnical properties were subsequently assessed using the Generalized Reciprocal Method (GRM). The initial layer, ranging from 0.89 meters to 1.50 meters in depth, exhibited notably low compressional and shear wave velocities, measuring between 178.17 to 264.40 meters per second and 104.83 to 155.50 meters per second, respectively. Correspondingly, this layer displayed low values for oedometric modulus, shear modulus, N-value, ultimate bearing capacity, and allowable bearing capacity. These characteristics collectively point to the presence of soft and weak alluvial deposits, rendering this layer unsuitable for supporting substantial structural loads. In contrast, the second layer, spanning from 1.52 meters to 3.84 meters in depth, presented significantly improved geotechnical parameters. It showcased notable values for ultimate and allowable bearing capacities, measuring between 460.15 to 716.80 kilopascals and 230.08 to 358.40 kilopascals, respectively. These findings indicate that the second layer can adequately support various construction loads. The third layer, extending from 15.00 meters to 26.05 meters in depth, exhibited variable thickness, ranging from 12.62 meters to 21.00 meters, and displayed moderately to competently compacted characteristics. Geographic Information System (GIS) analysis, employing the index overlay method, revealed that the top layer generally possesses fairly competent properties, with pockets of incompetency observed along the peripheries in Opolo. Conversely, the second and third layers at Opolo demonstrated fairly competent attributes, rendering them suitable for shallow footing and foundation design consid-

erations. However, it is crucial to note that the first layer is deemed unsuitable for construction due to its inherent incompetency.

4.2 Recommendations

Based on the geotechnical findings, it is advisable to exercise caution when selecting construction sites in Opolo, Yenagoa, Bayelsa State. Avoid building on the initial layer due to its inadequate bearing capacity. Opt for the second and third layers, which exhibit competent properties, especially for shallow footing and foundation designs. Further site-specific assessments and engineering solutions should be considered for safe and sustainable construction in Opolo.

Author Contributions

O.E. developed the study with part of the writing and Formatting, E.D. processed the data and also assisted with writing. The final version was co-written by all authors.

Conflict of Interest

There is no conflict of interest.

References

- [1] Rowland, E., Ejaita, E., Omietimi, E.J., 2020. Foundation materials bearing capacity of Tombia Yenagoa, Bayelsa State Nigeria using multichannel analysis surface waves method. *International Journal of Advance Research and Innovative Ideas in Education*. 6(5), 811-823.
- [2] Omonefe, F., Desmond, E., Ebiegberi, O., et al., 2019. Analysis of near surface seismic refraction for geotechnical parameters in Opolo, Yenagoa of Bayelsa State. *Journal of Engineering Research and Reports*. 4(4), 1-12.
- [3] Roy, S., Bhalla, S.K., 2017. Role of geotechnical properties of soil on civil engineering structures. *Resources and Environment*. 7(4), 103-109.
- [4] Nouwakpo, S.K., Huang, C.H., 2012. A fluidized bed technique for estimating soil critical shear stress. *Soil Science Society of America*

- Journal. 76(4), 1192-1196.
- [5] Nwankwoala, H.O., Warmate, T., 2014. Geotechnical assessment of foundation conditions of a site in Ubima, Ikwerre local government area, Rivers State, Nigeria. *International Journal of Engineering Research and Development (IJERD)*. 9(8), 50-63.
- [6] Akintorinwa, O.J., Oluwole, S.T., 2018. Empirical relationship between electrical resistivity and geotechnical parameters: A case study of Federal University of Technology campus, Akure SW, Nigeria. *NRIAG Journal of Astronomy and Geophysics*. 7(1), 123-133.
- [7] Akinlabi, I.A., Adeyemi, G.O., 2014. Determination of empirical relations between geoelectrical data and geotechnical parameters in foundation studies for a proposed earth dam. *Pascal Journal Science Technology*. 15(2), 279-287.
- [8] Zhu, J., Wright, G., Wang, J., et al., 2018. A critical review of the integration of geographic information system and building information modelling at the data level. *ISPRS International Journal of Geo-Information*. 7(2), 66.
- [9] Bill, R., Blankenbach, J., Breunig, M., et al., 2022. Geospatial information research: State of the art, case studies and future perspectives. *PFG—Journal of Photogrammetry, Remote Sensing and Geoinformation Science*. 90(4), 349-389.
DOI: <https://doi.org/10.1007/s41064-022-00217-9>
- [10] Palmer, D., 1980. The generalized reciprocal method of seismic refraction interpretation. *Society Exploration Geophysics*: London.
- [11] Mohamed, A.M., Abu El Ata, A.S.A., Abdel Azim, F., et al., 2013. Site-specific shear wave velocity investigation for geotechnical engineering applications using seismic refraction and 2D multi-channel analysis of surface waves. *NRIAG Journal of Astronomy and Geophysics*. 2(1), 88-101.
- [12] Imaitor-Uku, E.E., Owei, O.B., Hart, L., et al., 2021. Impact of settlement growth on Yenagoa's urban environment. *European Journal of Environment and Earth Sciences*. 2(1), 24-29.
- [13] Asare, E.N., Klu, A.K., 2019. The use of seismic refraction and geotechnical parameters to conduct site investigation—A case study. *International Journal of Advanced Engineering Research and Science*. 6(9).
DOI: <https://doi.org/10.22161/ijaers.69.36>
- [14] Adewoyin, O.O., Joshua, E.O., Akinyemi, M.L., et al., 2021. Engineering site investigations using surface seismic refraction technique. *IOP Conference Series: Earth and Environmental Science*. 655(1), 012098.
DOI: <https://doi.org/10.1088/1755-1315/655/1/012098>
- [15] Yilmaz, O., 2001. *Seismic data analysis: Processing, inversion, and interpretation of seismic data*. Society of Exploration Geophysicists: Tulsa, OK.
- [16] Khalil, M.H., Hanafy, S.M., 2008. Engineering applications of seismic refraction method: A field example at Wadi Wardan, Northeast Gulf of Suez, Sinai, Egypt. *Journal of Applied Geophysics*. 65(3-4), 132-141.
DOI: <https://doi.org/10.1016/j.jappgeo.2008.06.003>
- [17] Mageshkumar, P., Subbaiyan, A., Lakshmanan, E., et al., 2019. Application of geospatial techniques in delineating groundwater potential zones: A case study from South India. *Arabian Journal of Geosciences*. 12, 1-15.
- [18] Kearey, P., Brooks, M., Hill, I., 2002. *An introduction to geophysical exploration*, third edition. Blackwell: London.
- [19] Lowrie, W., 2007. *Fundamentals of geophysics*, second edition. Cambridge University Press: Cambridge.
- [20] Reynolds, J.M., 2011. *An introduction to applied and environmental geophysics*. John Wiley & Sons: Hoboken.
- [21] Telford, W.M., Geldart, L.P., Sheriff, R.E., 1990. *Applied geophysics*. Cambridge University Press: Cambridge.
- [22] Atat, J.G., Akpabio, I.O., George, N.J., 2013. Allowable bearing capacity for shallow foundation in Eket local government area, Akwa Ibom State, southern Nigeria. *International Journal of*

- Geosciences. 4, 1491-1500.
- [23] Tezcan, S.S., Ozdemir, Z., Keceli, A., 2009. Seismic technique to determine the allowable bearing pressure for shallow foundations in soils and rocks. *Acta Geophysica*. 57, 400-412.
- [24] Essien, U.E., Akankpo, A.O., 2013. Compressional and shear-wave velocity measurements in unconsolidated top-soil in Eket, South-Eastern Nigeria. *The Pacific Journal of Science and Technology*. 14(1), 476-491.
- [25] Hassan, M., 2023. *Avantgarde reliability implications in civil engineering*. IntechOpen: London.
DOI: <https://doi.org/10.5772/intechopen.102292>
- [26] Essien, U.E., Igboekwe, M.U., Akankpo, A.O., 2016. Determination of incompressibility, elasticity and rigidity of surface soils and shallow sediments from seismic wave velocities. *Journal of Earth Sciences and Geotechnical Engineering*. 6(1), 99-111.
- [27] Farauta, B.K., Egbule, C.L., Agwu, A.E., et al., 2012. Farmers' adaptation initiatives to the impact of climate change on agriculture in northern Nigeria. *Journal of Agricultural Extension*. 16(1), 132-144.
DOI: <https://doi.org/10.4314/jae.v16i1.13>
- [28] Imai, T., Fumoto, H., Yokota, K., 1976. *P- and S-wave velocities in subsurface layers of ground in Japan*. Urawa Research Institute: Tokyo.
- [29] Stümpel, H., Kähler, S., Meissner, R., et al., 1984. The use of seismic shear waves and compressional waves for lithological problems of shallow sediments. *Geophysical Prospecting*. 32(4), 662-675.
- [30] Parry, R.H., 1977. Estimating bearing capacity in sand from SPT values. *Journal of the Geotechnical Engineering Division*. 103(9), 1014-1019.
- [31] Abd El-Rahman, M., 1991. The potential of absorption coefficient and seismic quality factor in delineating less sound foundation materials in Jabal Shib Az Sahara area, Northwest of Sanaa, Yemen Arab Republic. *Egypt, MERC Earth Science*. 5, 181-187.
- [32] Clark, S.P., 1966. *Handbook of physical constants*. Geological Society of America: Boulder, Colorado, U.S.
- [33] Gassman, F., 1973. *Seismische prospektion (German) [Seismic prospection]*. Birkhaeuser Verlag: Stuttgart. pp. 417.
- [34] Tatham, R.H., 1982. Vp Vs and lithology. *Geophysics*. 47(3), 336-344.
- [35] Sheriff, R.E., Geldart, L.P., 1986. *Exploration seismology*. Cambridge University Press: Cambridge.
- [36] Abd El-Rahman, M.A.H.D.Y., 1989. Evaluation of the kinetic elastic moduli of the surface materials and application to engineering geologic maps at Maba-Risabah area (Dhamar Province), Northern Yemen. *Egypt Journal Geology*. 33(1-2), 229-250.
- [37] Nwankwoala, H.O., Amadi, A.N., 2013. Geotechnical investigation of sub-soil and rock characteristics in parts of Shiroro-Muya-Chanchaga area of Niger State, Nigeria. *International Journal of Environmental and Engineering*. 6(1), 8-17.

ARTICLE

Origin of the Dashuigou Independent Tellurium Deposit at the Southeastern Qinghai-Tibet Plateau: Based on the Abundances of Trace Elements in the Country Rocks

Jianzhao Yin^{1,2*}, Shoupu Xiang³, Haoyu Yin⁴, Hongyun Shi⁵, Yuhong Chao⁶

¹ College of Earth Sciences, Jilin University, Changchun, Jilin, 130061, China

² Wuhan Institute of Technology, Wuhan, Hubei, 430074, China

³ Silvercorp Metals Inc., Chaoyang District, Beijing, 100027, China

⁴ Guinea Westfield Mining Company-Sarlu, Jinzhong, Shanxi, 031300, China

⁵ Orient Resources Ltd., Richmond, BC, V7E 1M8, Canada

⁶ Ganzhongnan Institute of Geology and Mineral Exploration, Nanchang, Jiangxi, 330002, China

ABSTRACT

Through a detailed study of the abundances and spatial-temporal distribution patterns of Te, Bi, As, Se, Cu, Pb, Zn, Au, and Ag in the rock types of different geological epochs in the Dashuigou independent tellurium deposit, and in combination with other research findings of previous researchers in this area, the authors conclude as follows: Abundances of the main ore-forming elements Te, Bi, As, Se, Au, and Ag are not high in the regional geological background, generally lower or close to their respective crustal Clark values, but almost all altered country rocks contain high levels of ore-forming elements. This indicates that the deposit's ore-forming elements do not come from the country rocks. This also indicates that the geological thermal events that cause alteration and mineralization originate from depths and may be related to mantle plumes. Considering the distribution pattern of these ore-forming elements in the ore bodies' hanging wall and footwall, the metallogenic mechanism may be as follows: Mineralization is not achieved through lateral secretion in the horizontal or near horizontal direction, but rather through the upward movement and emplacement of deep ore-forming elements driven by geological processes such as mantle plumes. In addition, the migration of deep ore-forming elements is not achieved through dispersed infiltration between overlying rock particles, but through non widespread concentrated penetrating channels. This type of channel is likely to be the expansion structures where faults from different directions intersect, or where linear faults intersect with circular structures.

Keywords: Origin of ore-forming elements; The Dashuigou independent tellurium deposit; Trace element abundance; The country rocks; The mantle plume

*CORRESPONDING AUTHOR:

Jianzhao Yin, College of Earth Sciences, Jilin University, Changchun, Jilin, 130061, China; Wuhan Institute of Technology, Wuhan, Hubei, 430074, China; Email: jzyin7@jlu.edu.cn

ARTICLE INFO

Received: 16 September 2023 | Revised: 6 November 2023 | Accepted: 7 November 2023 | Published Online: 17 November 2023

DOI: <https://doi.org/10.30564/agger.v5i4.5967>

CITATION

Yin, J.Zh., Xiang, Sh.P., Yin, H.Y., et al., 2023. Origin of the Dashuigou Independent Tellurium Deposit at the Southeastern Qinghai-Tibet Plateau: Based on the Abundances of Trace Elements in the Country Rocks. *Advances in Geological and Geotechnical Engineering Research*. 5(4): 41-55. DOI: <https://doi.org/10.30564/agger.v5i4.5967>

COPYRIGHT

Copyright © 2023 by the author(s). Published by Bilingual Publishing Group. This is an open access article under the Creative Commons Attribution-NonCommercial 4.0 International (CC BY-NC 4.0) License. (<https://creativecommons.org/licenses/by-nc/4.0/>).

1. Introduction

The Dashuigou tellurium deposit, the only independent tellurium deposit in the world thus far, has attracted geologists' extensive attention, since its discovery in 1992. Thus many different views on its origins have been proposed^[1-7].

Yin and Yin et al. proposed that the deposit's tellurium and bismuth originated mainly from the mantle's degassing in the form of a mantle plume, and enriched through nano-effect^[1,5,6,8,9].

This paper's authors attempt to further prove the deposit's origin from the perspective of the abundance of trace elements in the deposit's country rocks.

2. Regional geology

2.1 General

Geotectonically in the transitional belt between the Yangtze platform and Songpan-Ganzi folded belt in the Qinghai-Tibet Plateau (**Figures 1 and 2**), the Dashuigou tellurium deposit is in the region where the crust-mantle structures and properties are the result of tectogenesis through various geological times, and have the following geophysical characteristics^[1,8,10]:

- The turning boundary of the Earth's crust's thickness and the gravity gradient zone controlling the earthquakes and a series of mineral deposits.
- The abnormal mantle available and the upper mantle below the region uplifting obviously.
- The region exhibiting high geothermal flow, low-velocity, high density, high resistance, high magnetism, and low resistivity.
- The region has properties of both geosyncline and platform and is a geo-tectonically active zone with very complicated igneous rock structures.

In short, the study area is a place where the upper mantle and crust react frequently and the geological tectonic activity is very intense. It has therefore become a very important south-north trending tectonomagmatic-mineral belt^[1,8,10].

2.2 Strata

Many of the strata in the study area are regional

low-grade metamorphic rocks of the Silurian, Devonian, Permian systems, and lower-middle Triassic series, with a large amount of Archaean high-grade metamorphic rocks of the Kangding Group emerging to the southeast of the deposit.

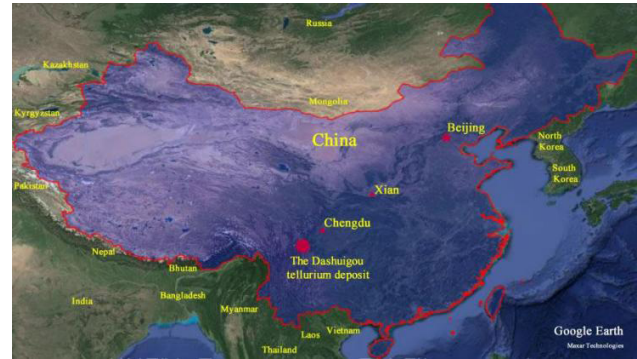


Figure 1. Location map of the deposit.

Source: Google Earth 7.1.8.3036 (32-bit): <http://download.pchome.net/industry/geography/detail-20351.html>, and 91 v17.5.8: www.91weitu.com; accessed January 25-27, 2020)^[10].

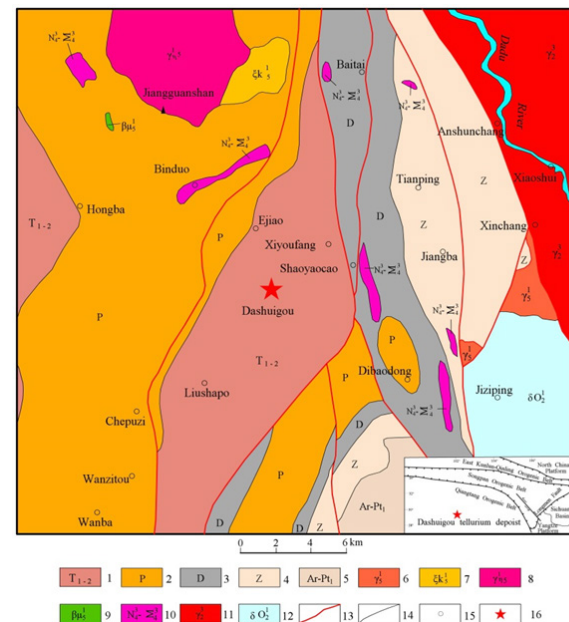


Figure 2. Regional geology.

1. The lower-middle Triassic metamorphic rocks; 2. The Permian metamorphic rocks; 3. The Devonian metamorphic rocks; 4. The Sinian metamorphic rocks; 5. Metamorphic complex of the Archean Kangding group; 6. Plutonic granite of the Indosinian orogeny; 7. Plutonic alkaline syenite of the Indosinian orogeny; 8. The Indosinian plutonic monzonitic granite; 9. The Indosinian hypabyssal sillite; 10. The late Hercynian basic-ultrabasic rocks; 11. The late Proterozoic plutonic granite; 12. The early Proterozoic-Archaean plutonic quartz diorite; 13. The deep and large fault zone; 14. The geological boundary; 15. Village and/or town; 16. The tellurium deposit.

Source: ^[1,8].

The lithology and lithofacies of the deposit's hosts rock schist and phyllite, which have undergone multiple geological tectonic movements, change significantly.

The rocks in the study area have undergone various alterations such as dolomitization, muscovitization, tourmalinization, silicification, sericitization, and chloritization, and localized mineralization such as pyrrhotite, lead-zinc, copper, pyrite, tellurium, bismuth, gold, and silver [1,8,10].

2.3 Igneous rock

The igneous rocks including ultrabasic, basic, neutral, acid, and alkaline produced in different geological times are well-developed in the study area [1,8,11]. Large basic-ultrabasic, neutral, acid, and alkaline intrusive bodies exist beyond 10 km of the deposit include (**Figure 2**) the Archean-early Proterozoic Jiziping-Caluo quartz diorite and diorite, the late Proterozoic Xiaoshui granite, the late Paleozoic basic-ultrabasic intrusive rocks, and the Mesozoic neutral, acidic, and alkaline intrusive bodies including Jiangguanshan alkaline syenite, Jiangguanshan quartz diorite, and Xinchang granite.

In addition, a series of veins/dykes including quartz veins, carbonate veins, diabase dykes, granitoid aplite dykes, granite pegmatite dykes, and lamprophyre dikes etc. are widely developed in the study area.

The favorable geological conditions of strata, igneous rocks, and structures have created abundant mineral resources in the area, some of which are well known both domestically and internationally, including Ti, V, Cu, Pb, Zn, SM, REE, coal, asbestos, and the Panzhuhua V-Ti-Fe deposit [1,8,11].

2.4 Structure

Well-developed annular and NW, NNE, NS, NWW, and NEE-trending linear structures are revealed by the remote sensing images in the study area (**Figures 3-6**) [1,8,11].

As we all know, the circular structure may be an external reflection of deep-buried igneous intrusive

and/or geotectonic/geophysical anomalies, which helps to determine the formation mechanism of tellurium deposits in the study area.



Figure 3. Linear-circular structures based on remote sensing satellite images and geochemical anomalies in the study area (1:200,000).

As the largest known annular structure with a diameter of about 8 km in the area (**Figures 3 and 4**), the Xiyoufang composite ring's southern part reaches the Dashuigou deposit. Inside the Xiyoufang large ring, there exist two small annular structures with a diameter of about 2 km. Moreover, around the big ring, there are two other small rings accompanying it.

The annular structures and linear structures with different mechanical properties in different directions are cut with each other to form typical Φ -shaped structures favorable for mineralization (**Figures 3-6**). More than 20 tellurium mineralization showings including the Dashuigou tellurium deposit, and more than 10 Au-Bi composite geochemical anomalies, as

well as several gold geochemical anomalies, are spatially related to these structures.

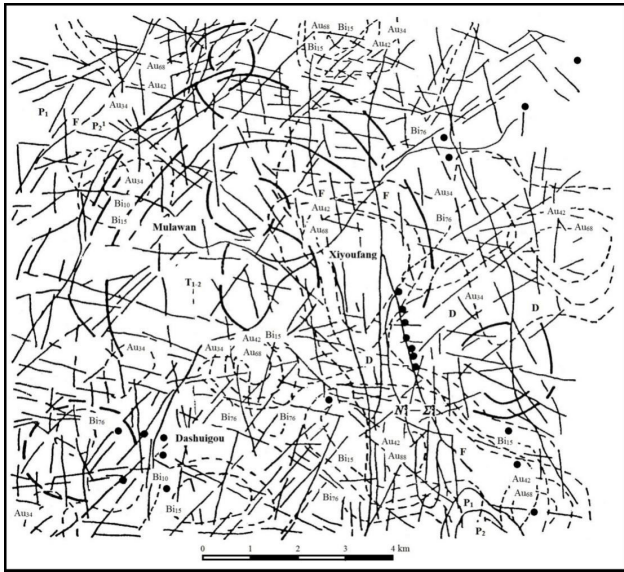


Figure 4. Linear-circular structures based on remote sensing satellite images and geochemical anomalies in the Xiyoufang area.

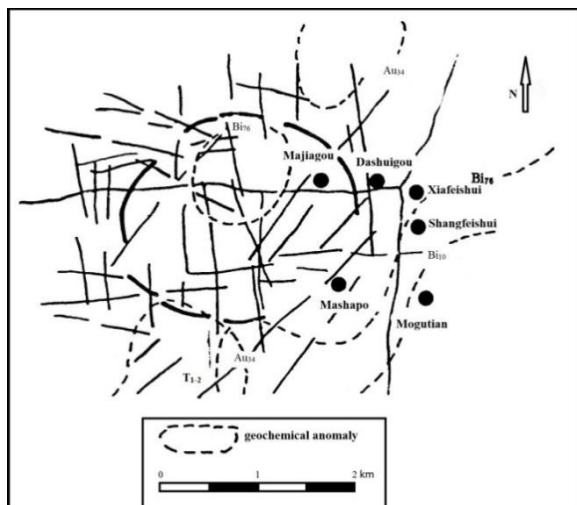


Figure 5. Linear-circular structures based on remote sensing satellite images and geochemical anomalies in the Dashuigou area.

As one of the Xiyoufang annular structure's sub-rings (**Figures 4 and 5**), the Dashuigou annular structure intersects with NE, EW, SN, and NW trending linear structures, forming a characteristic \emptyset -shaped structure controlling the unique deposit.

The perfectly circular Jinhudong ring structure, Xiyoufang annular structure's other sub-ring, intersects with NWW, NNW, and SN-trending linear structures, forming another \emptyset -shaped structure con-

trolling the Jinhudong, Qifenyao, and Bafenyao tellurium showings, and several Au and Bi geochemical anomalies (**Figures 4 and 6**).

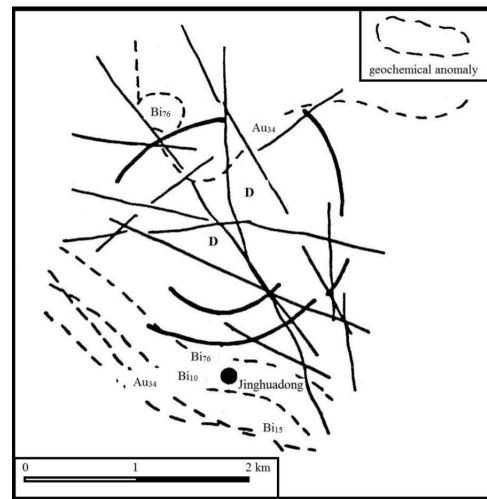


Figure 6. Linear-circular structures based on remote sensing satellite images and geochemical anomalies in the Jinhudong area.

Baita, Tianwan, Tangjiapo, and Jiangguanshan are other annular structures in the area (**Figure 3**), all of which have a close spatial relationship with the Bi and Au geochemical anomalies.

Relatively tight, narrow, and long folds including the Dashuigou dome and Bindo anticline are mostly NNE or nearly SN-trending.

The over 10 km long and roughly NNE trending Dashuigou dome is entirely composed of lower-middle Triassic rocks (**Figure 5**). The dome's four sides are cut and bounded by NNW-trending, near-north-south, and NNE-trending faults respectively, forming a clearly flattened rhombic block.

3. Mine geology

The deposit's country and/or host rocks are the lower-middle Triassic marble, phyllite, and schist (**Figure 7**).

From top to bottom, Dashuigou tellurium deposit's country/host rocks include ^[1,8]: schist and phyllite on the top, the upper thick fine-grained marble, the middle schist and phyllite formation, the lower fine-medium-grained marble, and thick coarse-grained marble at the bottom.

The deposit's direct host rocks are the middle

phyllite and schist including hornblende schist, garnet schist, tourmaline schist, and chlorite schist. Other minerals in the schist include quartz, plagioclase, potassium feldspar, muscovite, rutile, and magnetite (Figure 7).

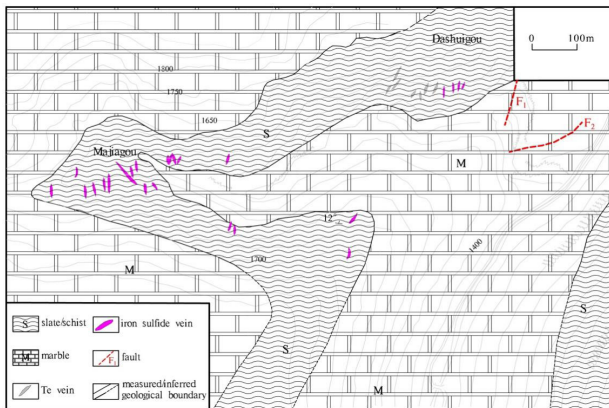


Figure 7. Mine geology.

Source: [1,8].

The NNE-trending Dashuigou dome is completely made up of the Triassic strata as mentioned above (Figures 3-5).

Most, if not all of the deposit's ore bodies in the shape of lenticular veins strike from 350 to 10 degrees, and dip at 55 to 70 degrees westward, with widths of which varying between 25 and 30 cm.

The alteration zones in the mining area are very narrow, generally ranging between several centimeters to one meter in width. The altered host rocks beside the massive ore bodies are narrower, at only several centimeters wide [1,6,8,10].

Approximately 40 minerals have been identified in the ore. Of all the ore types, the massive ore is the most important and disseminated ore is the secondary important. The tellurium grade in the ore varies between 0.01% and 34.58% [1,13-24].

Major ore textures and structures in the deposit include a replacement, remnant, reaction border, granular, massive, vein/veinlet, and stockwork veins [1,8,24].

Two paragenetic stages including five sub-stages in total have been recognized in the deposit; namely, the pyritic stage including carbonate sub-stage → pyrrhotite sub-stage → chalcopyrite sub-stage, and the tellurium stage including tetradymite sub-stage → tsumoite

sub-stage (from early to late) [1,6,8,10,24,25].

4. Analytical methods

Multi Element ICP Analysis/LA-ICP-MS: A 0.5-gram sample is digested with 3 mL of a 3:1:2 (HCl: HNO₃: H₂O) acid, which contains beryllium that acts as an internal standard for 90 minutes in a water bath at 95 °C. The sample is then diluted to 10 mL with water and then analyzed on a Jarrell Ash ICP unit.

If the quality control standard is outside 2 standard deviations, or if the blank sample is greater than the limit, the entire set of samples is redone. The analytical results are collated by computer and printed along with accompanying quality control data; namely, repeats and standards.

5. Ore-forming element abundance in the country rocks

There are many geochemical anomalies in the study area, such as the Baita-Xiyoufang lead heavy sand anomaly to the north of the mining area, the scheelite heavy sand anomaly in the Hongba area to the northwest, the Guanyinshan-Nibapengzi nickel-chromium-cobalt-copper stream sediment anomaly to the southeast, the Landiao nickel-chromium-cobalt-copper-tin stream sediment anomaly to the southwest, the Ziershan Pass lead heavy sand anomaly to the south, and the geophysical as well as Bi and Au geochemical anomalies shown in Figures 3-6, etc.

The research area is located in the No.1 ore-forming prospect area in the 1:200,000 regional survey results, which is the prospect area of asbestos, iron, copper, lead, zinc, gold, and polymetallic minerals [11].

Overall, the geochemical anomaly zones within the area are closely related to certain lithology and have certain mineralization specific characteristics, such as copper, nickel, chromium, and cobalt mainly distributed in the development areas of basic-ultra-basic rocks. On the other hand, these anomalies are mostly located near and along fault zones, especially in areas with strong structural fragmentation, dense linear structures, and Ø-shaped structures [1,26,27].

Due to the extremely low crustal abundance of tellurium (**Table 1**)^[28,30], coupled with previous human biases in understanding the mineralization ability of rare elements such as tellurium, as well as low

testing accuracy, and many other factors, the study area, like the vast majority of regions both domestically and internationally, lacks regional geochemical background data on tellurium.

Table 1. The crustal abundance of tellurium published by different researchers.

Researcher	Clarke & Washington	Goldschmidt	A. Abeyc	Tong Li		
Year	1924	1937	1975	1976	1994	
Abundance	$n \times 10^{-8}$	1.8×10^{-9}	1.0×10^{-9}	6.0×10^{-10}	2.0×10^{-8}	1.34×10^{-9}
Note	N/A	N/A	N/A	N/A	The Earth's crust in China	The Earth's crust world wide

6. Results and Discussion

In order to identify the abundance and distribution patterns of tellurium in the study area and provide sufficient basis for revealing the mineralization mechanism of the Dashuigou tellurium deposit, the authors of this article conducted quantitative chemical analysis of elements such as Te, Bi, Se, As, Au, Ag, Cu, Pb, and Zn in different rocks of different ages, including various metamorphic and igneous rocks, altered rocks, and highly developed carbonate veins in the study area. The results are shown in **Tables 2a and 2b**.

Among them, four elements, Te, Bi, Se, and As, were tested by atomic fluorescence spectrometry. Au, Ag, Cu, Pb, and Zn were tested by atomic absorption spectrometry. However, due to the limitation of the lower analytical limit, approximately 34% of the samples were unable to detect their exact abundance of Te. The detection limit of Te is 10^{-7} . As, Bi, Ag, Pb, Se, and Cu also have similar problems. This poses certain difficulties in accurately analyzing the abundance of relevant elements in different rocks and veins of different ages.

6.1 Te and Bi

According to **Tables 2a and 2b**, the distribution pattern of Te in the study area is summarized as follows:

The Te content in granite of different ages in the region is the lowest, less than 10^{-7} , close to the crustal abundance of tellurium (**Table 1**). This indicates a sense that the Dashuigou tellurium deposit's forma-

tion is not related to these granite intrusions. In addition, the three rock samples' $\delta^{30}\text{SiNBS}$ -28‰ values indicated that their protolith is an intermediate-basic volcanic rock^[1,8,12].

The abundance of Te in the metamorphic rocks is significantly higher than that in granites mentioned above. However, there are significant differences in tellurium content in metamorphic rocks of different ages. The main performance is that the tellurium abundance is the highest in the Middle and Lower Triassic rocks, followed by the Devonian rocks, and the lowest in the Upper Permian rocks (**Figure 8**).

In metamorphic rocks of the same age, different rock types contain different amounts of tellurium. In general, schist and phyllite contain more tellurium than marble. The same is marble, because of the different particle sizes, the abundance of tellurium is also different. Coarse-grained marble contains low tellurium abundance and is close to the crustal abundance of tellurium (**Table 1**), while fine-grained marble contains a higher amount of tellurium. That is, the abundance of tellurium is inversely correlated with the grain size of marble.

Both are lower-middle Triassic rocks, and the horizons are basically the same, but the tellurium content of the rocks inside and outside the mining area is also different (**Figure 8**). This should be related to the different degrees of alteration and mineralization of the metamorphic rocks in the mining area during the thermal dome process. The periphery of the mining area has low tellurium content because it has not been subjected to heat or to a lesser extent.

Table 2a. Analytical results of trace element content in different rocks in the research area.

Rock	Age	Series #	Sample #	Name	Location
Igneous rock	γ_5^1	1	SL-01	granite	Niubeishan, Xinchang
	Pt ₃	2	SL-26	KF granite	Sanxing, Fengle
		3	SL-22	granite	By the Dadu River
		4	SL-07	fg marble	West of Miaoping
		5	SL-19	schist	Near the mine
		6	SL-12	schist	peripheral Near Miaoping
		7	SL-17	fg marble	Near Tizigou
		8	SL-18	banded marble	Near Tizigou
		9	SL-16	mg marble	Near Tizigou
		10	SL-14	cg marble	East of Miaoping
		11	SL-15	cg marble	Near Tizigou
Metamorphic rock	T ₁₋₂	12	SD-12-2	slate	Between ore zones # II-III
		13	SD-18	green schist	In the hanging wall of # III-3 ore body
		14	SD-32	slate	In the hanging wall of # I-4 ore body
		15	SD-43	green schist	In the hanging wall of # I-1 ore body
		16	SD-38	green schist	mine In the footwall of # I-1 ore body
		17	SD-35	amphibole schist	In the hanging wall of # I-5 ore body
		18	SD-22	banded marble	In the foot wall of # III-3 ore body
		19	SD-69	cg marble	In the bottom of the Dashuigou ditch
		20	SL-03	slate	Near the river dam
		21	SL-04	green schist	Near the river dam
	P ₂	22	SL-02	slate	North of Wanzitou
		23	SL-10	metamorphosed basalt	peripheral Near Miaoping
		24	SL-21	marble	Northeast of Xiyoufang
	D	25	SL-20	slate	Northeast of Xiyoufang
		26	SD-02	sericite schist	In the adit of # II ore zone
		27	SD-37	sericite schist	In the hanging wall of # I-5 ore body
		28	SD-42	slate	In the hanging wall of # I-1 ore body
		29	SD-39	slate	mine In the foot wall of # I-1 ore body
		30	SD-54-1	schist	In # 4 adit
		31	SD-68	green schist	at the portal of # 4 adit
		32	SD-49	banded marble	at the portal of # 4 adit
		33	SL-05	slate	peripheral At Liushapo
		34	SD-65-1	dolomite	mine In # I-8 ore body
Strongly altered rock	177-80 Ma	35	SL-08	dolomite	peripheral At Liushapo

Note: KF—potassium feldspar, fg—fine grained, mg—medium grained, cg—coarse grained.

Table 2b. Analytical results of trace element content in different rocks in the research area ($\times 10^{-6}$).

Series #	Te	Bi	As	Se	Au	Ag	Cu	Pb	Zn	Average value
1	< 0.10	0.89	0.30	< 0.10	0.00	0.01	20.00	< 10	86.00	Te < 0.10, Bi < 0.37, As 0.47, Se < 0.10, Au 0.02, Ag 0.01, Cu 10.67, Pb < 30.33, Zn 71.33
2	< 0.10	0.18	0.80	< 0.10	0.00	0.01	4.00	63.00	42.00	
3	< 0.10	< 0.05	0.30	< 0.10	0.00	0.01	8.00	18.00	86.00	
4	0.90	1.34	1.10	< 0.10	0.00	< 0.01	1.00	< 10	98.00	
5	< 0.10	0.20	14.10	< 0.10	0.00	0.01	26.00	13.00	78.00	
6	< 0.10	< 0.05	0.10	< 0.10	0.02	0.06	122.00	12.00	122.00	Te < 0.50, Bi < 0.88, As 2.78, Se < 0.10, Au 0.01, Ag < 0.02, Cu < 19.75, Pb < 15.75, Zn 61.38
7	2.50	5.09	1.00	< 0.10	0.00	0.01	4.00	< 10	38.00	
8	< 0.10	< 0.05	5.60	< 0.10	0.01	0.01	2.00	< 10	41.00	
9	< 0.10	0.24	0.10	< 0.10	0.00	0.01	1.00	< 10	41.00	
10	< 0.10	< 0.05	0.10	< 0.10	0.00	0.06	1.00	51.00	21.00	
11	< 0.10	< 0.05	< 0.10	< 0.10	0.00	0.01	1.00	< 10	52.00	Te 8.35, Bi 12.27, As < 0.48, Se < 0.10, Au 0.004, Ag < 0.023, Cu < 21.75, Pb < 10.00, Zn 99.25
12	0.50	1.07	0.20	< 0.10	0.01	0.02	50.00	< 10	84.00	
13	4.50	10.60	< 0.10	< 0.10	0.01	0.05	6.00	< 10	142.00	
14	4.70	9.17	0.20	< 0.10	0.00	0.01	20.00	< 10	99.00	
15	2.70	4.05	0.20	< 0.10	0.00	0.02	9.00	< 10	197.00	
16	5.50	1.13	1.20	< 0.10	0.00	0.01	3.00	< 10	125.00	Te < 0.13, Bi 0.26, As 1.95, Se 0.10, Au 0.01, Ag 0.04, Cu 38.75, Pb 10.50, Zn 83.75
17	37.10	56.10	0.20	< 0.10	0.01	0.06	81.00	< 10	78.00	
18	11.60	15.50	1.10	< 0.10	0.00	0.01	4.00	< 10	56.00	
19	0.20	0.52	0.60	< 0.10	0.00	0.01	1.00	< 10	13.00	
20	< 0.1	0.10	4.10	< 0.10	0.01	0.02	12.00	12.00	86.00	
21	< 0.1	0.19	0.40	< 0.10	0.00	0.06	102.00	< 10	154.00	Te 0.60, Bi 0.47, As 0.63, Se 0.10, Au 0.01, Ag 0.06, Cu 2.00, Pb < 10.00, Zn 157.50
22	0.20	0.43	0.90	< 0.10	0.00	0.05	17.00	< 10	38.00	
23	< 0.1	0.31	2.40	< 0.10	0.01	0.03	24.00	< 10	57.00	
24	< 0.1	0.39	1.90	< 0.10	0.00	0.01	2.00	< 10	118.00	
25	1.10	1.49	0.60	< 0.10	0.012	0.10	2.00	< 10	197.00	
26	1.10	2.66	< 0.1	< 0.10	0.00	0.01	34.00	< 10	92.00	Te 44.15, Bi 52.77, As < 4.76, Se < 0.24, Au 0.02, Ag 0.06, Cu 68.50, Pb < 10.00, Zn 77.13
27	11.00	15.50	3.60	0.30	0.04	0.04	212.00	< 10	83.00	
28	4.60	5.98	0.20	0.40	0.00	0.01	130.00	< 10	145.00	
29	99.10	117.00	0.40	< 0.10	0.03	0.05	6.00	< 10	57.00	
30	56.80	84.60	32.80	0.70	0.09	0.06	6.00	< 10	14.00	
31	0.40	1.05	0.60	< 0.10	0.01	0.11	121.00	< 10	164.00	Te 31.90, Bi 20.39, As 0.15, Se < 0.10, Au 0.004, Ag 0.04, Cu 2.00, Pb < 10.00, Zn 7.50
32	178.00	191.00	0.20	< 0.10	0.01	0.12	3.00	< 10	4.00	
33	2.20	4.38	0.20	< 0.10	0.01	0.09	36.00	< 10	58.00	
34	2.30	3.44	0.20	< 0.10	0.00	0.03	3.00	< 10	10.00	
35	61.5	78.1	< 0.10	< 0.10	0.0	0.0	1.0	< 10	5.0	

Note: If there is no definite value in the original numerical value, the average value is calculated according to its lower limit of analysis.

Laboratory: National Geological Chemical Analysis Center.

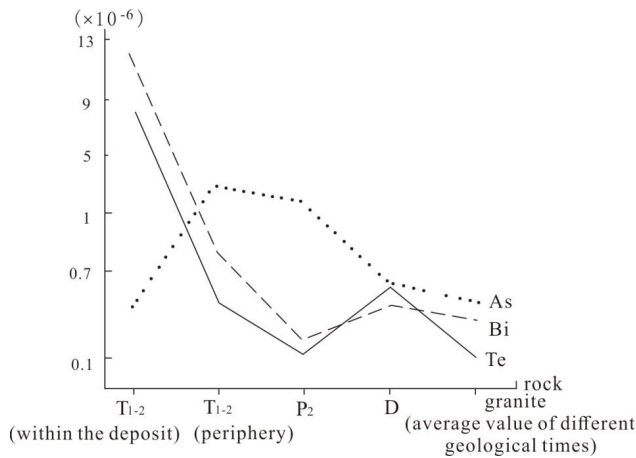


Figure 8. Te, Bi, and As abundances in metamorphic rocks and granites of different ages in the study area.

An important fact is that in the T1-2 formation outside the mining area, except for the two fine-grained marble samples near the Tizigou Pb-Zn showing (two samples with series numbers 4 and 7 in **Tables 2a and 2b** respectively), which may have undergone alteration, the crustal abundance of tellurium is slightly higher or close to that of tellurium in the Earth's crust. All other samples are lower or close to the crustal abundance of tellurium.

Anyway, the stronger the alteration that rocks undergo, the higher their tellurium content. This may to some extent indicate that the source of tellurium is not related to the host rock, but is closely related to alteration. In other words, the metamorphic rocks and granites of different ages in the study area are not the origin of Dashuigou independent tellurium deposit. The ore-forming materials, namely, Te, Bi, etc. come from mantle exhalation or mantle plumes that cause alterations.

Various geochemical evidence shows that the study area is an area where the deep crust and mantle materials are relatively developed. The $\delta^{30}\text{SiNBS-28}\%$ of the deposit's schist samples indicate that the schist's protolith is basalt [1,8,11,12]. The REEs of the lower-middle Triassic phyllite, marble, and tourmaline quartz vein in the study area are similar to those of modern mid-ocean ridge tholeiite. The REE geochemistry indicated that the lower-middle Triassic phyllite evolved from basalt magma.

There is no doubt that the tellurium abundance

of the rocks in the study area is positively correlated with the intensity of the alterations that these rocks undergo. Strongly altered rocks almost always have high tellurium content.

In both the periphery of the mine and the mining area itself, all dolomite in the study area has high tellurium content. This is consistent with the fact that dolomite is one of the important tellurium carriers in the mining area. This also indicates that dolomite veins are one of the important indicators for searching for potential tellurium deposits in the research area. On the other hand, it also reminds us that understanding the origin of dolomite may be one of the key factors in deciphering the mineralization mechanism of the Dashuigou tellurium deposit.

Another noteworthy fact is that the ore body host strata, namely the upper part of the lower-middle Triassic schist, especially the banded marble in the lower part, has a higher tellurium content (samples #4, 7, 18, and 32 in **Table 2b**), which is much higher than the underlying coarse grained marble belonging to the same carbonatite. This seems to mean that the ore-forming materials are not concentrated in the ore body host strata through bottom-up diffusion and infiltration, otherwise the underlying coarse-grained marble should be richer in tellurium than the overlying fine-grained banded marble, but the opposite is true. That is to say, the ore-forming material is likely to move up along a relatively concentrated and unified tubular channel, ultimately emplace to form the deposit. The ore-bearing fluid or likely telluride ore magma from the deep underground, driven by temperature and pressure, migrates upwards along this tubular fault channel, successively passing through coarse-grained marble and fine-grained banded marble layers, entering the schist layers and forming deposits in the expansion structures within them. The finer and denser schist layers than marble serve as a barrier layer.

It should be pointed out that this is only a theoretical assumption based on the abundance and spatial distribution of tellurium in the surrounding rocks of the study area, and other various geological and geophysical evidence is needed to support it.

The altered, unaltered, or weakly altered rocks in the footwall of the tellurium ore bodies all have higher tellurium content than similar rocks in the hanging wall (**Tables 2a and 2b, Figure 9**). This may mean that the ore-forming material is not accumulated through horizontal lateral secretion, but rather comes from the deep. In other words, the ore-forming elements do not originate from the host rock, but from the deep.

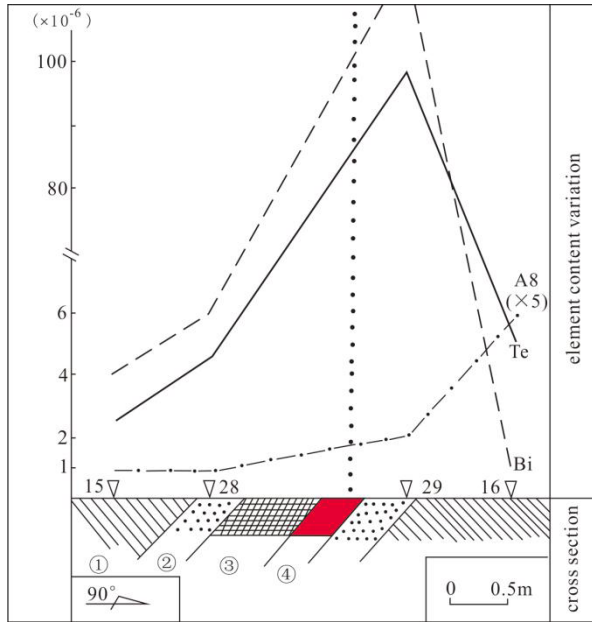


Figure 9. Cross section and trace element variation diagram of I-4 ore body in pit 1 of the mine.

① green schist, ② altered rock, ③ pyrrhotite vein, ④ tellurium ore body.

Bi and Te have almost identical patterns of change (**Tables 2a and 2b, Figures 8 and 9**). The abundance of Bi in Devonian rocks and granite is significantly higher than that in the Permian. In addition, the content of Bi in the Indosinian granite (0.89×10^{-6}) is also higher than that in the Chengjiang orogenic granite. In the Chengjiang granite, Bi tends to be enriched in alkaline granite rather than ordinary granite. But overall, the Bi content in these granites is still close to its abundance in the Earth's crust (0.17×10^{-6} , Taylor, 1964) and within the range of acidic igneous rocks. The abundance of Bi in acidic igneous rocks is 0.02×10^{-6} – 0.90×10^{-6} , with an average of 0.18×10^{-6} [29].

Durin Balkovskaya (1976) found through a de-

tailed study of the distribution of Bi in various ages of igneous rocks in the Kuraming Mountains of the former Soviet Union that the content of Bi significantly increased during the evolution process from early basic rocks to late acidic rocks, indicating that the enrichment of Bi in igneous rocks occurred in the late stages of each intrusive formation. After studying the distribution of Bi in the batholith of southern California and Iowa, Glenland (1976) reached a similar conclusion that Bi tends to accumulate in residual magma during magma differentiation [1,29].

The geochemical behavior of Bi mentioned above and its enrichment pattern in the study area indicates that the source and formation mechanism of the ore-forming material of the Dashuigou tellurium deposit is related to deep geological processes such as mantle plumes, but not directly related to the surrounding rocks.

6.2 As, Sn, Au, and Ag

The abundance of As in the Earth's crust is 1.7×10^{-6} (Vinogradov, 1962) or 1.8×10^{-6} (Taylor, 1964) [28-30]. In addition, the abundance of As in various rocks does not change much. In granite, neutral rocks, basalt, diabase, and gabbro, the abundance and distribution pattern of As are very consistent (Onich, H). Like Bi, As is mainly enriched in late rocks of magmatic differentiation series and tends to concentrate in residual solutions (Esson, J.R.) [28-30].

Arsenides are often found in the gasification products of volcanic processes. V. M. Goldschmidt discovered two types of arsenides, AsS and As₂S₃, in volcanic eruptions. W. Geilmann determined that two volcanic sulfur samples from West Java contained As of 62×10^{-6} and 9×10^{-6} , respectively. The average As content in the condensation water of the Hokkaido volcano in Japan is 0.49×10^{-6} . These constantly indicate a close relationship between As and volcanic exhalation. According to the related research, the intensity of metamorphism is inversely correlated with the As content of metamorphic rocks.

From **Tables 2a and 2b**, it can be seen that the As content of the vast majority of samples in the study area is lower than their crustal Clark value, and only

the average value of the Upper Permian samples is close to the crustal Clark value. The content of As in the middle and lower Triassic series around the mining area is slightly higher than its crustal Clark value (**Figure 8**), and the content of As in some strongly altered rocks is significantly increased. This also indicates that the As content is closely related to alteration, indirectly indicating that mineralization is controlled by deep geological processes and not related to surrounding rocks.

The Se content of almost all samples in the study area is below its detection limit, which is $< 0.1 \times 10^{-6}$. This may be equivalent to the crustal Clark value of Se (0.05×10^{-6} - 0.09×10^{-6})^[28,29], with only a few strongly altered rocks showing significant Se content (**Tables 2a and 2b**).

Research has shown that Se does not accumulate during the main crystallization and pegmatization stages of magma^[29]. However, during volcanic eruptions and gas generation hydrothermal processes, Se undergoes a certain degree of enrichment. The post magmatic hydrothermal activity stage is the main enrichment stage of Se and Te. Based on this, the enrichment of Se in the study area seems to be related to deep geological thermal events, such as mantle plumes.

The abundance of Au in various rocks in the study area is not high, lower or close to its Clark value in the Earth's crust, i.e. 0.004×10^{-6} (**Tables 2a and 2b, Figure 10**), with only a few altered rocks showing significantly higher Au abundance.

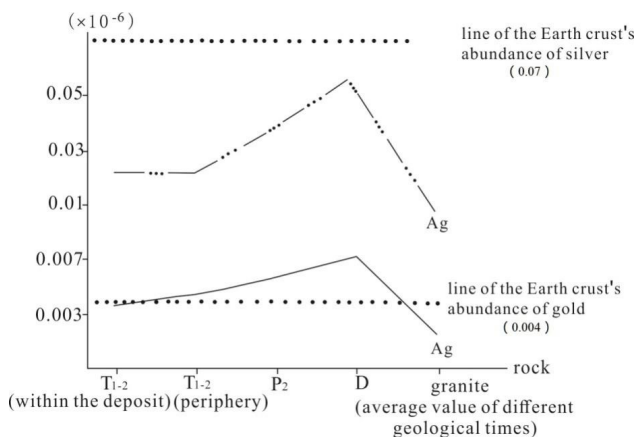


Figure 10. Comparison of Au and Ag contents in the country rocks and regional granites of different ages around the mining area.

The abundance of Au in the Devonian rocks is slightly higher than its Clark value in the Earth's crust, and the Au content is the highest in rocks of different ages in the study area. This is consistent with the fact that most of the gold deposits and gold showings in the study area occur in the Devonian system.

Ag and Au have obvious positive correlations and similar distribution patterns (**Figure 10**).

6.3 Cu, Pb, and Zn

The Clark value of Cu in the continental crust is 55×10^{-6} (Taylor, 1964)^[28,29]. The Cu content of most rock types in the study area is lower than its Clarke value (**Tables 2a and 2b, Figure 11**). There is only one sample from the Upper Permian and five samples from the lower-middle Triassic, including 3 strongly altered rock samples containing Cu above the Clark value. This also shows that the copper content has nothing to do with the country rock itself, but is closely related to deep geothermal events such as mantle plumes.

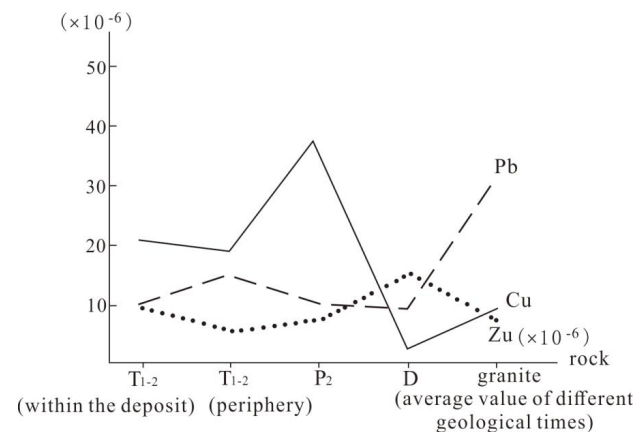


Figure 11. Comparison of Cu, Pb and Zn contents in the country rocks and regional granites of different ages.

The Clarke value of Pb in the Earth is 13×10^{-6} , and that of Pb in the Earth's crust is 10×10^{-6} - 16×10^{-6} (Li Tong, 1976)^[28,29]. Based on this and comparing **Tables 2a and 2b** and **Figure 11**, it can be seen that the Pb abundance of most rock types in the study area is lower than its crustal Clark value. Only the Chengjiang orogenic granites in the periphery of the mining area, and the lower-middle Triassic

samples from Miaoping-Liushapo in the periphery of the mining area contain significantly higher Pb. This may be related to the nearby Guanyinshan lead-zinc mine, but has nothing to do with the lead contained in the surrounding rocks.

The Clark value of Zn in the Earth's crust is shown in **Table 3**. The Zn content of about half of the samples in the study area is greater than or close to its crustal Clark value (**Tables 2a and 2b, Figure 11**), and has the following distribution rules:

Table 3. The Clark value of Zn in the Earth's crust.

Researcher	Vinogradov	Taylor	Song Miao	Weidelpol
Year	1962	1964	1966	1967
Abundance ($\times 10^{-6}$)	83	70	70	60

Source: ^[1].

The Zn content in acidic granite is higher than that in alkaline granite.

Regardless of the mining area or the periphery, the content of Zn in the Middle and Lower Triassic ore-hosting schist is higher than that in marble, and the strongly altered schist contains higher Zn.

No matter in the mining area or the periphery, the Zn content in all kinds of dolomite veins in the study region is low.

Combining the host rock's geology, geochemistry, and previous researchers' study on REE and silicon isotope of the lower-middle Triassic rocks ^[1,8-10,17-19], the following preliminary conclusions can be reached:

The ore-forming elements do not originate from various rocks around the deposit. The existence of numerous basalts from different geological ages in the study area, as well as the frequent and unusually active interactions between the crust and the upper mantle, all prove from one aspect that the deposit's ore-forming elements originate from the mantle.

Previous studies on sulfur isotopes and mineral fluid inclusions have also shown that the ore forming minerals of the Dashuigou tellurium deposit originated from the upper mantle ^[9,10].

Its enrichment mechanism is that these substances in the nanometer level from the mantle are enriched into

ore bodies through the unique nano-effect, and then were brought to the Earth's crust to settle down to form the deposit in the late Yanshanian orogeny ^[5,6,25].

7. Conclusions

In summary, this article draws the following conclusions:

The distribution of Te, Bi, As, Se, Cu, Pb, Zn, Au, and Ag in different rock types of different ages shows that the abundances of the main ore-forming elements Te, Bi, As, Se, Au, and Ag in the regional geological background are not high, generally lower than or close to their respective crustal Clark values. The enrichment of these elements is obviously closely related to the later alteration. The geological processes that cause this alteration and mineralization come from deep underground such as mantle plumes.

Mineralization is not achieved through horizontal or near-horizontal lateral secretion; that is, the ore-forming materials do not originate from ore-hosting wall rocks, but from deep.

The migration of deep metallogenic elements is not achieved through the diffuse infiltration between particles in the overlying formation rocks, but through non-widely distributed concentrated penetrating faults, such as the intersection of two groups of faults in different directions, or the expansion structure formed by the intersection of linear and circular structures.

Existing geophysical, geological and geochemical evidence shows that the study area located on the edge of the Qinghai-Tibet plateau is an area with an extremely active crust and upper mantle. It is both an area where geological structures including deep and large lithospheric faults are well developed and an area where mantle materials work well. It is under this very favorable geological background that the ore-forming elements such as tellurium were enriched in the upper mantle through nano-effects and then intruded along deep and large faults into appropriate parts of the crust to precipitate and form the deposit.

Author's Contributions

The whole research included in the paper was proposed and supervised by the first two authors J. Yin and S. Xiang. The chemical compositions were analyzed by the second and third authors H. Yin, H. Shi, and Y. Chao of this paper. All authors prepared and reviewed the manuscript and approved the final version of the manuscript.

Conceptualization: J. Yin; Investigation: J. Yin, S. Xiang, H. Yin, H. Shi, and Y. Chao; Project administration: J. Yin, S. Xiang; Writing—original draft: J. Yin.

Conflict of Interest

There is no conflict of interest.

References

- [1] Yin, J.Z., 1996. Shi jie shou li du li di kuang chuang de cheng kuang ji li ji cheng kuang mo shi (Chinese) [The first and only independent tellurium deposit in the world]. Chongqing Publishing House: Chongqing. pp. 190.
- [2] Chen, Y.C., Mao, J.W., Luo, Y.N., et al., 1996. Si chuan da shui gou di (jin) kuang chuang di zhi he di qiu hua xue (Chinese) [Geology and geochemistry of the Dashuigou tellurium (gold) deposit in Western Sichuan, China]. Atomic Energy Press: Beijing. pp. 146.
- [3] Luo, Y.N., Fu, D.M., Zhou, S.D., et al., 1994. Si chuan shi mian xian da shui gou di kuang chuang di zhi yu cheng yin (Chinese) [Genesis of the Dashuigou tellurium deposit in Sichuan Province of China]. Bulletin of Sichuan Geology. 14(2), 101-110.
- [4] Luo, Y.N., Cao, Z.M., Wen, C.Q., 1996. Da shui gou du li di kuang di zhi (Chinese) [Geology of the Dashuigou independent tellurium deposit]. Southwest Communication University Publishing House: Chengdu. pp. 30-45.
- [5] Yin, J.Z., 1996. The metallogenetic model and mineralizing mechanism of Dashuigou independent tellurium deposit in Shimian County, Sichuan; the first and the only independent tellurium deposit in the world. *Acta Geoscientia Sinica*. 17, 93-97.
- [6] Yin, J.Z., Shi, H.Y., 2019. Nano effect mineralization of rare elements-taking the Dashuigou tellurium deposit, Tibet Plateau, Southwest China as the example. *Academia Journal of Scientific Research*. 7(11), 635-642.
DOI: <https://doi.org/10.15413/ajsr.2019.0902>
- [7] Wang, R.C., Lu, J.J., Chen, X.M., 2000. Si chuan shi mian da shui gou di kuang chuang cheng yin tan tao (Chinese) [Genesis of the Dashuigou tellurium deposit in Sichuan Province, China]. *Bulletin of Mineralogy, Petrology and Geochemistry*. 4, 348-349.
- [8] Yin, J., Xiang, S., Chao, Y., et al., 2023. Petrochemical eigenvalues and diagrams for the identification of metamorphic rocks' protolith, taking the host rocks of Dashuigou tellurium deposit in China as an example. *Acta Geochimica*. 42(1), 103-124.
DOI: <https://doi.org/10.1007/s11631-022-00583-6>
- [9] Yin, J., Shi, H., 2021. Fluid inclusions and metallogenic conditions of the Dashuigou tellurium deposit, Tibet Plateau, southwest China. *Geology, Earth & Marine Sciences*. 3(3), 1-15.
DOI: <https://doi.org/10.31038/GEMS.2021331>
- [10] Yin, J., Shi, H., 2020. Mineralogy and stable isotopes of tetradyte from the Dashuigou tellurium deposit, Tibet Plateau, southwest China. *Scientific Reports*. 10(1), 4634.
DOI: <https://doi.org/10.1038/s41598-020-61581-3>
- [11] Geological Bureau of Sichuan Province, 1974. Zhong hua ren min gong he guo qu yu di zhi diao cha bao gao. 1: 200,000, Shi mian fu, Kuang chan (Chinese) [Regional geological survey report of the People's Republic of China. 1: 200,000, Shimian Sheet, Minerals]. Geological Bureau of Sichuan Province: Chengdu.
- [12] Ding, T.P., Jiang, S.Y., Wan, D.F., et al., 1995. Gui tong wei su di qiu hua xue (Chinese) [Silicon isotope geochemistry]. Geological Publishing House: Beijing. pp. 122.
- [13] Cao, Z.M., Luo, Y.N., 1994. Zhong guo si chuan

- mo zhuang di kuang cheng yin ji cheng kuang xu lie. Zhong guo kuang wu, yan shi ji di qiu hua xue yan jiu jin zhan (Chinese) [Mineral sequence and ore genesis of the Sichuan telluride lode deposit in China. New research progresses of the mineralogy, petrology and geochemistry in China]. Lanzhou University Publishing House: Lanzhou. pp. 476-478.
- [14] Cao, Z.M., Wen, C.Q., Li, B.H., et al., 1995. Shou li du li di kuang chuang cheng yin tan tao (Chinese) [Genesis of the Dashuigou tellurium deposit in Sichuan Province of China]. *Science China (B)*. 25(6), 647-654.
- [15] Yin, J.Z., Shi, H.Y., 2020. Mineralogy of tsu-moite based on samples from the Dashuigou tellurium deposit, Tibet plateau, China. *Geological Society of America Abstracts with Programs*. 52(6).
DOI: <https://doi.org/10.1130/abs/2020AM-349615>
- [16] Yin, J.Z., Zhou, J.X., Yang, B.C., et al., 1994. Zhong guo si chuan da shui gou du li di kuang de di zhi te zheng (Chinese) [Geological characteristics of the Dashuigou tellurium deposit in Sichuan Province, China]. *Earth Science Frontiers*. 1(4), 241-243.
- [17] Yin, J.Z., Chen, Y.C., Zhou, J.X., et al., 1995. Shi jie shou li du li di kuang chuang fu kuang wei yan de yuan yan hui fu (Chinese) [Original rock of the host rock of the Dashuigou independent tellurium deposit in Sichuan Province, China]. *Bulletin of Mineralogy, Petrology and Geochemistry*. 2, 114-115.
- [18] Yin, J.Z., Chen, Y.C., Zhou, J.X., et al., 1996. Shi jie shou li du li di kuang chuang fu kuang wei yan de di zhi di qiu hua xue yan jiu (Chinese) [Geology and geochemistry of host rocks of the Dashuigou independent tellurium deposit in Sichuan Province, China]. *Journal of Changchun University of Earth Sciences*. 26(3), 322-326.
- [19] Yin, J.Z., Chen, Y.C., Zhou, J.X., et al., 1996. Si chuan shi mian da shui gou du li di kuang chuang shi bian yan de di zhi di qiu hua xue yan jiu (Chinese) [Geology and geochemistry of altered rocks of the Dashuigou independent tellurium deposit in Sichuan Province, China]. *Journal of Xi'an College of Geology*. 18(4), 19-25.
- [20] Chen, Y.C., Yin, J.Z., Zhou, J.X., 1994. The first and only independent tellurium ore deposit in Dashuigou, Shimian County, Sichuan Province, China. *Scientia Geologica Sinica*. 3(1), 109-113.
- [21] Chen, Y.C., Yin, J.Z., Zhou, J.X., et al., 1994. Si chuan shi mian xian da shui gou du li di kuang chuang di zhi te zheng (Chinese) [Geology of the Dashuigou independent tellurium deposit of Sichuan Province]. *Acta Geoscientia Sinica*. 29(2), 165-167.
- [22] Yin, J.Z., Zhou, J.X., Yang, B.C., 1994. Rock-forming minerals and ore-forming minerals of the Dashuigou tellurium ore deposit unique in the world—A preliminary study. *Scientia Geologica Sinica*. 3(2), 197-210.
- [23] Yin, J.Z., Chen, Y.C., Zhou, J.X., 1994. Zhong guo si chuan da shui gou du li di kuang de kuang wu xue yan jiu (Chinese) [Mineralogical research of the Dashuigou independent tellurium deposit in Sichuan Province, China]. *Bulletin of Mineralogy, Petrology and Geochemistry*. 3, 153-155.
- [24] Yin, J., He, D., Yin, Y., et al., 2022. On ore from the Dashuigou tellurium deposit, Tibet Plateau, Southwest China. *European Journal of Applied Sciences*. 10(6), 458-472.
DOI: <https://doi.org/10.14738/aivp.106.13599>
- [25] Yin, J.Z., Chen, Y.C., Zhou, J.X., et al., 1995. K-Ar isotope evidence for age of the first and only independent tellurium deposit. *Science Bulletin*. 40(22), 1933-1934.
- [26] Shen, F.Q., 1985. Trace elements geochemistry of igneous rocks assemblage in Panxi rift. *Scientific Sinica*. (9), 844-855.
- [27] Zhang, Q.S., 1984. Zhong guo zao qian han wu ji di zhi ji cheng kuang zuo yong (Chinese) [Geology and metallogeny of the early Precambrian in China]. Jilin People Press: Changchun. pp. 536.
- [28] Li, T., 1976. Di qiu zhong hua xue yuan su feng du (Chinese) [Abundance of chemical elements

- in the Earth]. *Geochemistry*. 3, 167-174.
- [29] Liu, Y.J., Cao, L.M., Li, Z.L., et al., 1984. Yuan su di qiu hua xue (Chinese) [Element geochemistry]. Science Press: Beijing. pp. 510.
- [30] Yin, J., Xiang, S., Yang, K., et al., 2023. Review of tellurium resources in the world and in China. *Advances in Social Sciences and Management*. 1(1), 41-51.

EDITORIAL

Editorial for *Advances in Geological and Geotechnical Engineering Research*: Vol. 5 Issue 4 (2023)

Amin Beiranvand Pour 

Institute of Oceanography and Environment (INOS), Universiti Malaysia Terengganu (UMT), Kuala Nerus, Terengganu, 21030, Malaysia

1. Introduction

The scope of *Advances in Geological and Geotechnical Engineering Research* journal covers a variety of geology and environmental earth sciences. This journal is preparing to rivet a diversity of research and support the Earth in the imminent future. The achievements of articles presented in this volume are summarized in the following section.

2. Summary of paper presented in Vol. 5, Issue 4 (2023)

Rasouli and Vaseashta ^[1] studied groundwater quality assessment in Pul-e-Charkhi region, Kabul, Afghanistan for different types of usage, such as

drinking water, agriculture, and industries. The study presented the assessment of groundwater quality observed on several water samples taken from water supply sources in the Pul-e-Charkhi region, which is located near the eastern part of Kabul and has seen steady growth in population after the U.S. military left Afghanistan. The Pul-e-Charkhi region has experienced momentous industrial growth ranging from pharmaceuticals, metals, auto-repair, construction, and even bakeries—all producing CO and CO₂ emissions as well as a mixture of waste discharge in the water basin including micro/nano plastics, metals, volatile organic compounds, and new and emerging contaminants. The contaminants in groundwater were determined to observe what restrictions might pose for recycling and reusing. The samples were

*CORRESPONDING AUTHOR:

Amin Beiranvand Pour, Institute of Oceanography and Environment (INOS), Universiti Malaysia Terengganu (UMT), Kuala Nerus, Terengganu, 21030, Malaysia; Email: beiranvand.amin80@gmail.com

ARTICLE INFO

Received: 14 November 2023 | Accepted: 16 November 2023 | Published Online: 22 November 2023

DOI: <https://doi.org/10.30564/agger.v5i4.6080>

CITATION

Pour, A.B., 2023. Editorial for *Advances in Geological and Geotechnical Engineering Research*: Vol. 5 Issue 4 (2023). *Advances in Geological and Geotechnical Engineering Research*. 5(4): 56-58. DOI: <https://doi.org/10.30564/agger.v5i4.6080>

COPYRIGHT

Copyright © 2023 by the author(s). Published by Bilingual Publishing Group. This is an open access article under the Creative Commons Attribution-NonCommercial 4.0 International (CC BY-NC 4.0) License. (<https://creativecommons.org/licenses/by-nc/4.0/>).

analyzed for temperature, electro-conductivity, dissolved oxygen, total dissolved solids, salinity, pH, color, turbidity, hardness, chemicals, and heavy metals. The groundwater samples and parameters showed virtuous results with national and international standards, indicating that water can be recycled using standard coagulation, flocculation, and bleaching methods.

Oborie et al.^[2] integrated GIS with the Generalized reciprocal method (GRM) for determining foundation bearing capacity in Opolo, Yenagoa Bayelsa State, Nigeria. The study utilized Geographic Information System (GIS) with the Generalized Reciprocal Method (GRM) for construction planning in the region. The near-surface seismic refraction surveys were conducted along three designated lines, utilizing ABEM Terraloc Mark 6 equipment, Easy Refract, and ArcGIS 10.4.1 software. Key geotechnical parameters essential for soil characterization at potential foundation sites were determined using the methodology. Three different geoseismic layers were identified, including (1) the uppermost layer, within a depth of 0.89 to 1.50 meters, exhibited inadequate compressional and shear wave velocities, (2) the second layer (1.52 to 3.84 m depth) displayed favorable geotechnical parameters, making it suitable for various construction loads, (3) the third layer (15.00 to 26.05 m depth) exhibited varying characteristics. The GIS analysis emphasized the unsuitability of the uppermost layer for construction, while the second and third layers were found to be fairly competent and suitable for shallow footing and foundation design. The results highlighted the variations in soil competence in the study area, which can guide site selection for specific projects and inform decisions about foundation types and construction techniques.

Yin et al.^[3] identified the origin of the Dashuigou independent tellurium deposit at the southeastern Qinghai-Tibet plateau based on the abundance of trace elements in the country rocks. Abundances of the main ore-forming elements such as Te, Bi, As, Se, Au, and Ag are not high in the regional geological background, normally lower or close to their respective crustal Clark values, but almost all altered

country rocks contain high levels of ore-forming elements. This designates that the deposit's ore-forming elements do not come from the country rocks and the geological thermal events causing alteration and mineralization originated from depths and may be related to mantle plumes. The migration of deep metallogenic elements is not achieved through the diffuse infiltration between particles in the overlying formation rocks, but through non-widely distributed concentrated penetrating faults, such as the intersection of two groups of faults in different directions, or the expansion structure formed by the intersection of linear and circular structures. Existing geophysical, geological and geochemical maps show that the study area is located on the edge of an extremely active crust and upper mantle in the Qinghai-Tibet plateau. Geological structures including deep and large lithospheric faults are well developed in this zone. This is a favorable geological background that the ore-forming elements such as tellurium were enriched in the upper mantle through nano-effects and then intruded along deep and large faults into appropriate parts of the crust to precipitate the tellurium deposit.

3. Concluding remarks

The considerate and thoughtful comments conveyed by the reviewers enriched each of the papers published in this volume. We would like to express our appreciation to the Editorial Office, all authors and reviewers who contributed their time, research, and speciality for this volume. We hope to receive a variety of manuscripts from different fields in the future.

Conflict of Interest

There is no conflict of interest.

References

- [1] Rasouli, H., Vaseashta, A., 2023. Groundwater quality assessment in Pul-e-Charkhi Region, Kabul, Afghanistan. *Advances in Geological and*

- Geotechnical Engineering Research. 5(4), 1-21.
DOI: <https://doi.org/10.30564/agger.v5i4.5949>
- [2] Oborie, E., Desmond, E., 2023. Integration of GIS with the generalized reciprocal method (GRM) for determining foundation bearing capacity: A case study in Opolo, Yenagoa Bayelsa State, Nigeria. *Advances in Geological and Geotechnical Engineering Research*. 5(4), 22-40.
DOI: <https://doi.org/10.30564/agger.v5i4.5969>
- [3] Yin, J., Xiang, S., Yin, H., et al., 2023. Origin of Dashuigou independent tellurium deposit at the southeastern Qinghai-Tibet plateau: Based on the abundances of trace elements in the country rocks. *Advances in Geological and Geotechnical Engineering Research*. 5(4), 41-55.
DOI: <https://doi.org/10.30564/agger.v5i4.5967>

ARTICLE

Geophysical Approach for Groundwater Resource Assessment: A Case Study of Oda Community Akure, Southwestern Nigeria

S. J. Abe, I. A. Adeyemo, O. J. Abosede-brown*

Federal University of Technology Akure, Ondo State, 340110, Nigeria

ABSTRACT

The geophysical investigation for groundwater was carried out at Oda town, Akure south local government area of Ondo State. Fourteen (14) points were sounded using a Schlumberger array with AB/2 of 80 m and the resulting geoelectric parameters were used in the estimation of the aquifer layer parameters of the subsurface. The first layer resistivity value ranges from 29 to 164 Ωm and thickness ranges from 0.6 to 2.5 m. The second layer has a resistivity value ranging from 21-1361 Ωm with a thickness ranging from 1.5 m to 14.6 m. The third layer resistivity value is from 68 to 297 Ωm with thickness ranging from 4 m to 12.4 m. The fourth layer which is the deepest layer has a resistivity value ranging from 180 to 4364 Ωm with depth ranging from 4 m to 19.5 m. The parameters interpreted from the geoelectric data were used to generate the aquifer thickness and resistivity maps, with bedrock relief which were combined to produce the groundwater potential map of the area. These maps were used to characterise the study area into low to high groundwater potential zones. The southwestern and eastern parts were identified as productive groundwater potential zones. The result was validated by taking water column depth from eight existing hand-dug wells. A significant correlation was obtained between the groundwater potential model and the well water column. The surveyed area is generally suitable for hand-dug well aside from the north-eastern part where groundwater potential is low and water volume is observed.

Keywords: Geoelectric; Aquifer; Lithology; Bedrock

1. Introduction

Groundwater is an invaluable water supply source

for agricultural, industrial and domestic use in the world. Thus, the search for excellent and quality groundwater is remarkably significant to human

*CORRESPONDING AUTHOR:

S. J. Abe, Federal University of Technology Akure, Ondo State, 340110, Nigeria; Email: jsabe@futa.edu.ng

ARTICLE INFO

Received: 19 September 2023 | Revised: 13 November 2023 | Accepted: 14 November 2023 | Published Online: 23 November 2023

DOI: <https://doi.org/10.30564/agger.v5i4.5978>

CITATION

Abe, S.J., Adeyemo, I.A., Abosede-brown, O.J., 2023. Geophysical Approach for Groundwater Resource Assessment: A Case Study of Oda Community Akure, Southwestern Nigeria. *Advances in Geological and Geotechnical Engineering Research*. 5(4): 59-69. DOI: <https://doi.org/10.30564/agger.v5i4.5978>

COPYRIGHT

Copyright © 2023 by the author(s). Published by Bilingual Publishing Group. This is an open access article under the Creative Commons Attribution-NonCommercial 4.0 International (CC BY-NC 4.0) License. (<https://creativecommons.org/licenses/by-nc/4.0/>).

existence. It is the primary supply of fresh water in several world regions ^[1]. The need for water is on the rise due to its incredible quality, low vulnerability to pollution, drought resistance, relative abundance, etc.

Water is obtained from two main natural sources: surface water such as rivers, freshwater lakes, streams, etc. and underground water such as boreholes and well water ^[2]. It is considered to be a universal solvent due to its unique chemical properties which means it is able to alter the properties of different compounds ^[3]. Water covers about 71% of the earth's surface as oceans and groundwater respectively ^[4]. It has been found that approximately one-third of the world's population uses groundwater for drinking. The major source of freshwater is the aquifer. Aquifers contain over 90% of the total fresh water available for human use ^[5]. The role of geophysics is important in groundwater studies. The method has helped in detecting the availability, quality and quantity of groundwater over the years ^[1]. The geophysical method can be used to map sub-surface lithology sequences and concealed geological structures like fractures, faults, joints, etc., which can be favourable for the presence of groundwater especially in the basement complex environment, hence its importance in groundwater potential evaluation. Groundwater is usually associated with low yield and the increasing demand for water and the cost involved in drilling boreholes therefore requires the application and the proper use of geophysical investigation techniques to locate high-yielding aquifers ^[6]. Geophysical investigation using electrical method involves the measurement of geo-electric parameters such as layer resistivity, thickness and depth for each lithological unit ^[7]. These parameters can be used to explain the subsurface hydrological condition and groundwater potentiality assessment.

It is due to this that a geophysical survey using a vertical electrical sounding technique was employed to delineate the lithology underlying the ground surface in the area which is used to study the groundwater potential. This is an effective method of inves-

tigating the subsurface without interfering with the hydrogeological system. To this effect, the electrical method has been successfully used to characterize the subsurface, especially the Vertical electrical sounding technique. Conclusively, these geo-electric parameters are superimposed to produce a comprehensive map showing the groundwater potential of the area.

1.1 Description and geomorphology of the study area

The site is located at Oda Community, Akure South local government, Ondo State, Nigeria. It can be accessed by road from the Akure Shoprite and the area lies within the central senatorial District of Ondo state. The study area is situated within geographic grids between 746400 m to 747300 m (Eastings) and 793000 m to 794000 m (Northings) defined by Minna-Nigeria 31N datum of the Universal Traverse Mercatum (UTM) as shown in **Figure 1** with topographic elevation ranging from 362 m to 325 m. **Figure 2** is a map showing the elevation of the study area.

It has a seasonal climate characterised by dual seasons. The rainy season is from April to October, with rainfall of about 1524 mm per year. The average temperature is about 27 °C during harmattan (December-February) and 32 °C in March with an annual relative humidity of about 80%. The natural vegetation is tropical rainforest (en.wikipedia.org/wiki/Akure).

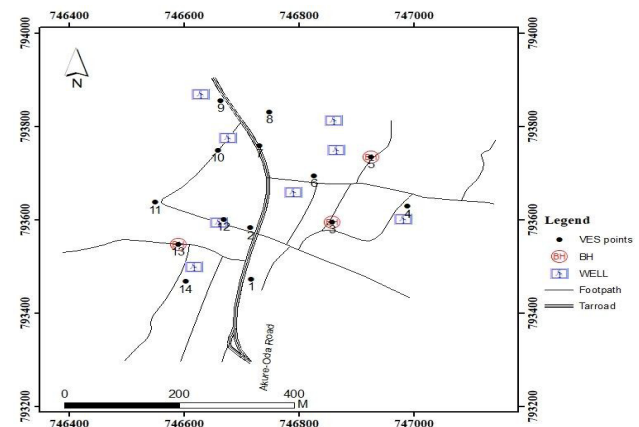


Figure 1. Basemap of the study area.

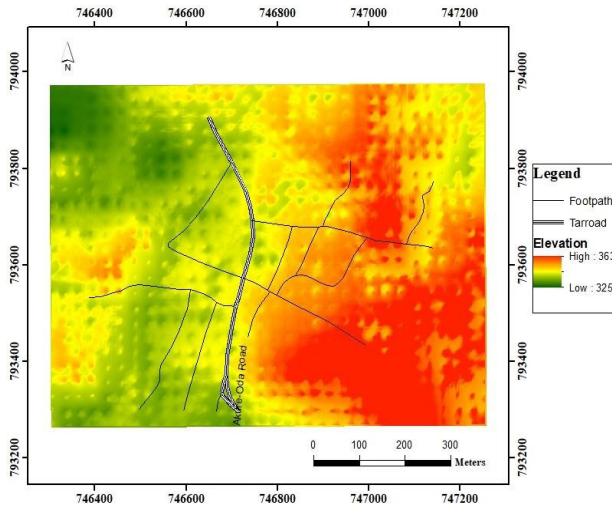


Figure 2. Elevation of the study area.

1.2 Local geology and hydrogeologic settings

Akure is underlain by the Precambrian Basement Complex rocks of Southwestern Nigeria which is typical of the Migmatite gneiss [8], comprising undifferentiated granite, Charnokitic rocks, medium to coarse granite and Migmatite gneiss rocks. The area is monolithic of Migmatite gneiss (**Figure 3**) and is highly weathered and fractured, with the prominent direction of foliation lying between 178° and 182° with easterly dips of 46° and 102° [9]. The hydrogeology system of this study area belongs to the hydrologic system of the basement complex terrain of Nigeria and groundwater is usually found in the weathered mantle, joints, and fractured bedrock in the surface. The basement rock may contain faulted areas, and incipient and fractured systems derived from tectonic activity earlier experienced. Therefore, the detection of these hydrogeologic structures may enhance the location of groundwater prospective zones in a typical basement setting.

2. Methodology

The vertical electrical sounding technique was used. **Figure 4** is a map showing the VES locations. Fourteen VES points in total were sounded and the electrode spread was varied from 1 to 80 m while the potential electrode ranged from 0.25 m to 5 m.

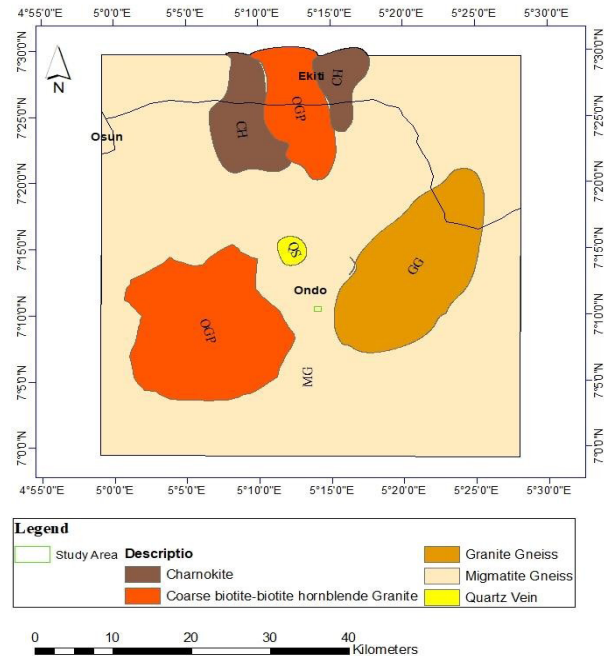


Figure 3. Geology map of Akure showing the study area (After NGS 2008).

The apparent resistivity data generated from the VES survey were presented as depth sounding curves on bi-log paper. After acquiring all the data, it was then checked and corrected for error in order to have a good result. The data was manually curve matched and interpreted with WINRESIST software.

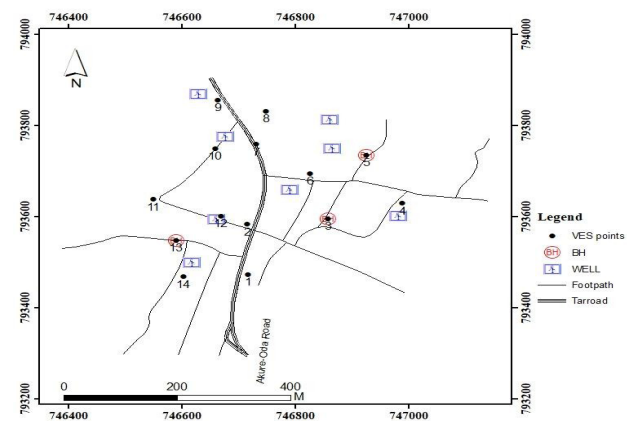


Figure 4. VES location map.

3. Results and discussion

3.1 Geoelectric sounding results

The geoelectric layers delineated across the study

area ranged from three to four layers. The first layer resistivity value ranges from 29 to 164 Ωm and thickness ranges from 0.6 to 2.5 m. The second layer has a resistivity value ranging from 21-1361 Ωm with a thickness ranging between 1.5 m to 14.6 m. The third layer resistivity value is from 68 to 297 Ωm with thickness ranging between 4 m to 12.4 m. The fourth layer which is the deepest layer has a resistivity value ranging from 180 to 4364 Ωm with a depth ranging from 4 m to 19.5 m as shown in **Table 1** below.

The sounding curve types obtained from the study area are A, AA, H, HA and KH curve types. A and H curve types have three layers while the four layers comprise AA, HA and KH. The A and H type curves

are the predominant curve type in the area, accounting for 36% each, and KH type curve accounts for 14% each and AA, HA curve type accounts for 7% of curve type in the study area. The KH curve type indicates a fractured or weathered layer between the second layer and basement rock which is often associated with groundwater possibilities. The H curve has a weathered layer as the middle layer which is usually regarded as the saturated zone in the basement complex and the aquifer varies depending on the material that overlain it. The resistivity values of the layers alone are not sufficient enough to serve as a guide during the investigation of areas for groundwater, the thickness and depth of each layer are also carefully considered in the assessment of groundwater.

Table 1. Geo-electric resistivities and thicknesses.

VES NO	Layer NO	Layer resistivity (Ωm)	Thickness (m)	Depth (m)	Curve type	Nature of rocks
1	3	94	1.1	----	H	Top soil
		21*	3.3	1.1		Weathered layer
		247	----	4.4		Fresh basement
2	4	46	1.4	---	KH	Top soil
		356	1.5	1.4		Weathered layer
		68*	4.5	2.9		Weathered basement
3	3	344	----	7.4	A	Fresh basement
		44	1.7	----		Top soil
		105*	11.6	1.7		Weathered layer
4	4	965	----	13.3	KH	Fresh basement
		57	2.5	----		Top soil
		530	4.6	2.5		Weathered layer
5	4	88*	12.4	7.3	AA	Weathered basement
		664	0.8	19.5		Fresh basement
		49	2.1	0.8		Top soil
6	3	66	1.1	0.8	A	Weathered layer
		297*	----	2.9		Weathered basement
		470	----	4.0		Fresh basement
7	3	29	1.1	-----	H	Top soil
		113*	8.0	1.1		Weathered layer
		340	----	9.1		Fresh basement
8	3	49	2.7	----	A	Top soil
		16*	7.3	2.7		Weathered layer
		460	-----	10.0		Fresh basement
		83	0.9	----		Top soil
		106*	3.9	0.9		Weathered layer
		338	-----	4.7		Fresh basement

Table 1 continued

VES NO	Layer NO	Layer resistivity (Ωm)	Thickness (m)	Depth (m)	Curve type	Nature of rocks
9	3	77	0.6	----	A	Top soil
		361*	6.9	0.6		Weathered layer
		1308		7.5		Fresh basement
10	3	54	1.1	----	H	Top soil
		29*	5.6	1.1		Weathered layer
		180	----	6.7		Fresh basement
11	3	164	0.6	----	A	Top soil
		332*	5.7	0.6		Weathered layer
		4364	----	6.3		Fresh basement
12	4	148	0.6	----	HA	Top soil
		59	1.2	0.6		Weathered layer
		145*	4.0	1.8		Weathered basement
13	3	244	----	5.9	H	Fresh basement
		215	0.9	----		Top soil
		62*	14.6	0.9		Weathered layer
14	3	1392	----	15.5	H	Fresh basement
		64	1.0	----		Top soil
		29*	5.9	1.0		Weathered layer
		234	----	6.9		Fresh basement

Note: * = aquifer layer.

3.2 Geo-electric section results

Geo-electric section 1

Figure 5 shows the geo-electric section observed on each VES point along the southwest-northeast trend. VES11, VES 10, VES 7, and VES 8 were shown. It comprises 3 layers. The resistivity of the top soil is from 49 to 164 Ωm and a thickness of 0.6 to 2.7 m, the weathered layer had a resistivity range of 16 to 332 Ωm and a thickness of 3.9 to 7.3 and the resistivity of the fresh basement ranged from 180 to 4364 Ωm with a depth range from 4.7 to 10 m. VES 8 is observed at a higher elevation which is a basement ridge indicating the region is of low groundwater potential.

Geo-electric section 2

Figure 6 shows the geoelectric section along the southwest-northeast trend drawn through VES 13, 12, 2, 6 and 5. It comprises three to four geoelectric layers. The resistivity of the top soil ranged from 39 to 215 Ωm and thickness between 0.6 to 1.4 m, the weathered layer had a resistivity range of 59 to 356 Ωm and thickness of 1.2 to 14.6 m. Beneath this layer in VES 13 and 6 is the fresh basement while the other VES 12, VES 2 and VES 5 have beneath them

the weathered basement with a resistivity range of 68 to 297 Ωm and thickness range of 1.1 to 4.5 m. VES 6 is seen to be on a depressed elevation and with the highest thickness. It has a good groundwater potential.

Geo-electric section 3

Figure 7 is a geoelectric section drawn through VES points 1, 3, 4 and 14 in the southwest to northeast trend comprising three to four geoelectric layers. The top soil has resistivity values ranging from 44 to 94 Ωm and thickness values between 0.6 and 2.5 m. Beneath the top soil layer, the layer identified as the aquifer unit characterized by resistivity values between 21 and 104 Ωm and thickness ranging from 3.3 and 11.6 m respectively, diagnostic of the weathered basement.

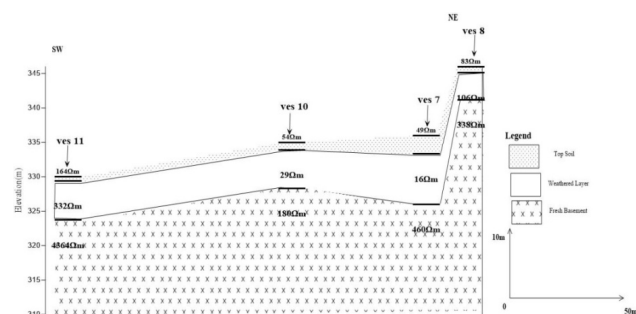


Figure 5. Geo-electric section 1.

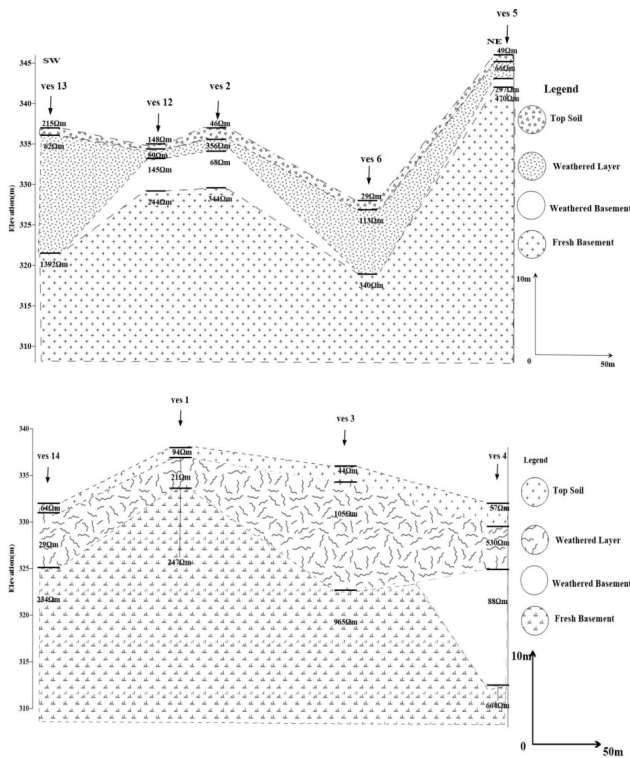


Figure 7. Geo-electric section 3.

3.3 Isopach and iso-resistivity map of the study area

Aquifer resistivity map

This is a contoured map that depicts the resistivity of the aquifer layer in the study area. The area was characterised into four zones very high resistivity, high resistivity, moderate and low resistivity. These zones have been indicated by different colour types as presented in **Figure 8**. Areas of low resistivity values between 16 to 100 Ωm on the map are depicted in green colour indicating highly saturated zones. This occupies the major zones in the study area. These areas occupy the central southern part and northern part of the area.

Areas with very high resistivity values are indicated by the red colour and range from 251 to 360 Ωm . These areas occupy the extreme western, eastern, northern parts of the study area excluding the location of VES 12 which has moderate resistivity value of 145 Ωm and is indicated by the light green colour. Areas with high resistivity have low conductivity which indicates low moisture content while ar-

reas with low resistivity value have high conductivity which indicates high moisture content. Hence these values give insight into the hydrogeological features.

Aquifer thickness map

The thickness varies from 1.1 to 14.5 m (**Figure 9**). The aquifer unit in the entire area is generally characterized by moderate thickness ranging from 6 to 10 m. They are indicated with light green colour on the map. Zones of low thickness are observed in the northern, north-eastern and southern parts of the area. They are indicated with green colour. However, some areas have relatively thick aquiferous units with thickness greater than 10 m i.e., VES points 3, 4, and 13. They are indicated in yellow colour on the map. Thickness plays an important role in groundwater abstraction, areas with high aquifer thickness are considered of good potential in hydrogeology.

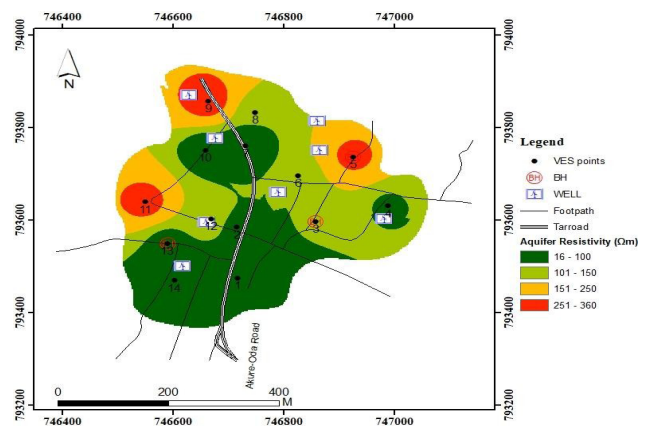


Figure 8. Aquifer resistivity map of the study area.

Bedrock relief map

This shows the relief of the basement rock in the area (**Figure 10**). It was derived by subtracting the overburden thickness values from the elevation values all measured in meter. This indicates the hydro-topographic condition of the basement rock underlying the study area. According to Adiat et al., (2009), groundwater flows from areas of high pressure (such as bedrock ridge) to areas of low pressure (such as bedrock depression) [9]. The study area is divided into basement ridges, slopes and depressions. The basement depression areas are indicated with green colour on the map and they are found in the western and eastern part of the study area while the slope area is observed in the central part

indicated with yellow colour. The ridge is indicated with red colour and is located in the southern part and north-eastern part of the study area. Areas with depressions on the map have a significant role in groundwater potentiality because they act as groundwater collection points as a result of flow directed towards these areas from the basement ridge through the slope area which is an intermediate between the two.

3.4 Groundwater potential mapping

The groundwater potential map was generated by overlaying the aquifer parameters extracted from the geoelectric results above using the weighted overlay algorithm in ArcGIS and by assigning weight to the three parameters using Analytical Hierarchy Process (AHP).

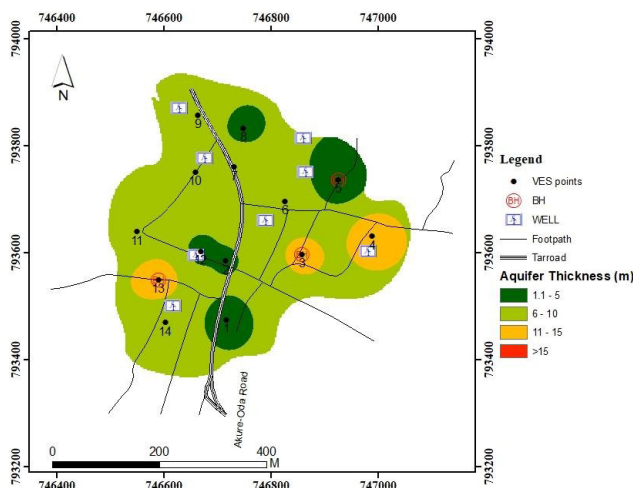


Figure 9. Aquifer thickness map of the study area.

3.5 Weight assignment

Weights were assigned to the isopach and iso-resistivity maps of the study area using Analytical Hierarchy Process (AHP) in order to overlay them to produce the groundwater potential map of the study area. Weight describes the degree of influence of each factor with respect to the groundwater potential of the study area. The resulting priority vector and weights obtained by estimating the average of all the elements of each row, **Tables 2 and 3** respectively below indicate that in terms of criterion aquifer

thickness is prioritized, with alternatives bedrock relief ranking second and aquifer resistivity ranking third and the assigned weight for the parameters from the AHP process are 0.48, 0.41 and 0.11 respectively. The result has a consistency ratio of 3% which shows that the result is accepted and the decision is valid. The result was used to assign weight to the geo-electric parameters.

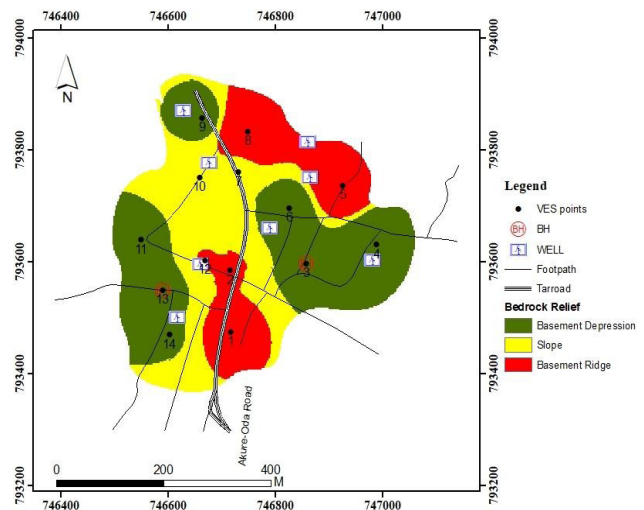


Figure 10. Bedrock relief map of the study area.

3.6 Estimation of groundwater potential index

This is the sum of products of weights (W) and ratings (R) overall factors used for the estimation. Mathematically, it is expressed as:

$$\text{Groundwater Potential Index} = \text{ArR} * \text{ArW} + \text{AtR} * \text{AtW} + \text{BrR} * \text{BrW} \quad (1)$$

where A.R = aquifer resistivity, A.T = aquifer thickness, B.R = bedrock relief and subscript R and W represent rating and weight respectively.

The weights were substituted into (1) to become:

$$\text{Groundwater Potential Index} = 0.11\text{Ar} + 0.48\text{AtR} + 0.41\text{BrR} \quad (2)$$

3.7 Groundwater potential index map

This was generated using Equation (2) in the ArcGIS environment using the weighted overlay algorithm. The individual maps were reclassified first into 4 rates depending on their contribution

factor. The weighted overlay was used to classify the groundwater potential of the study area into four areas; namely the low, moderate, high and very high potential regions. Areas of low potential were indicated by the colour blue. These areas occupied the north-eastern part of the area and the area VES 5 and 10 were sited. Areas of moderate potential were indicated by the colour green and it is predominant in the area. These areas mostly occupied the central area covering the western, north-western and north-eastern parts. The southwestern and eastern parts are occupied by high to very high groundwater potential zone which is indicated by the colours red and orange. VES 13 and 3 are very high potential points and they also coincide with the existing borehole in the area, this indicates the accuracy of the model (Figure 11).

3.8 Groundwater potential index map validation

The groundwater potential index map was validated by taking the hydrological parameters of 8 existing hand-dug wells in the area. The parameters include static water level, well depth and water column. The water column level was obtained by subtracting the static water level from the well depth. These parameters are valuable in validating the accuracy of the calculated groundwater potential index

map taking into cognizance the relationship between the map and the well parameters.

Table 4 shows the results of the validation parameters and their groundwater potential category. The hand-dug wells depth ranges from 6.27 to 12.6 m, static water level ranges from 6.36 to 15 m and the water column varies between 0.09 to 4 m. The water column which implies the volume of water present in the well was used for the final validation. It was categorized into three classes namely low, moderate and high depending on the column length in meter. This was superimposed on the established groundwater potential index map for correlating both results (Figure 12).

The two wells with low water volume (0.09-0.1 m) coincide with low-moderate groundwater potential zones in the north-eastern part of the study area, while the remaining wells have water volumes ranging from 1.18 to 4 m fall and are categorized as moderate to high potential. These wells coincide with the moderate to high groundwater potential zones.

The ratings of the well water column significantly coincide with the groundwater potential index map of the study area, which implies that the groundwater potential index validates the groundwater productivity of the study area. Hence, the generated groundwater potential map has good prediction accuracy.

Table 2. A matrix of pair-wise comparisons of the parameters for the AHP process.

	A.R	A.T	B.R
A.R	1	1/5	1/3
A.T	5	1	1
B.R	3	1	1
Column sum	9	2.2	2.33

Note: A.R = Aquifer Resistivity, A.T = Aquifer Thickness, B.R = Bedrock Relief.

Table 3. Weight determination.

	A.R	A.T	B.R	Weights
A.R	1/9=0.11	0.2/2.2=0.091	0.333/2.33= 0.143	0.344/3 = 0.11
A.T	5/9=0.556	1/2.2=0.455	1/2.33=0.429	1.44/3=0.48
B.R	3/9=0.333	1/2.2= 0.455	1/2.33=0.429	1.217/3=0.41
Column sum	1	1	1	1

Note: Consistency ratio = 3.0.

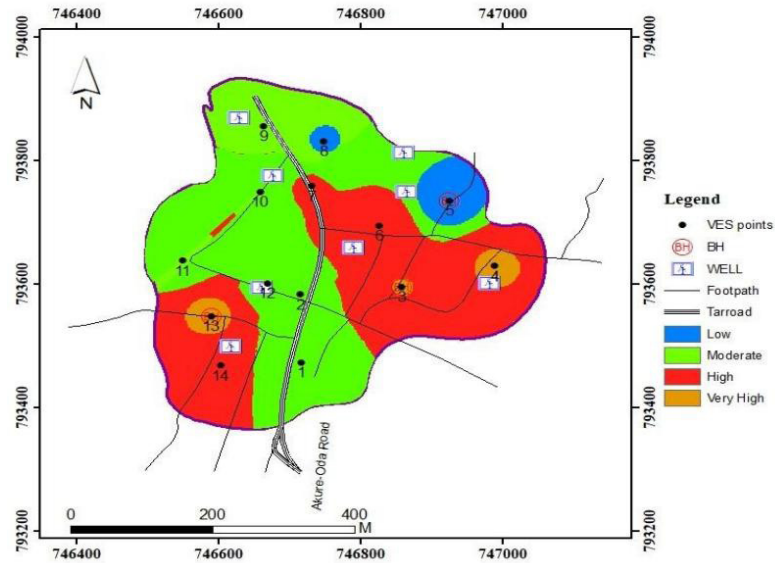


Figure 11. Groundwater potential map of the study area.

Table 4. Hydrological parameters of the hand-dug wells in the study area.

S/N	Longitude	Latitude	Well depth (m)	Static water level (m)	Water column (m)	Groundwater potential category
1	5.2353	7.1754	12	15	3	High
2	5.2357	7.1761	11	15	4	High
3	5.2362	7.1739	12.6	12.7	0.1	Low
4	5.2346	7.1746	11.81	13.6	1.18	Moderate
5	5.2328	7.1736	8.18	10	1.18	Moderate
6	5.2335	7.1740	6.27	6.36	0.0	Low
7	5.2336	7.1757	8.18	9.54	1.36	Moderate
8	5.2332	7.1765	7.27	9.09	1.81	Moderate

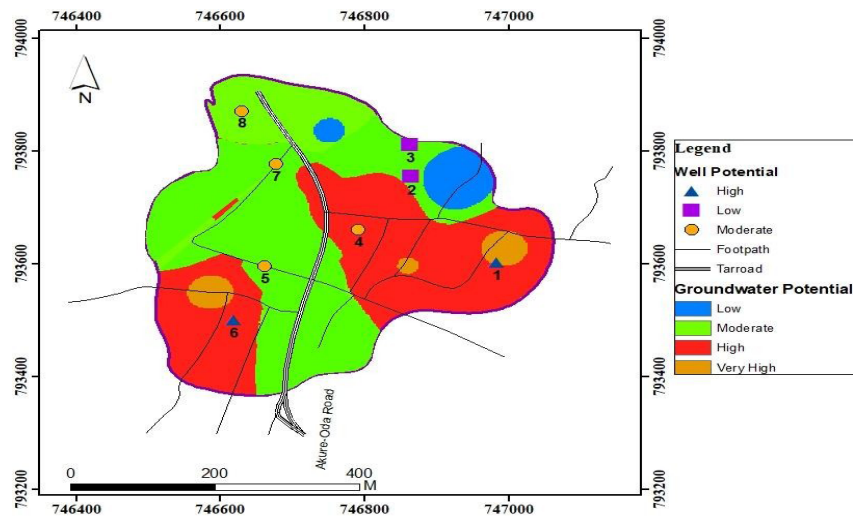


Figure 12. Correlation of hand-dug well and groundwater potential index map.

4. Conclusions

The electrical method using vertical electrical soundings technique was carried out at several locations with the aim of evaluating the groundwater potential of the study area. The study area is characterized by fresh basement rocks. A total of 14 VES data were acquired from the study area using a Schlumberger array with a maximum spacing ($AB/2$) of 80 m. The first layer resistivity value ranges from 29 to 164 Ωm and thickness ranges from 0.6 to 2.5 m. The second layer has a resistivity value ranging from 21-1361 Ωm with a thickness ranging between 1.5 m to 14.6 m. The third layer resistivity value is from 68 to 297 Ωm with thickness ranging between 4 m to 12.4 m. The fourth layer which is the deepest layer has a resistivity value ranging from 180 to 4364 Ωm with depth ranging from 4 m to 19.5 m. The geoelectric parameters obtained were used to generate and evaluate the groundwater potential in the study area. The parameters interpreted from the geoelectric data were used to generate the aquifer resistivity map, aquifer thickness map and bedrock relief which were combined to produce the groundwater potential map of the area. These maps were used to classify the study area into zones ranging from low to high groundwater potential zones. The southwestern and eastern parts are identified as productive groundwater potential zones. VES 13 and 3 coincide with the existing borehole in the area, this is indicating a good accuracy of the model.

In order to validate the results, water column depth was taken from 8 existing hand-dug wells. Major parts of the study area fall within the moderate to high potential while the rest has low potential. Therefore, the area can be concluded to have moderate groundwater potential.

The ratings of the well water column significantly coincide with the groundwater potential index map. Hence, the generated groundwater potential map has good prediction accuracy.

Authors Contributions

The first and the third authors Abe, S.J. and Adeyemo, I.A. supervised and provided the technical direction for the research while the second author was a student. He acquired the data and did the interpretation.

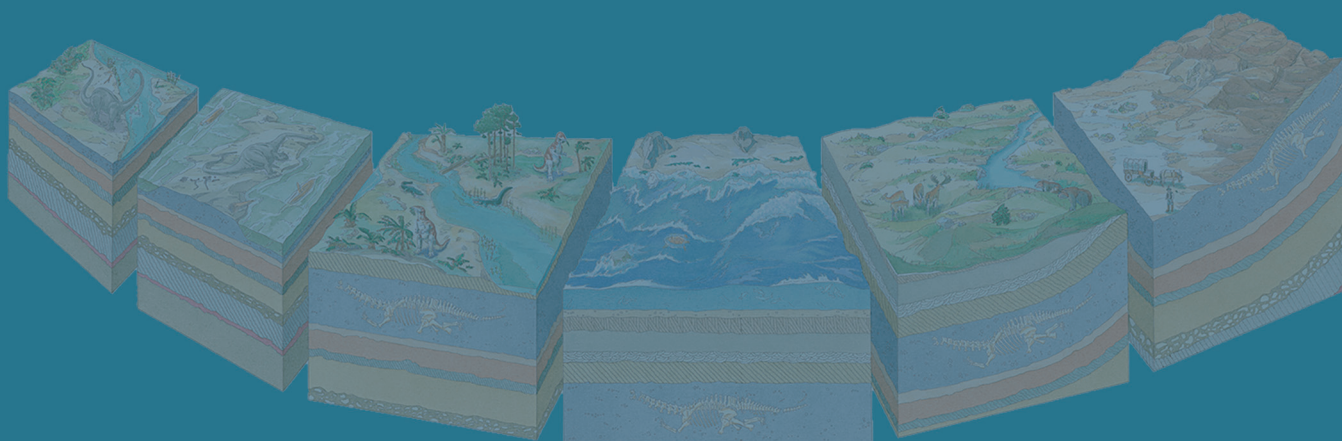
Conflict of Interest

There is no conflict of interest.

References

- [1] Khan, Q., Liaqat, M.U., Mohamed, M.M., 2022. A comparative assessment of modeling groundwater vulnerability using DRASTIC method from GIS and a novel classification method using machine learning classifiers. *Geocarto International*. 37(20), 5832-5850.
- [2] McMurtry, J., Fay, R., 2004. Hydrogen, oxygen and water. Pearson Education: New Jersey. pp. 575-599.
- [3] A Snapshot of Drinking Water and Sanitation in Africa [Internet]. WHO/UNICEF; 2008. Available from: https://sswm.info/sites/default/files/reference_attachments/UNICEF%20WHO%202008%20A%20Snapshot%20of%20Drinking%20Water%20and%20Sanitation%20in%20Africa.pdf
- [4] The State of the World's Land and Water Resources for Food and Agriculture: Managing Systems at Risk [Internet]. FAO; 2011. Available from: https://haseloff.plantsci.cam.ac.uk/resources/SynBio_reports/FAO2011-i1688e.pdf
- [5] Oluyemi, E.A., Makinde, W.O., Oladipo, A.A., 2009. Potential groundwater contamination with toxic metals around refuse dumps in some parts of Lagos metropolis, Nigeria. *Toxicological & Environmental Chemistry*. 91(5), 933-940.
- [6] Adagunodo, T.A., Akinloye, M.K., Sunmonu,

- L.A., et al., 2018. Groundwater exploration in Aaba residential area of Akure, Nigeria. *Frontiers in Earth Science*. 6, 66.
DOI: <https://doi.org/10.3389/feart.2018.00066>
- [7] Olusola, E.F., Ayodele, Y.G., 2021. Geophysical investigation of groundwater potential of a site in Obale area of Akure, Nigeria. *International Journal of Engineering Applied Sciences and Technology*. 6(1), 88-93.
- [8] Rahaman, M.A., 1976. Review of the basement geology of SW Nigeria in geology of Nigeria. Elizabethan Publishing Company: Lagos. pp. 41-58.
- [9] Adiat, K.A.N., Olayanju, G.M., Omosuyi, G.O., et al., 2009. Electromagnetic profiling and electrical resistivity soundings in groundwater investigation of a typical Basement Complex—a case study of Oda Town Southwestern Nigeria. *Ozean Journal of Applied Sciences*. 2(4), 333-359.



Tel: +65 65881289

E-mail: contact@bilpublishing.com

Website: <https://journals.bilpubgroup.com>

2810-9384



04